PETROLOGY OF THE LAVAS OF GRANDE COMORE

by

DAVID F. STRONG, B.Sc.,M.Sc.

Thesis presented for the Degree of Doctor of Philosophy
of the University of Edinburgh in the Faculty of Science.

1970

ABSTRACT

The Comores archipelago consists of four volcanic islands situated on a linear rise across the northern entrance to the Mozambique Channel. These islands are, from east to west, Mayotte, Anjouan, Moheli, and Grande Comore. There are geomorphological indications that volcanism migrated westward, from deeply dissected and submerged Mayotte to the active Kartala volcano on Grande Comore. The volcanic rocks on all the islands appear to consist of silica-undersaturated basalts and their derivatives.

Grande Comore comprises two shield volcanoes, La Grille in the north and Kartala in the south. There is a complex suite of collapse calderas at the summit of Kartala, marking the centre of historic volcanic activity in the archipelago. Each volcano is elongated, which, along with the abundant aligned and coalescing pyroclastic cones, reflects the importance of fissure eruptions in their development.

The lavas of Kartala are primarily alkali basalts, with abundant ankaramitic and oceanitic varieties, containing an average of 3·7 wt % normative nepheline. From a detailed evaluation of the chemistry and petrography of these lavas it is postulated that they represent a series resulting from low-pressure fractional crystallization of alkali basalt magma. The magmas can be explained as resulting from more than 10% partial melting of garnet lherzolite upper mantle at pressures around 30 kb, with some high-pressure (> 25 kb) fractionation of harzburgite, garnet harzburgite, and either garnet wehrlite or eclogite, followed by subsequent polybaric fractionation of olivine

± clinopyroxene during ascent.

The lavas of La Grille volcano are more undersaturated in silica than those of Kartala, containing an average of 11·5 wt % normative nepheline, and many containing normative leucite. They also have higher average concentrations of Ba, Sr, Rb, CaO, MgO, P_2O_5, and MnO than Kartala lavas. They have been classified in the present study as a basanitic series, and contain only olivine as an important phenocryst phase. The lack of any systematic relation between chemical and mineralogical composition precludes the possibility of their having a similar petrogenetic development to the Kartala lavas. They are explicable as originating from less than 10% partial melting of garnet lherzolite upper mantle, with substantial high-pressure fractionation of garnet wehrlite or eclogite. Interruption of this high-pressure fractionation at different stages produced one trend of chemical variation, on which was superimposed a second trend resulting from polybaric fractionation of lherzolite, wehrlite and dunite, now found as ultramafic inclusions in the lavas.

C O N T E N T S

4. MINERALOGY

5. PETROCHEMISTRY

- 4 -

FIGURES

- 5 -

PLATES

1. Typical coastal exposure, southeast Grande Comore.

2. Columnar-jointed lavas exposed in walls of Chagnoumeni pit crater.

3. Plagioclase-phyric flow, Foumboudzivouni.

4. Aerial view of aligned cinder cones, Massif de la Grille.

5. Haboho cinder cone.

6. Sima cinder cone.

7. Goudjoulachamle cinder cone.

8. Typical cinder cone with breached walls.

9. N'Gouni tuff cone.

10. Panoramic view of the Kartala caldera.

11. Vertical basaltic dyke in caldera wall.

12. Photomicrograph of typical alkali basalt.

13. Photomicrograph of typical alkali olivine basalt.

14. Photomicrograph of typical oceanite.

15. Photomicrograph of typical ankaramite.

16. Photomicrograph of typical feldspar-phyric basalt.

17. Photomicrograph of typical basanite.

18. Photomicrograph of typical nepheline basalt.

19. Photomicrograph of orthopyroxene xenocrysts.

20. Photomicrograph of quartz xenocrysts.

1. GENERAL INTRODUCTION

1.1 THE COMORES ARCHIPELAGO

1.1.1. Introduction

The Comores Archipelago is situated at the northern entrance to the Mozambique Channel, between $10^{\circ}21'$ and $13^{\circ}03'$ south and $43^{\circ}15'$ and $45^{\circ}20'$ east (Fig. 1). It comprises four principal islands distributed over a distance of 275 km along a NNW-trending submarine plateau which rises from depths in excess of 3 km. These islands are, from east to west, Mayotte, Anjouan, Moheli, and Grande Comore. Two atoll groups, Banc du Geyser and Isles Glorieuses, are found ENE of Mayotte, offset from the linear trend of the Comores Archipelago (Fig. 1). These may represent the earliest manifestations of Comores volcanism.

The Archipelago has a tropical climate, with abundant rainfall and high temperatures, and trade winds (or monsoon) blowing more or less continuously from southerly directions. This produces a deep lateritic soil and lush vegetation which, particularly in the older islands, makes geological investigation difficult.

The essentially volcanic nature of the islands was discussed by Voeltzkow (1906) and later by Lacroix (1922), who provided the first petrographic descriptions and chemical analyses of the rocks. However, the first detailed geological study was made by De Saint Ours (1960), who was particularly interested in the geomorphology and economic geology of the islands.

The present study commenced in 1967 when geologists from Edinburgh and Manchester Universities (Esson, Flower, Upton and
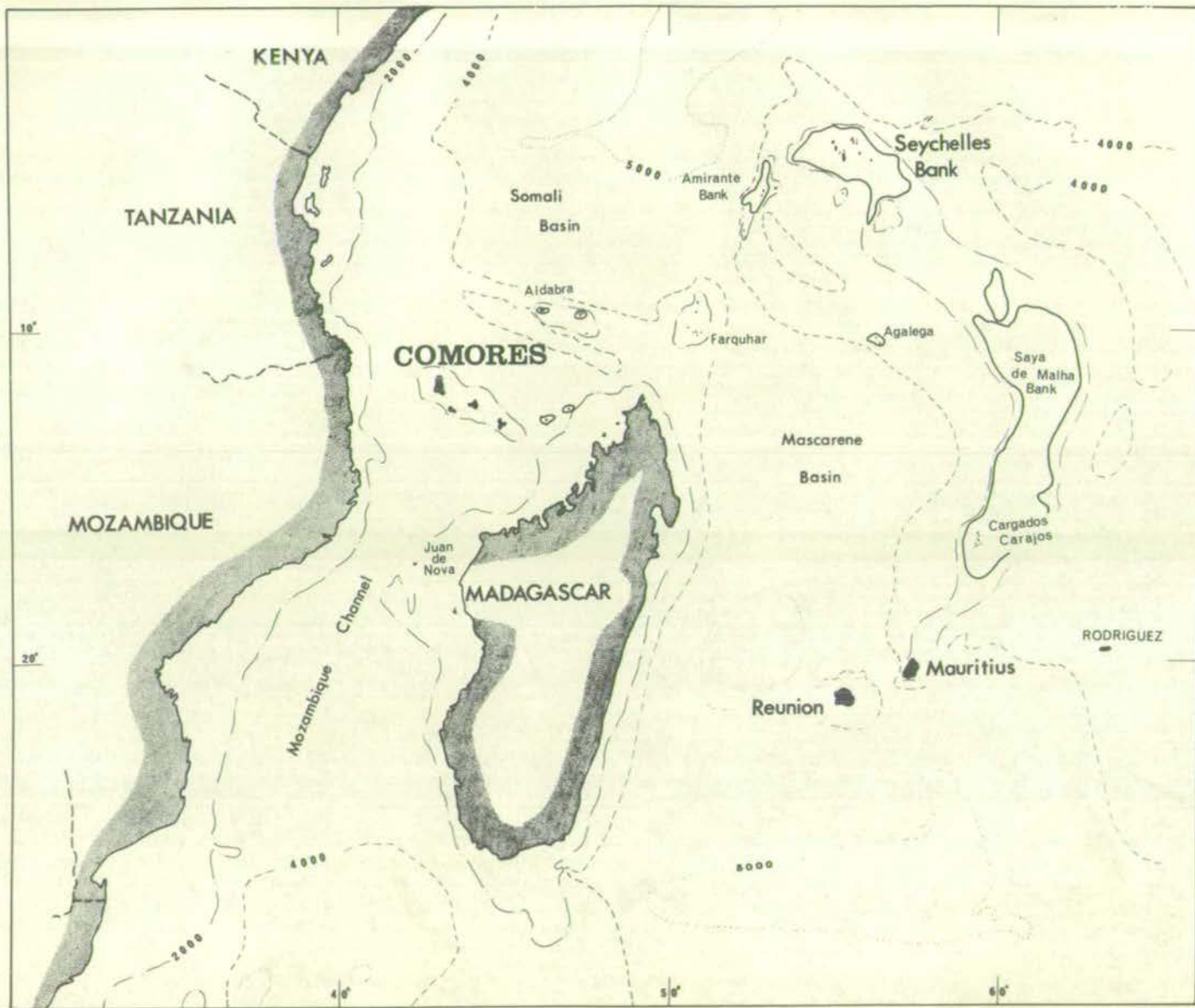
Fig. 2.

Local setting of the Comores archipelago.

Submarine contours, given in metres, were drawn from
data points on the 1/500,000 scale map of the
archipelago published by the Institut Geographique
National of France, 1964.
Contours on the islands at intervals of 500 metres.

MAYOTTE

MOHELI

ANJOUAN

GRANDE
COMORE

10 20 30 40 50 km
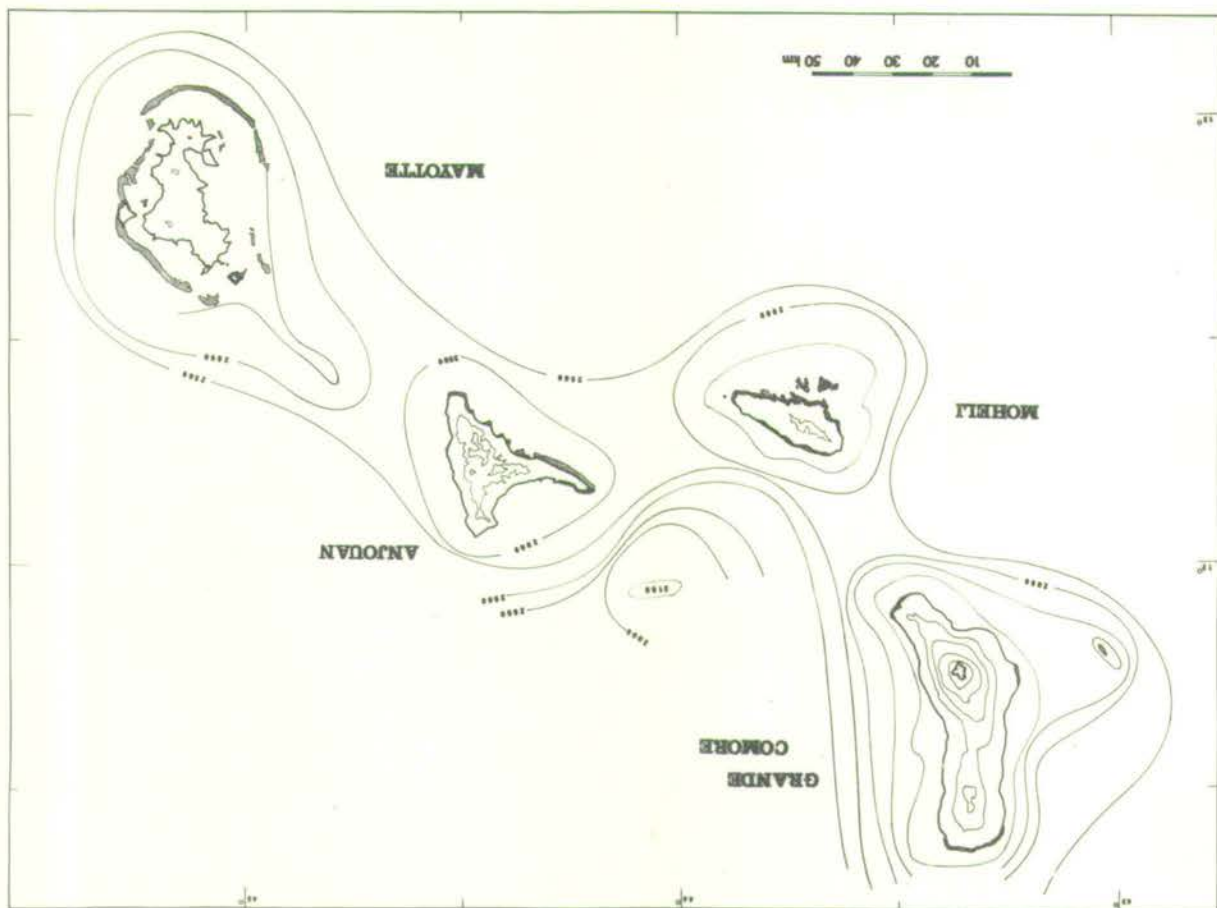
Wadsworth) spent several weeks on reconnaisance field-work in preparation for detailed studies. Flower and the present writer returned to the islands in 1968, and further field-work was carried out on Grande Comore, Anjouan, and Moheli. The whole study forms part of a more general research programme on the volcanic islands of the western Indian Ocean.

The following general account is based primarily on the work of De Saint Ours (1960) and a preliminary report by the present investigators (Esson, _et al._, in press).

1.1.2. Mayotte

Mayotte, 320 km from Madagascar and most easterly of the Comores islands (Fig. 2), is the most low-lying of the group, with maximum altitude of only 660 metres. It has undergone deep submergence and dissection, resulting in a deeply embayed coastline and rugged topography. Nevertheless, it retains a strong pattern of NW- and N-trending lineations in the form of mountain ridges, coast lines, submarine escarpments, and reef margins, which is probably controlled by a fundamental pattern of rifts and faults in these two principal directions.

The island is surrounded by fringing reefs, and an almost continuous barrier reef. The barrier reef has a smooth elliptical form which stands in marked contrast to the islands jagged coastline. This elliptical form may represent the periphery of an ancient Mayotte volcano. If this is the case, it implies that the ancient volcano was some 55 km long and 35 km wide, and assuming slopes of $8°$, probably more than 3 km high. The reefs and lagoon were studied by Guilcher (1965), who explained submerged river valleys and karst topography as

resulting from subaerial erosion during a Pleistocene period of low sea level.

The oldest rocks of Mayotte consist of deeply eroded basalts, which form small hills and low-lying plateaux with a maximum relief of 450 metres. De Saint Ours, by comparison of geomorphology with Mt. Ambre in Madagascar, considered it possible that these basalts are Turonian-Cenonian (Upper Cretaceous) in age. Phonolitic plugs form resistant masses up to 660 metres high, and appear to make up much of the central ridge of the island. Resistant ribs running down to the coast from this central ridge consist of flows of trachy-basalt, basanite, nephelinite, and phonolite. The only constructional volcanic features remaining are the deeply dissected pyroclastic craters Karani and Kaweni, in the northeast part of the island. An extensive blanket of lateritic clay covers the northern inland regions of the island. Xenoliths of hornblendite, anorthosite, peridotite, gabbro, and syenite have been found by Esson in the lavas and tuffs.

Although the Mayotte volcano shows every sign of extinction and advanced decay, the eruption of three tuff cones through the reef at Pamanzi show that there has been a rejuvenation of activity in the recent past.

1.1.3. Anjouan

Anjouan, 80 km northwest of Mayotte (Fig. 2), is dominated by a central peak, N'Tingui, which rises to a height of 1,595 metres. According to De Saint Ours (1960, p. 226), the ancient N'Tingui volcano, probably reaching heights of 3 km, is now eroded into deep gorges and cirques comparable to the classical amphitheatre-headed

valleys of the Hawaiian islands (cf. Stearns and Vaksvik, 1935).

The rocks of the central N'Tingui massif are chiefly alkali basalts of ankaramitic type. These were assigned to a Miocene phase of eruption by De Saint Ours, which he termed the "phase inferieur".

According to De Saint Ours, the three main peninsulas of Anjouan were formed by fissure eruptions during lower to middle Quaternary times, and he referred to these as the "phase intermediare". Lavas of this phase also occupy the gorges and river valleys eroded into the N'Tingui massif. These younger lavas are more undersaturated in silica than the older ones, and include basanites, trachybasalts, trachytes, and phonolites. Over 50 tuff cones are present on Anjouan and, despite much variability in the state of dissection (and therefore age), most are assigned by De Saint Ours to a period of volcanism younger than the "phase intermediare". A body of quartz gabbro, about 250 metres in diameter, intrudes the lavas of the "phase inferieur" in the upper reaches of the Cirque de Bambao.

Xenoliths of gabbroic and ultramafic rocks (sometimes layered) are common in the more basic lavas, and xenoliths of syenite have been recovered from the phonolitic flows. Fragments of quartzitic and arkosic sandstone have been found in the younger basaltic lavas, and arkosic sandstone crops out over an area of 250 square metres in the Cirque de Bambao. The significance of these sandstones has been discussed by Flower and Strong (1969).

The southwest and east coasts of Anjouan are straight and regular, parallel to the fissure system inferred from Mayotte lineaments, and

the alignment of its southwest coast with the straight north coast of Mayotte is particularly striking (Fig. 2). The distinctly concave northern coast does not fit this regional pattern of fissures, and may be the result of slumping of the volcanic pile into the deep waters (greater than 3000 metres) just northwest of Anjouan (Fig. 2).

Anjouan is bordered by fringing reefs, but barrier reefs are only in an incipient state of development, an indication of the youthfulness of this island relative to Mayotte.

1.1.4. Moheli

Moheli, the smallest of the four main islands, lies 45 km to the southwest of Anjouan (Fig. 2). The island can be divided into two distinct topographic regions, viz. a relatively low-lying (less than 400 metres) eastern plateau, and a more mountainous western half. The latter is dominated by a jagged median ridge which rises to a maximum height of 790 metres. A group of small elongate islets off the south coast appear to radiate from this peak.

De Saint Ours (1960) recognized the same two phases of volcanism on Moheli as he did for Anjouan. The "phase inferieur" supposedly makes up the western mountainous area, which consists of basanites, nephelinites, ankaramites, and minor phonolitic rocks. The "phase intermediare" in the eastern half consists of more olivine-rich varieties of basaltic rocks. Some doubt is thrown on these relative ages, however, by an abundance of youthful flows in the western part and a deep soil cover in the eastern part of the island. These suggest that the relative ages of each area are in fact in the reverse order of that postulated by De Saint Ours, i.e.

with the older part being in the east.   Recent tuff cones are
seen in both areas, and their respective ages do not appear to have
any geographic correlation.

Samples of presumed intrusive rocks are found as boulders in
most riverbeds of Moheli.   These consist of gabbros, syenites, and
ijolites; none of these has been seen in situ.   Ultramafic inclusions
are found in basaltic lavas, both in flows and river boulders.   One
sandstone inclusion, 50 cm in diameter, was found in a younger
basaltic lava flow.

Although the present elongate form of the main island is
probably a reflection of repeated eruptions along WNW fissures, the
circular submarine contours (Fig. 2) suggest the former presence of
a large central volcano.   In this light, the southern islets may
be explained as younger lavas which occupied river valleys eroded
into this volcano, and which were preserved as positive relief
features after further erosion of the intervening spurs of older
basalt.

Moheli is completely surrounded by fringing reefs, but no
barrier reef, in contrast to Mayotte and Anjouan.

1.1.5. Grande Comore

As Grande Comore is described in detail in the following chapter,
only very general information will be given here.   It is the most
westerly of the four islands (Fig. 2), only 280 km from Cape Delgado
in Mozambique.   It is the largest island in the group, and is made
up of two volcanic massifs.

The northern volcano, La Grille, has the form of a gently domical

shield which reaches a maximum height of 1087 metres, and is covered by more than 120 tuff cones. Its lavas are chiefly olivine-phyric basanites, in some cases containing ultramafic and, more rarely, gabbroic inclusions. Scarce arkosic sandstone inclusions are also found in La Grille lavas, and are similar to those described for Anjouan and Moheli.

Kartala, the southern volcano, is a steep-sided shield volcano, 2361 metres high, and crowned by a large dome and a complex suite of collapse calderas. The Kartala lavas are all alkali basalts, with highly variable proportions of olivine and augite phenocrysts, and rarer plagioclase phenocrysts.

The smooth topography and coastline, and the scarcity of reef development, indicate the youthfulness of Grande Comore relative to the other three islands. Kartala is the only active volcano of the group, although La Grille has also been active in historic times.

1.1.6. Relative volumes of each volcano

As indicated above, each of the islands has undergone differing degrees of erosion, with the result that their present sizes are not representative of the volumes of the lava originally erupted. There is no exact way of obtaining these original volumes, but some approximate estimates can be made.

Although the lavas from each volcanic center probably overlap at depth, the individual domes appear to separate at depths around 2 km (Fig. 2). With this in mind, the volume of each volcano above this level can be arbitrarily estimated, although much of the total volcanic material (i.e. below 2 km) will not be included. These

volumes are given in Table 1, as calculated by assuming that each
volcano was conical, with its base at the -2 km contour, and a mean
radius calculated at this contour.   For the eroded eastern islands,
the height of each cone was calculated by assuming original slopes
of 9°, slightly greater than those of La Grille.   For the "Grande
Comore" calculation, Kartala, La Grille, and the Vailheu reef were
included as one volcano, and an altitude was assumed intermediate
between Kartala and La Grille.

It should be emphasized from Table 1 that any subsequent dis-
cussion of these volcanoes will be concerned only with the subaerial
parts, certainly less than 7%, and probably less than 3% of the
total volume of erupted magma.

Table 1

Estimated volumes of each volcano

Volcano	Subaerial Volume, km^3	Total Volume, km^3	Subaerial as Percentage of Total Volume
Mayotte	58	6,880	0·8%
Anjouan	262	1,800	14·6%
Moheli	41	2,300	0·02%
"Grande Comore"*	749	4,220	17·7%
Kartala	625	"	14·8%
La Grille	124	"	2·9%

* "Grande Comore" estimate includes an allowance
   for the Vailheu reef.

1.1.7. Tectonic setting

The scanty evidence bearing on the tectonics of the western Indian Ocean have been reviewed by Flower and Strong (1969), and the following summary is taken directly from this paper.

There are two essentially contradictory views on the tectonics of the western Indian Ocean. Fisher et al. (1968), mainly on the basis of oceanographic studies, suggested that Madagascar was once twenty degrees north of its present position relative to Africa, and connected to the Seychelles Bank. These were then separated by the southward movement of Madagascar by left lateral faulting sometime between the Permian and Cretaceous periods, and the ocean floor between Madagascar and the Seychelles was subsequently developed during Cretaceous volcanism. The merits of this interpretation are that it agrees with an hypothesis of sea floor spreading from the Carlsberg Ridge, it can explain the pattern of magnetic anomalies and bottom topography in the area, and a north-northeast projection of the proposed fault coincides with the Owen Fracture Zone.

This southerly faulting mechanism does not, however, account for the present eastward position of the Saya de Malha micro-continent, which Fisher et al. (1967) earlier proposed to extend from the Seychelles to Cargados Carajos. The northern coincidence of the proposed fault zone with the Owen Fracture should not be relied upon too heavily for several reasons; i.e. correlation of the very old and seismically inactive southern fault with the presently seismically active Owen Fracture is hardly justified, and the right lateral displacement on the Owen Fracture is opposite to that required.

Perhaps the most serious objection to their interpretation is that it requires the crust in the southern part of the Somali Basin to be basaltic.   Although Fisher et al. (1968) interpret seismic data (Francis et al., 1966) as indicative of rocks "wholly volcanic except for an uppermost layer of sediments", Francis et al. (1966) find Karroo beds well out into the Somali Basin, and a layer with seismic velocities of 2·5 km/sec almost as far east as the Seychelles (page 259, Fig. 19), which they correlate with African drill core data and explain as "probably consolidated sediments of Jurassic and Cretaceous age".   Thus, any separation of Madagascar and the Seychelles would have occurred before the Jurassic, and the required basaltic material does not appear to be present to any large extent.

An additional important criticism to the hypothesis of southward movement of Madagascar is that it conflicts with the tensional environment of the area, well established through studies of the African rift systems.

The second major interpretation of the tectonics is that put forth by Dixey (1956), who suggests that the Mozambique Channel is geosynclinal in nature, having resulted from Karroo (late Carboniferous) and later subsidence along normal faults in a tensional environment. Dixey suggests that this geosyncline may extend over the full length of the east coast of Africa.   By extrapolation of data from both sides of the channel he concludes that it contains about 8 km of Karroo sediments and 6 km of post-Karroo sediments, with Precambrian basement at a depth of about 14 km.   This conclusion is supported by Pepper and Everhart (1963) who, on the basis of seismic and drill core data, put the basement at a depth of 7·5 km near the southwest

coast of Madagascar, and who also point out that granite on the island of Juan de Nova supports this conclusion. The sediment thicknesses postulated by Dixey (1956) are also in agreement with thicknesses for the Somali Basin given by Francis et al. (1966). The gravity data for the Mozambique Channel given by Talwani (1962) may be interpreted as indicative of continental crust, overlain by the thick Karroo and Cretaceous lavas, and work of H.M.S. Owen in 1961-1962 indicates that Madagascar is connected to Africa by continental crust (Holmes, 1965, p. 936). There is clearly much evidence in favour of Dixey's hypothesis.

If the Mozambique Channel is underlain by Precambrian basement, then Madagascar has probably never been in other than its present position relative to Africa; if the Channel contains only Karroo and post-Karroo sediments and lavas, then Madagascar may have moved eastward from Africa. Either way, the evidence is conclusive that Madagascar did not move into its present position from the north. In the light of this discussion it is clear that there is a need for direct evidence as to the nature of crust beneath the Mozambique Channel or the Somali Basin.

As shown in Fig. 1, the Comores Archipelago lies in a critical position between the Mozambique Channel and the Somali Basin. Vienne (1900) reported "grey-blue granite and quartz rocks" from southern Grande Comore at Morotso, Roveni, and Chindini, but no source for these rocks was given. Lacroix (1922) gave detailed descriptions of metamorphic rocks found at Mutsamudu, Anjouan, and quartz monzonite inclusions in the tuffs at Dzaoudzi. The orthogeneiss consists of almandine, biotite, microline, oligoclase, and

quartz, and is common in Madagascar. He also describes amphibole granite, granodiorite rich in diopside, hornblende and biotite, as well as quartz monzonite, anorthosite, olivine gabbro, and serpentinzed peridotite from the same locality. From these rocks Lacroix concluded that the islands were underlain by crystalline basement. De Saint Ours (1960), unable to find any such rocks, did not accept Lacroix's conclusions, and suggested that dredging of the submarine plateau might solve the problem. Whether or not these rocks were derived from underlying basement, the sandstone inclusions found by the present workers is unequivocal evidence that the islands are at least underlain by sedimentary rocks. In this light the Comores volcanoes cannot be described as truly oceanic, as they must have passed through some highly silicic material.

1.1.8. Summary

1. The Comores islands are situated on a long linear rise and show geomorphological indication of a decrease in age westwards.

2. Two principal regional fissure systems appear to have controlled the volcanism.

3. Inclusions of sandstone are found in lavas of three of the four islands, indicating the presence of underlying silicic material through which the lavas were erupted.

4. The dominant petrological association is alkali basalt, basanite, nephelinite, trachyte, and phonolite.

1.2. GENERAL REVIEW OF ALKALINE IGNEOUS ACTIVITY

1.2.1. Introduction

If this study of the Comores islands is to be of more than just local significance, it must be related to other occurrences of similar rocks, very common in both oceanic and continental crustal environments. Unfortunately, the crustal structure in the Comores area cannot, with any certainty, be described as truly continental nor oceanic. Consequently, both continental and oceanic occurrences, and the hypotheses surrounding them, may be relevant to the Comores volcanoes. Accordingly, the following is a brief review of occurrences from each environment that are petrologically similar to the rocks of the Comores islands, and Grande Comore in particular.

1.2.2. Oceanic occurrences

Although, unlike the Comores situation, alkalic lavas make up less than 3% of the volume of any Hawaiian volcano, the detail in which these islands have been studied makes them a reference point for any other volcanic studies. As a detailed discussion of the Hawaiian alkaline lavas has recently been presented by Macdonald (1968a), only a brief summary of his views are given here.

The Hawaiian alkali basalts were erupted after voluminous out-pourings of tholeiitic lavas, and after long quiescence, these are followed by relatively small amounts of nepheline basalt and nepheline melilite basanite ("the nephelinic series"). According to Macdonald (1968a), the magmas producing the alkalic and nephelinic suites were formed from an olivine tholeiite magma by fractionation (of unspecified phases) at depths around 30 km and 50 km respectively,

the olivine tholeiite having formed by partial melting of the mantle at depths around 60 km.

Differentiation of the alkalic magma (into an ankaramite - alkalic olivine basalt - hawaiite - mugearite - benmoreiite-soda trachyte suite) was thought to be brought about by fractional crystallization of augite, olivine, bytownite and magnetite, in the approximate proportions 5:2·5:2:0·5. This accounts for the dominance of ankaramitic and absence of olivine-cumulitic rocks in the alkalic series, and in this respect they are clearly comparable to those of the Kartala volcano on Grande Comore. The nephelinic suite shows two fractionation trends. The first, (alkali olivine basalt - basanitoid - basanite), results from fractionation of "pyroxene and olivine, and perhaps some feldspar". The second trend leads to the nephelinites and melilite nephelinites, and "may be largely controlled by the separation of orthopyroxene in place of olivine in a high pressure environment".

There are many oceanic volcanoes that appear to be more closely comparable to the Comores than those of Hawaii in that they show no visible indication of being underlain by tholeiitic basalts (e.g. Tutuilla, Macdonald, 1968b; Manu'a Island, Stice, 1968; Gough Island, LeMaitre, 1962; Tristan da Cunha, Baker, et al., 1964; St. Helena, Baker, 1969; Rodriguez, Upton, Wadsworth, and Newman, 1967; Cook Islands, Wood, 1969; Marshall, 1929; Clarion Island, Bryan, 1967; Truk Islands, Stark and Hay, 1963; Ponape Island, Yagi, 1960; Mauritius, Walker and Nicolaysen, 1953; Tahiti, Williams, 1933; McBirney and Aoki, 1968).

Tahiti is particularly similar to the Comores Islands in the range of rock types represented. Like Grande Comore, it is formed of two coalescing shield volcanoes, although it is more deeply dissected, and displays both plutonic and extrusive differentiates which are absent on Grande Comore, but present on Moheli, Anjouan, and Mayotte. Furthermore, both ankaramite and basanite are abundant on both volcanoes of Tahiti, whereas on Grande Comore they appear to be restricted to separate volcanoes. According to McBirney and Aoki (1968), a Tahitian parental alkali basalt differentiated into two divergent series, one trending towards trachyte and the other towards phonolite. They considered that fractionation of the observed mineral phases could not account for these trends, and postulated that they resulted from fractionation at greater depth, where other phases would be stable.

1.2.3. Continental occurrences

As for oceanic volcanoes, chemical diversification of alkali olivine basalt in continental environments has most commonly been explained by some process involving crystal fractionation. One well-known example of this is the Eastern Otago province of New Zealand, recently reviewed by Coombs and Wilkinson (1969), who propose for these, and alkaline lavas in general, three "fractionation lineages". These are (1) alkali basalt - hawaiite - mugearite - benmoreite - trachyte; (2) basanite - nepheline hawaiite - nepheline mugearite - nepheline benmoreite - phonolite; (3) a nephelinite series of restricted compositional range. Except for minor differences these lineages are similar to the differentiation series reviewed above

for Hawaii and Tahiti, suggesting that the continental environment was not an important factor in their development. Although the Otago lavas have reacted to some extent with the underlying silicic basement, indicated by "half digested inclusions of quartzose schist" (Turner and Verhoogen, 1960, p. 167), (cf. the sandstone inclusions in Comores lavas), this had no detectable effect on the chemistry of the lavas (Coombs and Wilkinson, 1969, p. 496).

The Carboniferous lavas of the Scottish Midland Valley also show many similarities to the Hawaiian and Otago lavas, in particular the early eruption through central volcanoes of lavas showing ample evidence of fractionation of olivine, augite, and plagioclase, followed by a suite of more undersaturated basanites and nephelinites rich in ultramafic inclusions (MacGregor, 1948; Upton, 1969).

A similar suite of lavas has been erupted through and intruded into Cretaceous sedimentary rocks in the Balcones province of Texas (Spencer, 1969). According to Spencer (1969), these rocks represent two primary magmas. Fractional crystallization of an alkali basalt primary magma produced only small changes in chemical composition. A nephelinite primary magma differentiated, by fractionation of olivine, clinopyroxene, and nepheline into two separate trends. These trends, nepheline basanite - mafic phonolite - phonolite and nephelinite - melilite nephelinite, were, according to Spencer (1969), probably determined by the composition of the fractionating pyroxene.

In the East Rift of Kenya and northern Tanzania, great volumes of alkaline magmas have poured out through fissures and individual stratovolcanoes from the Miocene to the present (King and Sutherland,

1960; Williams, 1969). Activity began with olivine phonolite eruptions, followed up to the Quaternary with irregularly alternating phases of predominately alkalic basalt, basanites and nephelinites or phonolites, trachytes and nephelinites.

Saggerson and Williams (1964) divide these rocks into an ankaratrite - melanephelinite - nephelinite - phonolite series and an alkali basalt - trachybasalt - trachyte series, each of which they consider to be derived independently from some common source, possibly alkali peridotite, in the mantle, and differentiated by fractionation of olivine and other unspecified phases.

Varne (1968) recognized two similar series from Moroto Mountain, Uganda, and proposed that incongruent melting of pargasite gave rise to the nephelinite series, and that partial melting of the peridotite produced the alkali basalt series. However, Wood (1968) suggested that low concentrations of Rb, Sr, Ba, Zr, Nb, Y and La and high K:Rb and K:Ba ratios in the pargasite of these rocks invalidated Varne's hypothesis. Wood concluded that high pressure fractionation of magnesian clinopyroxene, along with wall-rock reaction during ascent, could produce the olivine nephelinites; these, by fractionation of olivine and spinel, could produce the olivine-poor nephelinites.

1.2.4. Summary

The above brief review has shown that:

1. There are numerous occurrences, in both oceanic and continental crustal environments, of rocks petrologically similar to those of the Comores. Hence any petrological conclusions from the present study should be of some general significance.

2. Although metasomatism, alkali transport, partial melting, and other processes have been proposed to account for the formation of such rocks, fractional crystallization of a basic magma is that most commonly accepted. Any such process might be valid for the Comores.

3. Much attention has been given to explaining the differentiation of these suites from the "parent magma", but little attention has been given to explaining the actual origin of the "parent magma" in question, a surprising fact in view of the theoretical and experimental interest in this problem.

1.3. THE PRESENT STUDY

The present study has been confined to Grande Comore since it displays the simplest geology and petrology of the group, and is consequently most amenable to a detailed petrochemical study, especially with regard to the genesis of any primary magma. At the same time it may well display relatively primitive stages of volcanic evolution through which the older Comores volcanoes themselves passed in their earlier development. Furthermore, should the study reveal little of general petrological significance, it would be of some intrinsic local value as a contribution to the geological knowledge of the archipelago as a whole. In this light, the objective of the present study is to provide an accurate geological and geochemical description of Grande Comore, and attempt to explain the petrogenesis of the lavas in the hope that any such explanation may be applicable to the many other occurrences of similar lavas.

2. <u>GEOLOGY OF GRANDE COMORE</u>

2.1. <u>INTRODUCTION</u>

A complex interplay of erosional and volcanic activity results in rugged topography on the three islands of Anjouan, Moheli, and Mayotte, making field-investigations slow and difficult.   On Grande Comore, however, constructional volcanic activity has been dominant, and the island has a relatively smooth and undissected topography. The resulting lack of vertical sections does, unfortunately, limit field work to sampling the thin veneer of lavas covering the island.

The present study is based on field work carried out over two separate periods, two weeks during the summer of 1967, and three weeks during the summer of 1968.   The extensive network of roads and footpaths permitted rapid coverage of most of the island, and a representative sampling of the island was obtained.   This, in conjunction with study of the aerial photographs and topographic map was considered adequate for the present investigation.   There is no doubt, however, that refinements and additions could be made, especially with the aid of drilling or geophysical techniques.

2.2. <u>TOPOGRAPHIC UNITS OF GRANDE COMORE</u>

2.2.1. <u>Introduction</u>

De Saint Ours (1960) divided Grande Comore into four topographic units.   These are, from north to south, the Massif de la Grille, the Diboini Plateau, the Massif de la Kartala, and the Massif de Badjini. These subdivisions are retained by the present writer, although not always with the same geological significance as given to them by De Saint Ours.

2.2.2. Massif de la Grille

The Massif de la Grille comprises the northern third of Grande Comore (Fig. 3). It has the form of a gently sloping dome about 15 km in diameter and 1087 metres high. It is slightly elongated in an ESE direction, with surface irregularities resulting from some 120 pyroclastic cones (Figs. 3, 4a). The slopes of this dome do not exceed 7° on the west and north, but the eastern slopes are steeper (up to 16°) and slightly concave (Fig. 4a).

2.2.3. Diboini Plateau

The Diboini Plateau was not precisely defined by De Saint Ours (1960), but used only to indicate the broad saddle between La Grille and Kartala. In the present study, the Diboini Plateau refers to the region indicated on Fig. 3 by the narrow NW-trending defile between Kartala and La Grille reaching a maximum height of 600 metres. It emphasizes the clear topographic break between La Grille and Kartala volcanoes, and is believed to represent a zone of inter-digitation of lava flows from each.

2.2.4. Massif de la Kartala

The Massif de la Kartala forms an elongate dome, about 30 km in diameter at sea level and 2361 metres above sea level, which makes up over half the island of Grande Comore (Fig. 3). It is elongated towards NNW and SE, due to fissure eruptions concentrated in these directions, and these elongations are hereafter referred to as the NNW and SE fissure zones. The western Kartala slopes have an average value of 15° (much steeper than those of La Grille) while

Fig. 3.

Topographic map of Grande Comore

————————— Roads

- - - - - - Footpaths

Pit crater

Approximate boundary of ancient
marine platform

Coral reef

Topographic boundaries

Topo. contours at 100 meters

A————B etc. Locations of profiles given in Fig. 4.

LA GRILLE

Diboini

N

KARTALA

C — — D

F

Badjini

1 2 3 4 5 6km

E

G
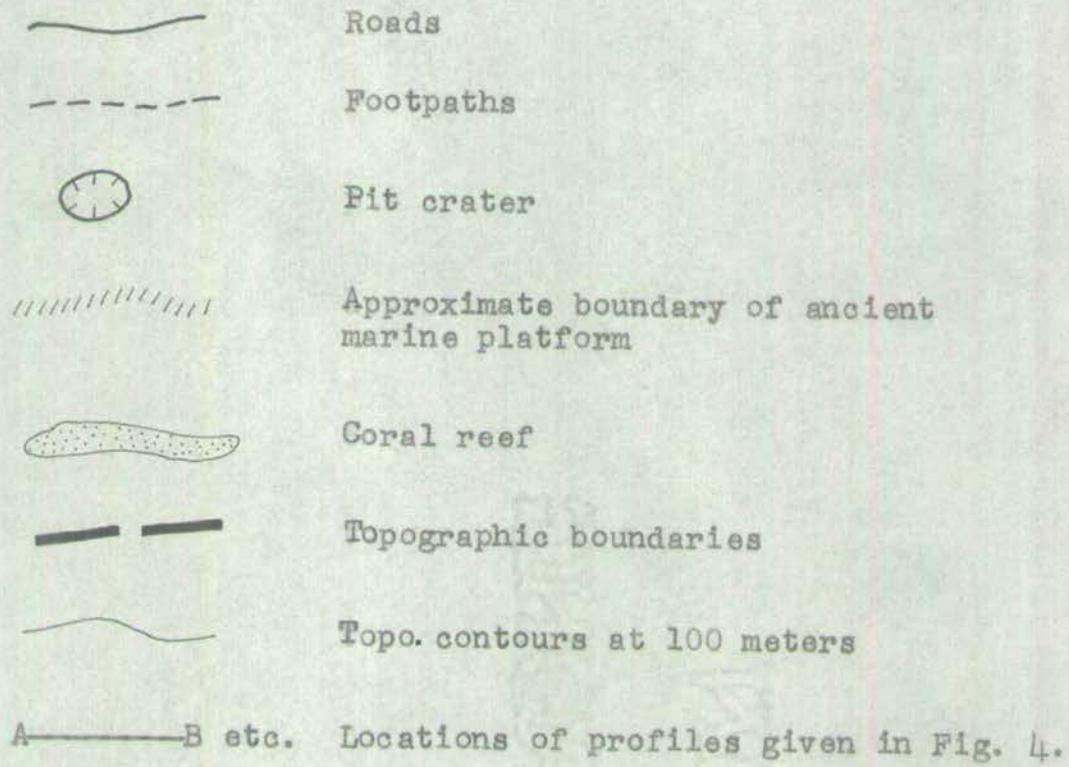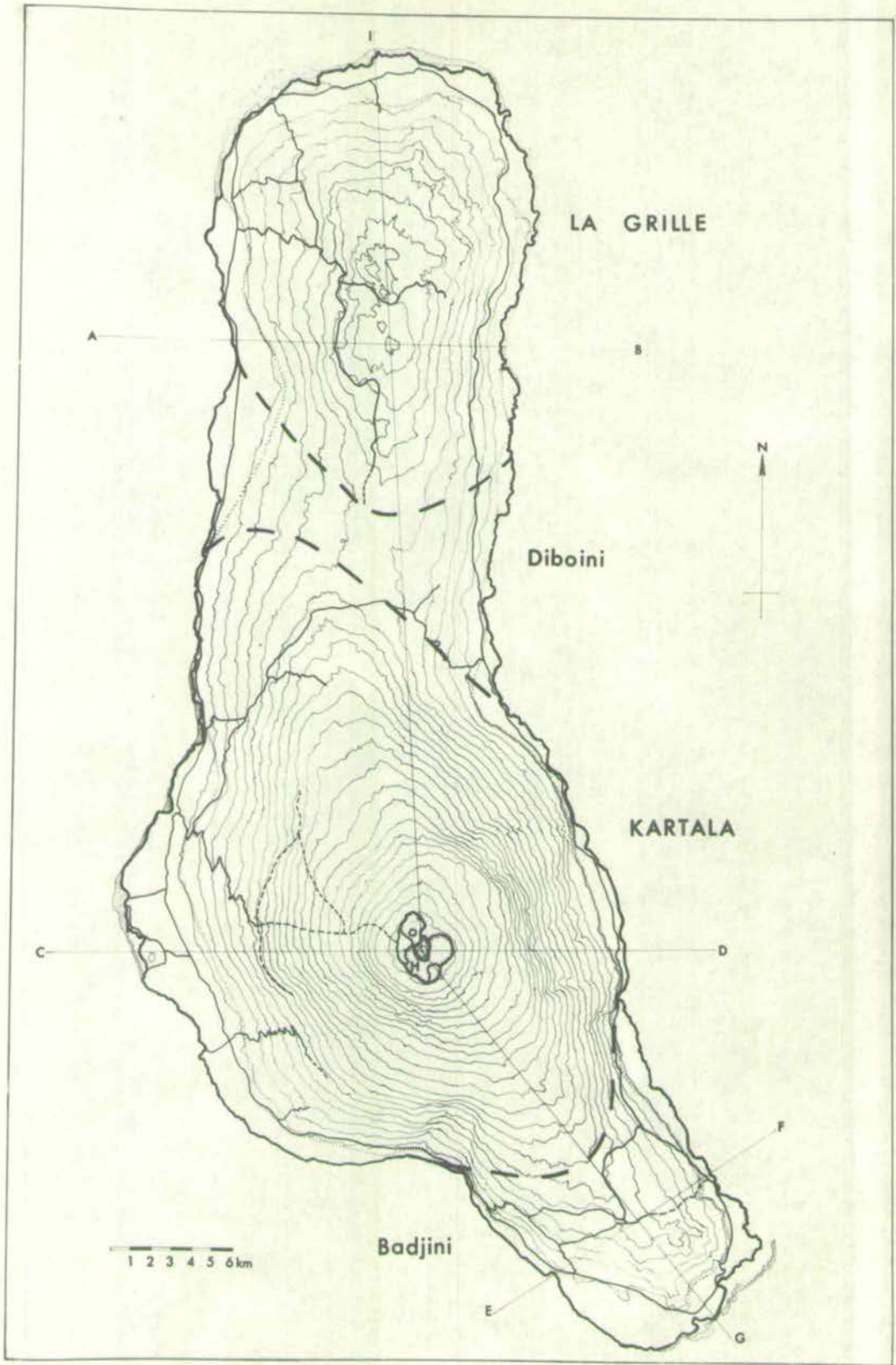
Fig. 4.

Profiles of Grande Comore

    a. La Grille

    b. Kartala

    c. Badjini

    d. Longitudinal profile (note different scale
                                     from a, b and c)

a.

LA GRILLE

1500
1000
500 m.

A   B

c.

BADJINI

1000
500 m.

E   F

b.

KARTALA

3000
2000
1000 m.

C   D

1   2   3 km.

d.

3000 m.

La Grille   Diboini Plateau   Kartala   Badjini

I   H   G

0   2   4   6 km.
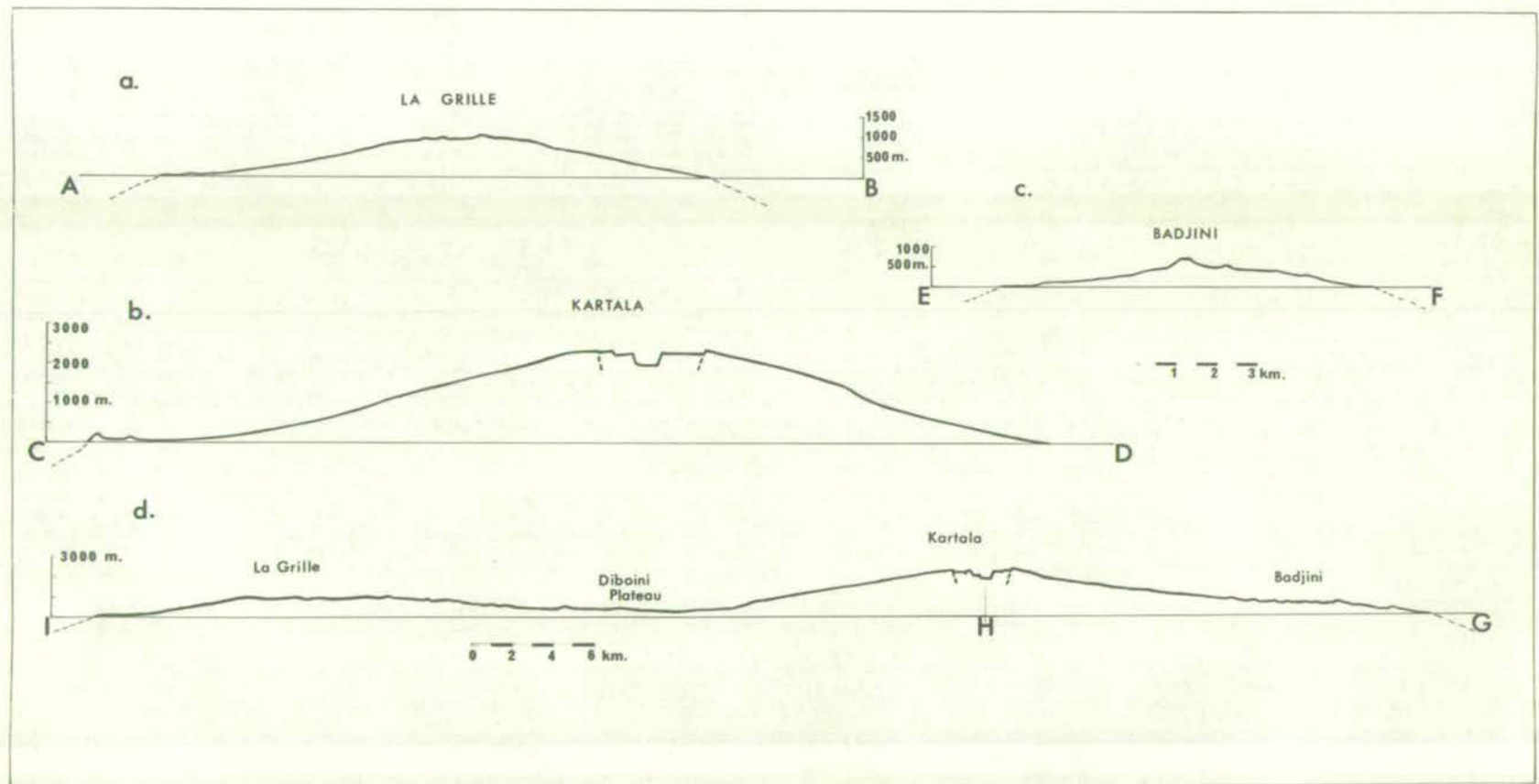
the eastern slopes are steeper, showing the concave form described
for the eastern slopes of La Grille (Fig. 4b).   The massif is capped
by a steeper dome, with average slopes of 24°, truncated by the
Kartala calderas.   De Saint Ours (1960) considered this dome to be
formed of interbedded lava flows and pyroclastic material, i.e. to
be a composite cone, but the caldera sections show that pyroclastic
rocks are rare.   Pyroclastic cones are far less common on Kartala
than La Grille.

2.2.5. The Badjini Peninsula

The Badjini Peninsula is a prominent extension of the Kartala
dome along the SE fissure zone (Fig. 3).   De Saint Ours considered
it to represent a separate volcanic center older than Kartala, but
no evidence was found for this in the present investigation.   It is
explicable as resulting from voluminous eruptions along the southeast
fissure zone of Kartala.   This is supported by Fig. 4d, which shows
no topographic break between Badjini and Kartala, as found for
example between Kartala and La Grille at the Diboini Plateau, and as
one would expect if there was a separate Badjini volcano.   There is
also a strong similarity between the east-west profiles of Kartala
(Fig. 4b) and Badjini (Fig. 4c) suggesting that they result from
similar volcanic and erosional activity.   Furthermore, the great
majority of lavas in this area are petrologically and chemically
similar to those of Kartala.   Nevertheless, several exposures on the
Badjini Peninsula are surrounded by deep soil, and consequently appear
to consist of lavas more ancient than any other Kartala lavas, and
possibly unconformably overlain by them.   It is useful to distinguish
these by the term "Badjini lavas".

2.3. GEOLOGICAL MAP OF GRANDE COMORE

The geological map of Grande Comore, like the topographic map described above, is based on the 1:50,000 scale topographic map of the island published by the Institute Geographique National of France. It was prepared from aerial photographs, the field observations described below, and the petrographic and chemical studies to be described in subsequent chapters.
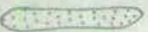
2.4. LAVA FLOWS

2.4.1. Sites of eruption

Where not obscured by soil or vegetation, the sites of lava eruption are commonly marked by breached cinder cones, which suggest that a gas phase separated from the magma preceding these eruptions. For some flows, e.g. the 1880 flow on the Badjini Peninsula near Nioumamilima (Fig. 5), these cones are aligned and coalesce, presumably defining the outcrop of fissures. Some flows, e.g. those of 1860 and 1918 (Fig. 5), emanate from fissures whose outcrop near the caldera is marked by a linear valley, with very minor pyroclastic material present. Still others, such as the 1859 and 1872 flows on the west coast (Fig. 5), have neither cones nor valleys marking the site of emission, but the alignment of their upper ends suggest that they were emitted from a single fissure. The fact that both Kartala and La Grille are elongated domes is taken as more general evidence for the dominance of fissure eruptions in their formation, at least in the later stages.

Fig. 5.

Geological map of Grande Comore

☀   Pyroclastic cones

◐   Craters

▱▱▱   Historic lava flows (with dates where known)

●   Analysed samples from La Grille

▲   "   "   "   Kartala

━ ━ ━   Approximate geochemical boundary between
              Kartala and La Grille

━ ─ ━   Fissures

‾‾‾‾ ---   Roads and footpaths

⬭   Coral reefs

LA
GRILLE

N

1859

HAHAIA
1872

1872

1859

1858

1904

ITSANDRA

MORONI

1860

1918

N'TSAOUENI

KARTALA

1862

1880

1857

1857

1 2 3 4 5 6 km
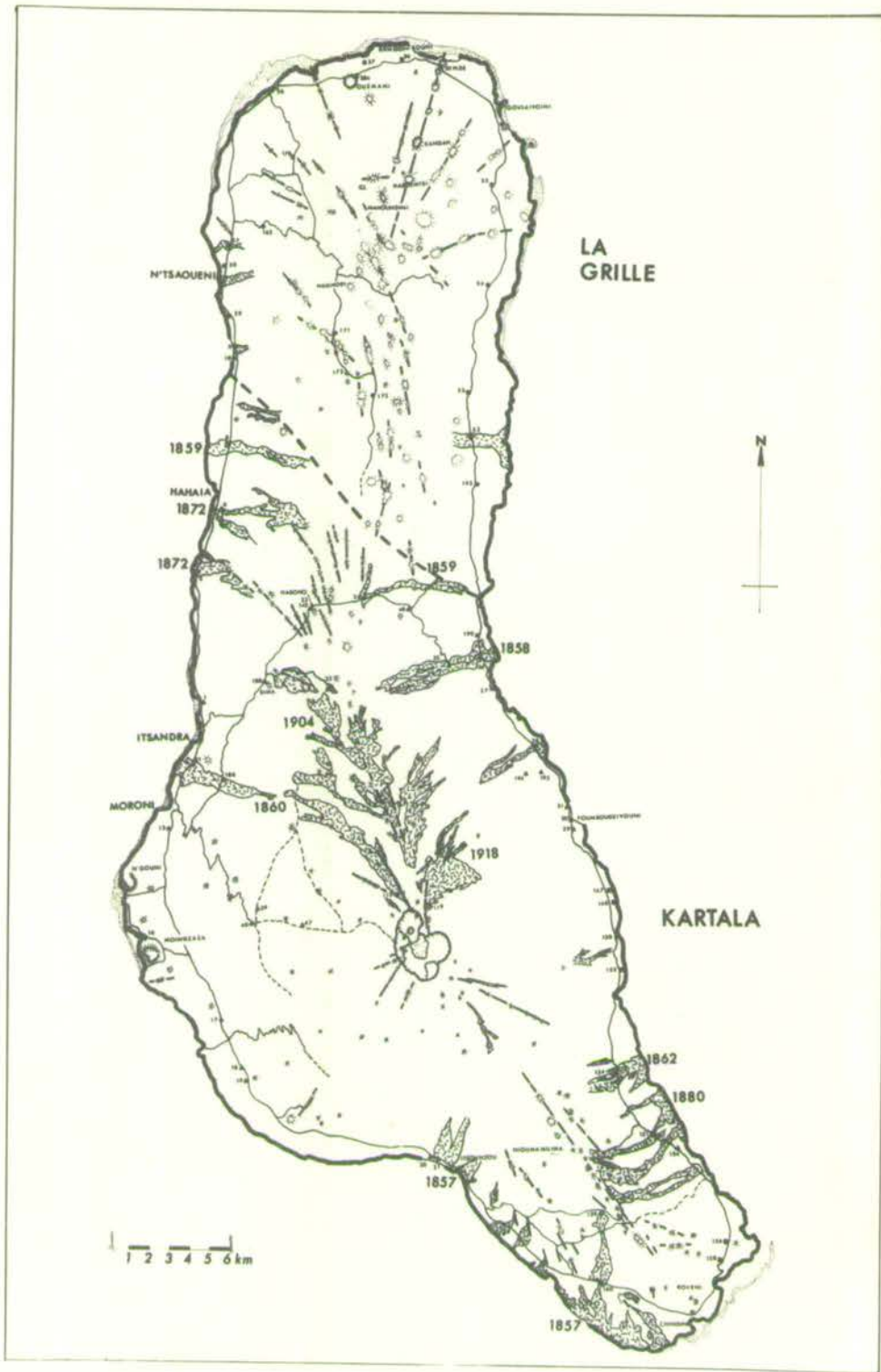
2.4.2. Dimensions of flows

The unvegetated lava flows, mostly dated as less than 150 years old, are clearly visible on aerial photographs, and so their lengths and widths can be accurately established. They show a range in length from 17 km (the 1860 Itsandra flow, Fig. 5) to less than 1 km (excluding possible submarine extensions). They generally increase in width downslope, to a maximum observed width of 6 km, but generally about 1 km wide.

The thicknesses of these lava flows are shown in numerous exposures provided by coastal cliff-sections, river channels, and caldera walls. There is no apparent difference in thickness between flows of Kartala or La Grille. Most are between one and three metres thick, and a typical coastal exposure is shown in Plate 1. The thickest coastal exposure observed was that of the feldspar-phyric flow near Foumboudzivouni. Its thickness was estimated at ten metres, but this may be excessive since the dip of separate units is highly variable and the true thickness may not have been measured. The horizontal flows exposed in caldera walls reach thicknesses up to 30 km, almost certainly a result of ponding within the caldera walls. The volume of lava produced in the average eruption is estimated at around $1 \cdot 5 \times 10^6 m^3$, less than a tenth of that for the average historic eruption in Hawaii (cf. Macdonald, 1967, Table 1).

2.4.3. Structures of flows

All uneroded lava flows observed on Grande Comore can be des-cribed as aa, rather than pahoehoe type, with their surfaces covered by a chaotic jumble of jagged, spinose blocks.

The centers of these flows are massive and often columnar-jointed the best examples of which are seen in the caldera walls, Plate 2. In some cases along the shore, the blocky surfaces have been removed by erosion, displaying small scale flow structures which could be described as pahoehoe.

Although lava tunnels do not appear characteristic for aa flows (cf. Macdonald, 1967), numerous examples can be found on Grande Comore (see Prosperi, 1957). One such tunnel was examined in the present study, on the west coast between Hahaia and N'Tsaoueni. The roadside entrance to this tunnel is about one metre in diameter and the tunnel is about four metres wide at the floor, two to three metres high in the center, with the roof curved down to the flat floor which is covered by fallen blocks. The tunnel extends for at least 200 meters, but its total length was not determined. Small hollow stalactites were collected from the roof, as well as a crust of calcite apparently resulting from groundwater deposition.

The lavas of Grande Comore are mostly dark grey with variable amounts of phenocrysts. The Kartala flows contain mostly phenocrysts of olivine and clinopyroxene, with rare plagioclase phenocrysts. The Foumboudzivouni plagioclase-phyric flow is particularly striking, showing, along with large clinopyroxene crystals, a range of sizes and orientations of plagioclase phenocrysts, from large (up to 2 cm) rosette-like clusters to the smaller flow-aligned laths,(plate 3). Only olivine phenocrysts are common in the lavas of La Grille, but rare clinopyroxenes can be seen.

Vesicularity of the lavas is highly variable, within flows as

well as between flows, and a quantitative estimate of vesicularity is given in Chapter 3 (Fig. 10). The type of vesicles varies from pipe vesicles, developed in the lower parts of flat-lying flows, to the cellular spatter which makes up most of the 1965 caldera flow.

2.5. HISTORIC VOLCANIC ACTIVITY

Both Kartala and La Grille volcanoes have been historically active, but the bulk of this activity has been confined to Kartala. The dates of flows shown on the map of Fig. 5 were taken from De Saint Ours (1960) and Lacroix (1938). Some undated lava flows have been mapped as "historic" (Fig. 5) because their complete lack of vegetation gives them a distinctly youthful appearance. However, one should make the reservation that a difference in climate, as well as age, controls the development of a vegetation cover, and lavas on the drier leeward parts of the island would take longer to become vegetated. The unvegetated "historic" flows of La Grille volcano are all undated, implying that they are appreciably older than those of Kartala.

The historic Kartala flows have been mostly erupted from fissures on the northern and southern rift zones of the dome, with no apparent correlation between geographic location and date of eruption (cf. Kilauea, Jagger, 1947). Since 1918 the activity has been confined to the Kartala caldera. The available descriptions of historic activity are given in Table 2, taken mostly from Van Padang (1963), and personal accounts by residents of Grande Comore.

Table 2

Historic volcanic activity on Grande Comore

Date	Effects	Type	Chemical Analysis of lava
May 1828	Eruption in parasitic crater		
1830	" " " "		
1848	Eruption in radial fissure with lava emission		
July 1855	Eruption in parasitic crater with normal explosions and lava emission		
1857	As above, along with caldera explosions	Strombolian	X
1858	As above, without caldera explosions	Strombolian	X
1859	As above	Strombolian	X
1860	Large lava flow from caldera		X
1862	Parasitic crater with lava emission	Strombolian	X
1865	Parasitic crater		
1872	Parasitic crater with much vapour and lava emission	Hawaiian	X
1876	As above		
1880	Eruption in radial fissure with vapour and lava emission	Strombolian	X
March 1883	Eruption in parasitic crater, with vapour and lava emission, arable land destroyed, and people killed (?)		
1884	Eruption in radial fissure, lava emission, arable land destroyed		
April - June 1903	Flank eruption at 1600 meters altitude; much suffocating gas, 17 people killed.		

Table 2 (Contd.)

Date	Effects	Type	Chemical Analysis of lava
Feb 25 to March 1904	Eruption in radial fissure with lava emission; arable land destroyed, people killed	Strombolian	X
Aug 11-26, 1918	Strong phreatic eruptions; large flank lava flow; Chagnoumeni pit crater formed	Vulcanian and Hawaiian	
Apr. 22, May 4, June 13-16, 1948	Great black clouds; strong tremors; eruption in lava lake; possible parasitic eruptions	Strombolian	
Feb. 1952	Explosions and vapour emission in caldera		
1953-1965	Fumarole activity		
July 1965	Lava and vapour emission from fissure on caldera floor; Brush fires started by bombs		X
Oct. 1967	Tremors, felt as far away as Anjouan		
Jan. 1968	Tremors, felt as far away as Moroni.		

2.6. PYROCLASTIC CONES

2.6.1. Introduction

Stearns and Vaksvik(1935) have subdivided the secondary cones of Oahu, Hawaii into three types, viz. lava, cinder, and tuff cones. Each of these has a characteristic profile, the latter two of which are reproduced in Fig. 6.   Although few secondary cones of Grande Comore have received detailed field study, it appears from the topographic maps and aerial photographs that they fall into one of these two categories, and assuming that these profiles are reliable indicators, the majority appear to be cinder cones.

2.6.2. Cinder Cones

Most cinder cones of Grande Comore are concentrated in the central parts of the island along the rift zones of each volcano. They are abundant on the crest of La Grille but rare on the higher parts of Kartala.   They are similar in profile and size to that shown in Fig. 6, and reach a maximum size of 600 metres diameter and 140 metres high.   Many are aligned along fissures (Plate 4).

The Haboho cinder cone, on the NW rift zone of Kartala volcano (see Fig. 5), was the best studied example in the present investigation.   It is composed entirely of black, glassy, highly vesicular (cellular) cinders and pumice, i.e. entirely magmatic ejecta.   It has been extensively quarried, and is consequently well exposed in a quarry section about ten metres high (Plate 5).   The material was deposited in distinct layers, dipping about 30°.   A thin soil zone about 50 cm from the top reflects a pause in activity before it completely ceased.   Two chemical analyses have been made of pumice
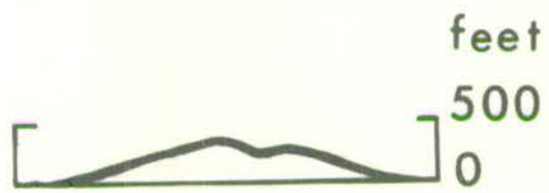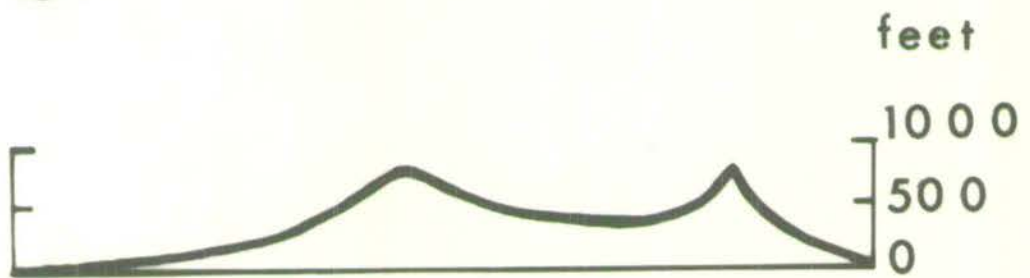
from different parts of this cone (23 and 142, Tables B-1 and C-1).

Weathering of the basaltic cinder causes a change in colour from black to yellow-brown, a good example of which is seen in the quarried cone near Sima (Plate 6). The layered cinder of this cone is cut by a sub-horizontal plagioclase-phyric dyke about one metre thick (Plate 6). This dyke has not undergone any weathering (see 188, Tables B-1 and C-1), and if its formation was contemporaneous with the cone, it indicates the much more rapid weathering of the cinders than the lava.

Some cinder cones are completely rounded in profile, with no central depression marking the vent, but rather a capping of cinders (Plate 7). However, most cones have a central depression, the walls of which are commonly breached, presumably by lava emission (Plate 8).

2.6.3. Tuff cones

As shown in profile b (Fig. 6), tuff cones are generally larger than cinder cones, and have large central flat-floored craters which have diameters of about half the total diameter (Stearns and Vaksvik, 1935). The tuff cones of Grande Comore, although similar in profile to those of Oahu, are generally smaller, on the average about one km in diameter as compared to two km diameter of those on Oahu. As on Oahu, most tuff cones on Grande Comore are found close to the seashore. If the Habointsi and Kandah cones on the northeast part of La Grille (Fig. 5) are tuff cones, as suggested by their size and form, they are exceptions to this general rule.

Two excellent examples of the Grande Comore tuff cones are N'Gouni and Moindzaza, found on the west coast just south of Moroni

(see Fig. 5).   The N'Gouni cone (Plate 9) is very similar in form to that of Koko Head, Oahu (Stearns and Vaksvik, 1935, Plate 1), but is slightly smaller, with a diameter of 1 km as compared to the 2 km of Koko Head.

Brief sampling of N'Gouni revealed very few lithic fragments, most samples obtained consisting entirely of olivine, clinopyroxene, and yellow-orange glass fragments.   The hand specimens are strikingly laminated, but no detailed study was made of dips of the bedding in this cone.   One hand specimen was studied petrographically and chemically (16, Tables B-1 and C-1).

The Goulaivoini tuff cone on the northeast coast of the island (Fig. 5), breached by marine erosion, shows the characteristic features of Hawaiian tuff cones, and differs from the Moindzaza cone in that lithic material is abundant.   Fragments of coral limestone, as well as the lava flows and the ultramafic inclusions which they contain, are found in the Goulaivoini cone, as well as further inland in the Dinde tuff cone (Fig. 5).

2.7. THE KARTALA CALDERA

2.7.1. Description of the caldera

The following summary is taken from the detailed description given by Strong and Jacquot (1969).

The main caldera is formed by the coalescence of at least five smaller calderas which have an average diameter of about 1500 metres (Fig. 7a).   These have combined to give the main caldera a roughly elliptical form, about 4 km by 3 km (Fig. 7a).   Superimposed on this elliptical form are the two sets of NNW- and N-trending regional

1860

1918

Chagnoumeni

1965

Chahale

N

500 M
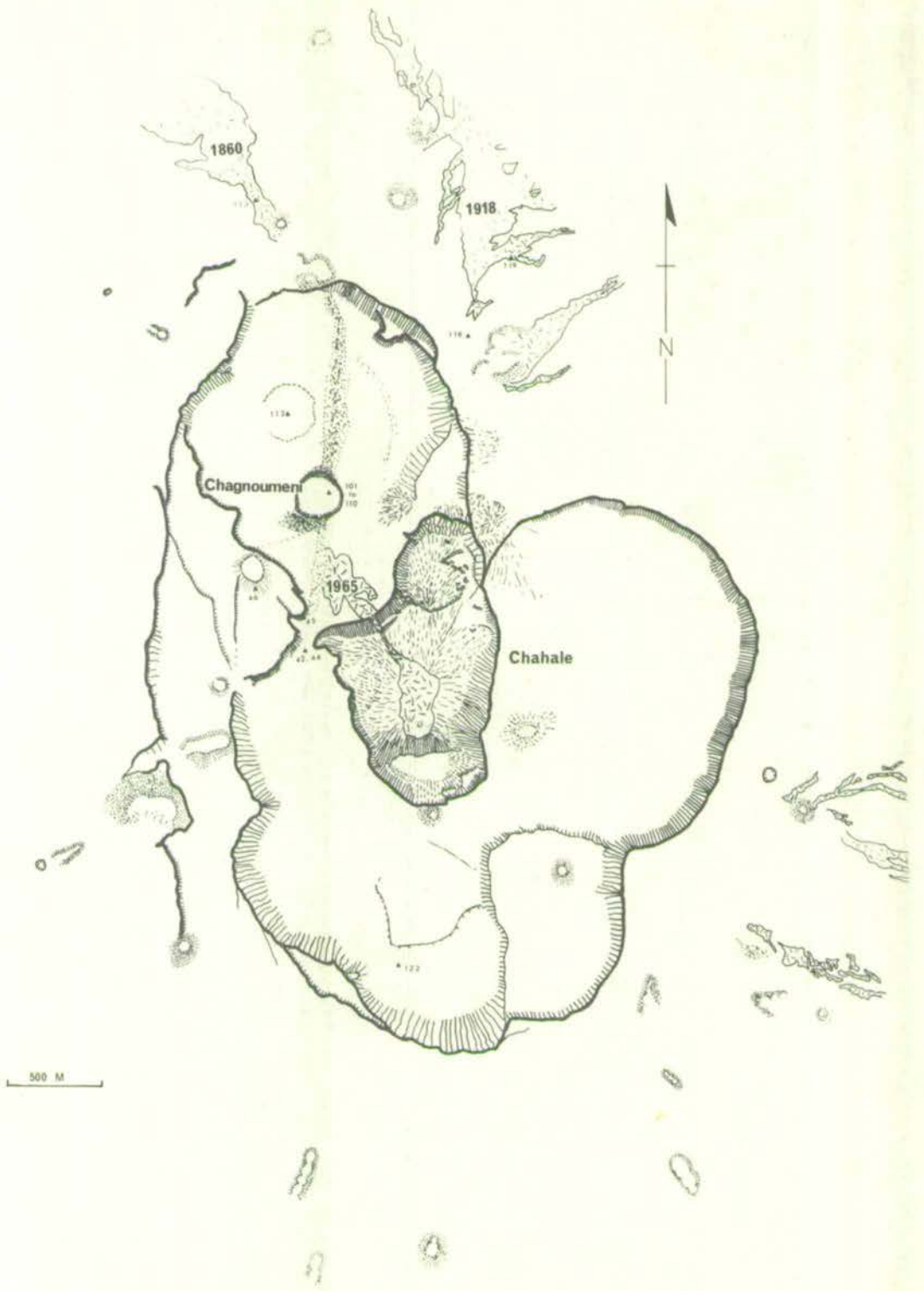
fissure systems, as well as local radial fissures. The caldera walls dip inwards from 90° to 70°, but only the vertical walls are unvegetated and uneroded (Plate 10).

The floor of the main caldera complex is broken by two pit craters (Fig. 7a, Plate 10). The southern pit crater, Chahale, is 1300 by 800 metres across and 300 metres deep. Chagnuomeni pit crater, about one km north of Chahale, is cylindrical in form, 250 metres in diameter and 30 metres deep. According to Lacroix (1938), Chagnuomeni was formed during the 1918 eruption.

The walls of these pit craters provide sections through some of the thick (up to 30 metres) horizontal lava flows which presumably ponded in the caldera (Plate 2). Chemical analyses of the bottom and centre of one of these flows are given in Table C-1 (101 and 102). Several thin vertical basaltic dykes cut these flows (Plate 11), and chemical analyses of these dykes are given in Table C-4 (105, 107, 110).

A straight, north-trending fissure zone runs through the central part of the northern half of the caldera floor (Fig. 7a), and it was from this fissure that the 1965 flow was emitted. This flow has been accurately surveyed by C. Jacquot, and its volume estimated at 1,500,000 cubic metres, similar to the average volume of flank eruptions. One specimen from the surface of this flow has been analysed (23, Tables B-1 and C-1).

Many angular blocks, almost certainly brought from depth during explosive activity, have been strewn over the caldera floor, especially around the Chahale pit crater. Many of these are of porphyritic ankaramitic basalt, while some are sufficiently coarse to be described

as dolerite and gabbro. It is uncertain whether these coarser-grained blocks were derived from thick lava flows or from intrusive bodies, but they have been listed as intrusive rocks for present purposes. Two chemical analyses of these are given in Table C-4 (42 and 44).

2.7.2. Formation of the caldera

Judging from the relative amounts of erosion and vegetation of the various fault scarps and walls of the caldera, the following sequence of events might be postulated. After completion of the Kartala dome, the stresses producing the regional north-south fissure systems still prevailed, facilitating graben-type collapse along fractures 1 and 2 (Fig. 7b). A gradual lessening of this regional stress, i.e. an effective increase of vertical stress, resulted in the development of radial and circular fractures. Subsequent eruptions emptied the underlying magma chambers, removing support, and causing collapse along the circular fractures, resulting in formation of the calderas in the sequence a to e (Fig. 7b). During the flank eruption of 1918, the calderas h (Chagnuomeni pit crater) and g were formed by collapse and explosion respectively.

As these regional fissures, radial fissures, grabens, and circular fractures represent a striking combination of the features discussed by Robson and Barr (1964), it is instructive to try and interpret the stress system in the light of their theoretical predictions. In applying these predictions to the Kartala caldera we might best assume that throughout the development of these features there was a vertical stress (p_{max}) which was greater than either of

Fig. 7b.

Schematic outline of the separate collapse calderas
(a to h, in order of formation) and graben-type
fractures (1 to 5, in order of formation) which
combined to produce the Kartala caldera.
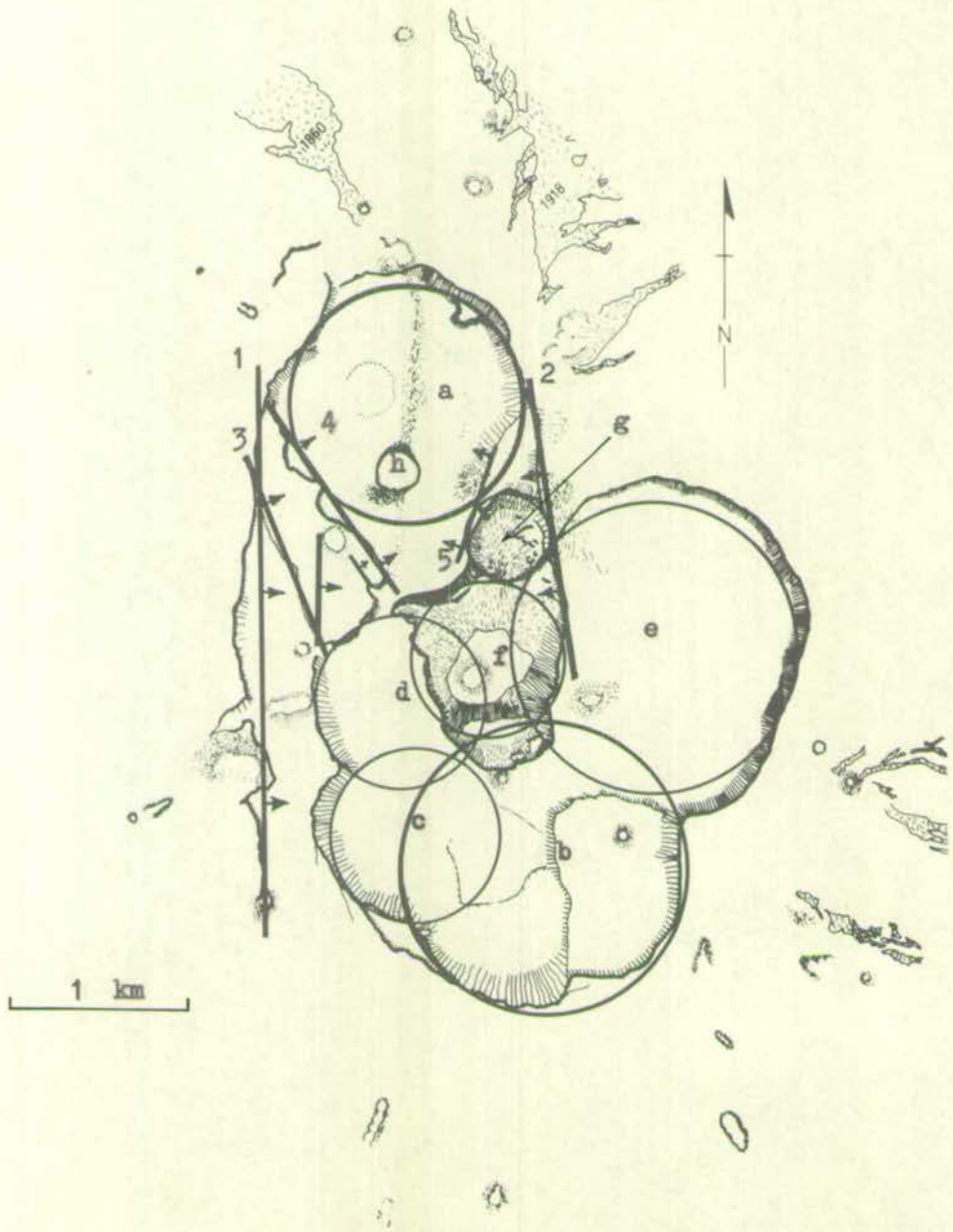
two horizontal stresses (p_{min} and p_{int}), a reasonable assumption
since a very considerable force is needed to transport the magma
upward to the surface in the first place. We must then assume that
at the beginning of volcanism via the regional fissures p_{int} was
much greater than p_{min}; this also seems perfectly reasonable because
otherwise the fissures would not have formed at all. As the Kartala
shield volcano grew, p_{int} appears to have approached p_{min} in value,
which could have taken place by an actual equalization of these regional
stresses, or more probably by a local equalization due to increasing
difficulty in transmitting stress through the growing pile of lava.
Associated with this equalization of stresses was an increasing
tendency for central type eruptions to take place, resulting in build-
up of the dome. After formation of the dome, however, there must
have remained sufficient difference in these horizontal stresses
to cause the initial graben-type collapse postulated above. When
the stresses were more or less equalized, the small circular calderas
and radial fractures were formed. Thus, using reasonable assumptions
about the stress environment, the theoretical considerations of
Robson and Barr (1964) can be used to explain the observed features.
Using these same assumptions, a more detailed application of their
predictions can be made to try and deduce something about the deeper
structure of the volcano.

Robson and Barr (1964, pp. 326-327) consider that when p_{max} is
vertical and applied at a depth greater than 4·7 km, and $p_{int} = p_{min}$,
shear failure should occur in the form of inward-dipping fractures,
with the resultant caldera about 4 km in diameter and increasing in

diameter with greater depth of the magma chamber. The walls of Kartala caldera appear to fit this requirement, and some of the widespread radial fractures (e.g. see Fig. 5) also appear to require a very deep source of upward pressure. However, the Kartala caldera results from the clustering together of individual smaller calderas which, according to the theories of Robson and Barr, are too small to have formed by shear failure from a deep source of upward stress.

The other possibility discussed by Robson and Barr (1964, pp. 326-327) for shallow magma chambers, i.e. at a depth less than 4·7 km, with p_{max} vertical and $p_{int}=p_{min}$, shows that the stress can be relieved by a single arcuate tension crack dipping outwards at an angle greater than 60°, or by vertical tension cracks radiating from the centre of stress. In the former case the arcuate cracks would form segments of a circle which form a ring dyke. As described above, the walls of the small circular calderas that are visible at the surface are vertical in the two cases where very recent and uneroded, and therefore possibly have been so in all cases. They may therefore be the surface expression of ring dyke type of fractures expected from shallow magma chambers. Although Robson and Barr do not make any statement concerning the relationship between diameter and depth of this fracture type (except that the magma chamber is less than 4·7 km deep), it appears that the Kartala caldera is most likely to have resulted from these ring-dyke type of tensional fractures rather than shear failure along inward-dipping cone-sheet type of fractures.

2.8 EROSIONAL FEATURES

2.8.1. River erosion

As noted above, the whole island of Grande Comore is asymmetrical in east-west profile, with the concave eastern slopes steeper than those of the west.   Because the eastern slopes face the prevailing winds, precipitation and run-off is far higher on the east coast than the west.   Thus, the asymmetry apparently results from different climatic conditions on opposite sides of the island.   Nevertheless, the relative insignificance of erosion in determining the gross topography of Grande Comore must be a reflection of the high productivity of both volcanoes.   It is possible, however, that long periods of dormancy have occurred in the past and that eroded landscapes have subsequently been obliterated by renewed volcanism.   This has been suggested by De Saint Ours (1960) for the Badjini Peninsula, but no evidence was found in the present study to support such an hypothesis.

2.8.2. Marine erosion

Surrounding most of Grande Comore is a narrow, gently sloping plain which is separated from the central parts of the island by an abrupt change in slope (Fig. 3), occurring at about 25 to 100 metres above sea-level.   This plain, varying in width from 0 to 3 km, is interpreted by the present writer as a wave-cut platform resulting from a former period of relatively higher sea level.   The change in slope is thought to represent ancient sea cliffs, now mostly covered by younger lava flows.   This platform is narrowest near the main rift zones (Fig. 3), presumably due to higher volcanic activity in these areas.

The changes in sea-level are thought to be eustatic rather than due to uplift of Grande Comore, since it seems unlikely that the whole island could undergo an equal amount of uplift. Furthermore, similar features are seen on the other Comores islands, as well as other islands of the Indian Ocean (cf. Gardiner, 1936; Upton and Wadsworth, 1966; Veeh, 1966).

2.8.3. Reefs

As shown in Fig. 3, fringing coral reefs are discontinuously developed around Grande Comore, and they are lacking in areas of higher volcanic activity, coinciding with the narrowest parts of the wave-cut platform (Fig. 3). The narrowness and discontinuity of these reefs compared with those of Mayotte serves to emphasize the great difference in age between these two islands.

2.9. SUMMARY

The island of Grande Comore is made up of two shield volcanoes, La Grille in the north and Kartala in the south, separated from one another by a zone of lava interdigitation referred to as the Diboini Plateau. Both volcanoes have been historically active, but since 1918 the activity has been confined to the caldera complex atop Kartala. The slopes of Kartala (at 15°) are steeper than those of La Grille (at 7°), and the whole island has an asymmetrical east-west profile due to the prevailing easterly winds.

Pyroclastic cones are common on each volcano, but are much more abundant on La Grille than on Kartala. Their alignment in specific zones indicates that fissure eruptions have been important in the formation of each volcano.

The lavas of Kartala contain phenocrysts of olivine, clinopyroxene, and plagioclase, whereas only olivine and rare clinopyroxene phenocrysts are found in those of La Grille.

3. PETROGRAPHY OF THE LAVAS

3.1. INTRODUCTION

Both Lacroix (1922) and De Saint Ours (1960) indicated that
all lavas on Grande Comore are basaltic, but they did not recognize
any differences between the lavas of Kartala and La Grille.   Thus,
they described basalt, "andesitic basalt", "labradoritic basalt",
limburgite, "basanitic ankaratrite", ankaramite, and oceanite, but
attached no significance to the geographic distribution of any rock
type.   The names "andesitic basalt" and "labradoritic basalt" have
little relevance to the present study, and the term "ankaratrite" was
misused by these writers (as no biotite-bearing rocks were found).
Neither is the term limburgite used in the present rock classification,
although it might properly be applied to some of the glassy lavas of
La Grille.

3.2. LAVAS

3.2.1. Classification of the lavas

The undersaturated basaltic rocks have in the past been given
many poorly-defined, redundant, and often inconsistent names, making
it difficult to classify any but the most distinctive of rock types.
This situation is aggravated by the variety of criteria used in such
classifications (e.g. modal composition, modal feldspar composition,
normative composition, normative feldspar composition, differentiation
index), a point discussed in some detail by Coombs and Wilkinson
(1969).   This difficulty is now particularly unfortunate because there

Fig. 8.

Projection of lava norms from plagioclase onto the
plane nepheline-diopside-forsterite. (mol. %)

    ○   = Kartala

    ●   = La Grille
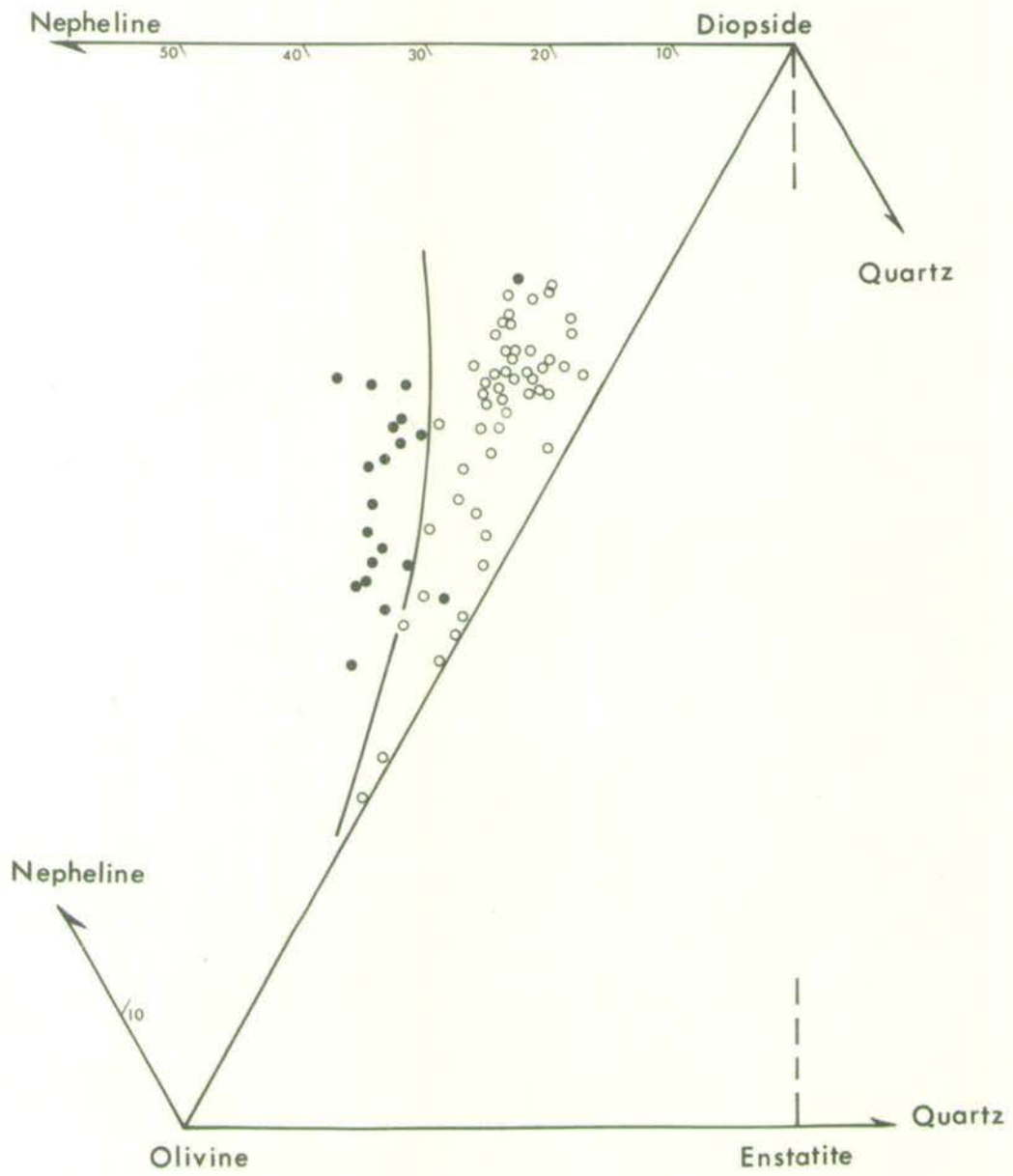
appears to be some divergence between field geologists and experimental petrologists, or even amongst experimental petrologists, and the same term may refer to different rocks when used by different workers. For example, "nephelinite" is used differently by Yoder and Tilley (1962) and Green (1969), although each paper seems to refer to rocks described as "nepheline basalt" by Turner and Verhoogan (1960), and neither uses "nephelinite" as defined by Johannsen (1938).

The objectives of the present classification are to (1) outline the differences between the lavas of Kartala and those of La Grille, and (2) provide a simple descriptive terminology for the rocks within each group. As there is a significant difference in normative nepheline content between each group (Table 3), the first of these objectives can be achieved on this normative basis. Thus, Fig. 8 shows that the La Grille lavas may be termed a basanitic group and an alkali basaltic group, as suggested by Coombs (1963).

The second objective is met on the basis of petrographic criteria alone, and the definitions of rock terms are given in Table 3. These terms are consistent with general usage (e.g. Lacroix, 1922; Macdonald, 1949; Yoder and Tilley, 1962), but the quantitative distinctions used for Kartala lavas are unique to the present study. Detailed petrographic descriptions of each analysed specimen are given in Appendix B, and representative photomicrographs in Plates 12 to 18.

Table 3

Classification of the lavas

Kartala (3·7% ne)		La Grille (11·5% ne)	
Rock name	Features	Rock name	Features
Alkali basalt (Plate 12)	less than 5% mafic pheno-crysts	Basanite (Plate 17)	Variable amounts of olivine ± augite phenocrysts, in groundmass of olivine, augite, plagioclase, opaque oxides, nepheline ± glass
Alkali olivine basalt (Plate 13)	5 to 15% mafic pheno-crysts		
Oceanite (Plate 14)	greater than 15% mafic pheno-crysts, with olivine dominant over augite	Nepheline basalt (Plate 18)	Similar to basanite, except that modal plagioclase is absent
Ankaramite (Plate 15)	greater than 15% mafic pheno-crysts, with augite dominant over olivine		
Feldspar-phyric basalt (Plate 16)	basalts with feldspar pheno-crysts		

3.2.2. Petrographic contrasts between Kartala and La Grille lavas

In addition to the chemical distinction between the lavas of each volcano there are consistent petrographic differences which should be emphasized from Tables B-1 and B-2.

1. Olivine, augite, and plagioclase are found as phenocrysts in Kart-ala lavas; the phenocryst assemblage in La Grille lavas is

commonly olivine alone though very rarely the assemblage olivine + minor clinopyroxene is found.

2. Plagioclase is a typical groundmass phase in the Kartala lavas; it is absent or accompanied by nepheline in La Grille lavas.

3. The analysed Kartala lavas show no sign of alteration; some lavas of La Grille contain slightly iddingsitized olivines.

4. Olivine phenocrysts in the Kartala lavas are mostly euhedral, with only minor signs of resorption or skeletal character (Plate 14). Those of La Grille lavas occur as three distinct types, often in the same rock (Plates 17, 18):

   a) euhedral crystals, apparently crystallized in equilibrium with the host lava;

   b) skeletal crystals, presumably formed during quenching of the magma;

   c) fragmented and resorbed crystals with deformation lamellae, probably derived from disaggregated ultramafic inclusions.

5. Orthopyroxene and translucent spinel crystals occur in the La Grille lavas, and probably these also result from disaggregation of ultramafic inclusions. The orthopyroxenes are surrounded by polysynthetically twinned clinopyroxene (Plate 19), presumably grown as a product of reaction between the orthopyroxene and the basanitic magma. Comparable xenocrysts are, so far as is known, wholly absent from the Kartala lavas.

6. Quartz grains, also surrounded by clinopyroxene reaction rims (Plate 20), have been found in two samples of the La Grille lavas, but not in any from Kartala.

A more quantitative indication of differences between the
Kartala alkali basalts and La Grille basanites can be obtained from
Fig. 9, which shows histograms of their respective phenocryst volumes.
Olivine phenocrysts are relatively abundant in the La Grille lavas,
accompanied, if at all, by scarce augite phenocrysts.   By contrast
olivine phenocrysts are invariably accompanied by substantial amounts
of augite phenocrysts in the Kartala lavas, occasionally with an
abundance of plagioclase phenocrysts.   It should also be noted that
the distribution of La Grille phenocrysts is more normal (i.e. gaussian)
than that of Kartala.

Figure 10 shows that there is no significant difference in the
degree of vesicularity of either group, at least not as indicated by
modal analysis.

3.2.3. Badjini lavas

The Badjini lavas (Table B-3) show petrographic affinities with
both those of Kartala and La Grille.   Specimens 156 and 158 are
similar to the La Grille basanites, while 132, 146, and 147 are more
similar to the Kartala alkali basalts.

3.3. OTHER ROCKS OF GRANDE COMORE

3.3.1. Pyroclastic rocks

Two types of pyroclastic rock have been chemically analysed
and studied petrographically.

Basaltic cinder (samples 23, 46, 122 and 142, Table B-1)
consists of cellular basaltic glass, with traces of olivine and/or
augite skeletal microphenocrysts.   This material is

Fig. 9.

Histograms of modal phenocryst contents
in lavas of La Grille (a) and Kartala (b).

■   Olivine

▨   Augite

▦   Plagioclase

☐   Aphyric
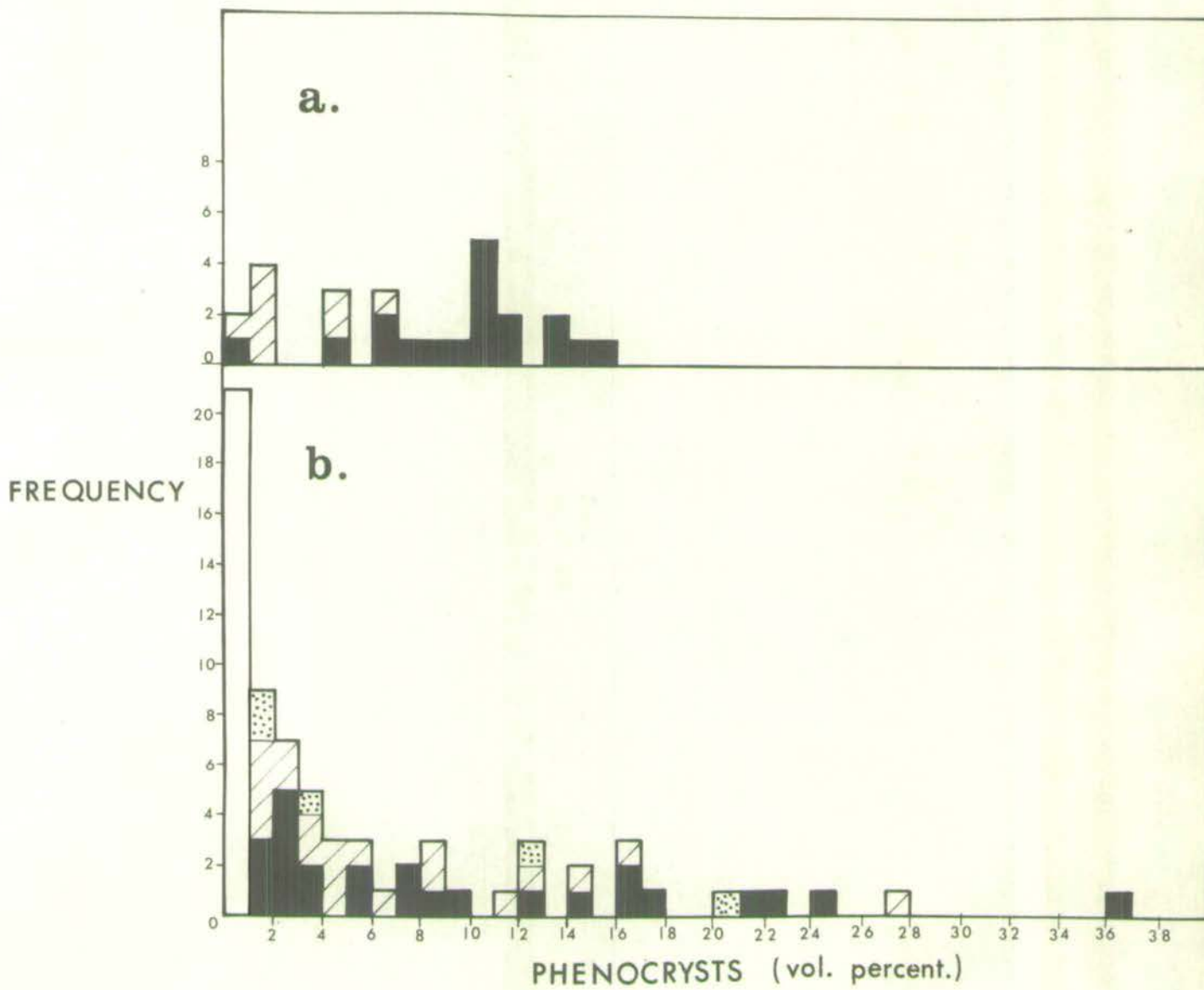
similar, in both microphenocrysts and refractive indices of the glass, to the glassy chilled margins and flow tops of lava flows (c.f. samples 6, 103, 109, and 123, Table B-1).

Finely bedded and friable vitric crystal tuff from the Moindzaza tuff cone consists of fragmented olivine and clinopyroxene phenocrysts in a clear yellow glass. Variation in proportions of these phases (see Table B-3, No. 16) is responsible for the striking fine-scale lamination in this rock.

The pyroclastic cones of La Grille volcano generally show some alteration due to weathering, and consequently were not sampled as thoroughly as those of Kartala, and none at all were chemically analysed. The one reasonably fresh cinder cone, Hamhori (Fig. 5), is formed of brown vesicular (cellular) glass with less than 1% olivine microphenocrysts, and some small (less than 1 mm) gabbroic inclusions. As described in Chapter 2, the tuff cones contain blocks of basaltic, ultramafic, and gabbroic rocks, similar to those described below, as well as limestone blocks. The limestone blocks of Dinde tuff cone (Fig. 5) consist of poorly sorted fragments of bryozoa, foraminifera, gastropods, echinoderms, ostracods, abundant green algae, and lava, set in a finer carbonate matrix. It may be described as an algal or foraminiferal biomicrite, probably deposited in a lagoonal environment (Dr. T.P. Scoffin, pers. comm.).

3.3.2. Intrusive rocks

The only unquestionably intrusive rocks found on Grande Comore are the thin basaltic dykes cutting the lava flows exposed in the walls of the Chagnuomeni pit crater on Kartala (Plate 11). These

FREQUENCY

VESICLES (vol. percent.)
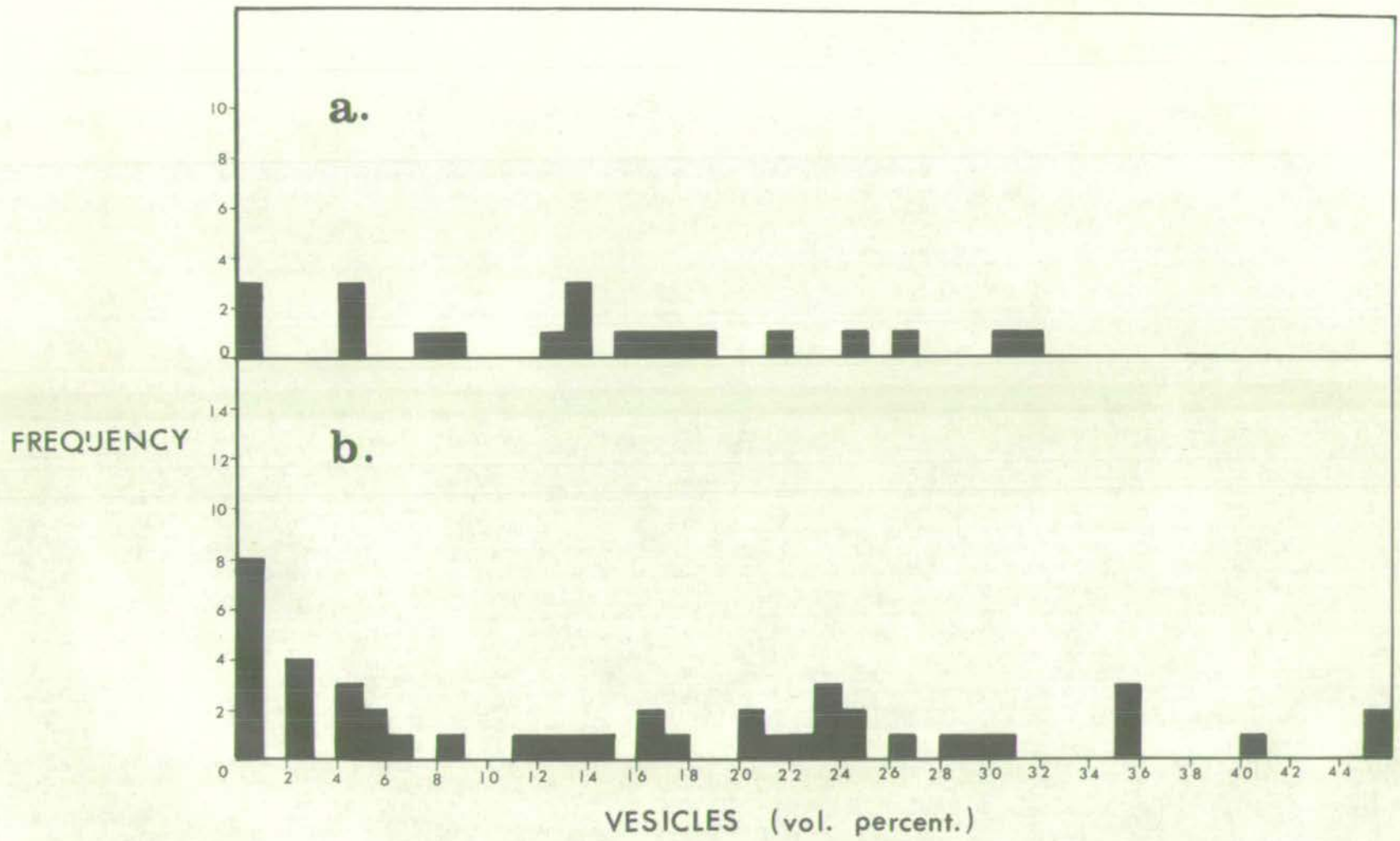
rocks (samples 105, 107, and 110, Table B-4) are petrographically similar to the alkali basalt flows. Blocks of variolitic gabbro and layered dolerite (samples 42 and 44, Table B-4) are strewn over the caldera floor near Chahale pit crater. Although it is questionable whether these rocks are truly intrusive, possibly being derived from the central parts of thick caldera-filling flows, they are classed as such in this study because of their distinctive gabbroic texture.

A single gabbroic inclusion, about 3 cm in diameter, was found in a historic oceanite flow near Itsoundzou, on the southwest slopes of Kartala. This was not examined in thin section, but it appears to be much richer in mafic minerals than those blocks found in the caldera.

No intrusive rocks were found in situ on La Grille, but one very coarse-grained inclusion was found in lava fragments from the Dinde tuff cone. This differs from the gabbroic blocks of Kartala, however, in that it consists of euhedral olivine phenocrysts set in a holocrystalline fluidal groundmass of plagioclase, titanaugite, magnetite, and calcite, with minor brown alteration along the cracks and vesicles. These features suggest that this specimen was in fact derived from a coarse-grained lava flow.

3.3.3. Ultramafic inclusions

Ultramafic inclusions were found in the lavas of Kartala in only two locations, although searched for throughout the field studies. A specimen of only one of these could be obtained, and it was too small for reliable separation and chemical analysis. However, thin sections

show it to be dunitic, consisting entirely of equigranular olivine crystals.

In contrast, ultramafic inclusions are common in the lava flows and pyroclastic cones sampled on La Grille, and one can see from Table B-2 that these occur in eleven of the nineteen samples analysed.   In one particular flow, at Goulaivoini (Fig. 5), they make up possibly 20% of the rock, and an inclusion-free hand specimen is difficult to obtain.   Wehrlite is the most abundant rock type, but dunite and lherzolite are also found.   Along with the variable amounts of olivine, pale green diopside, and orthopyroxene, these inclusions generally contain minor amounts of reddish-brown spinel, some in symplectic intergrowth with orthopyroxene·(Plate 23).   Granular aggregates and veins of euhedral olivine and diopside are commonly seen along the margins and cleavage of the orthopyroxene crystals. At contacts with the surrounding lava, orthopyroxenes of the inclusions are surrounded by polysynthetically twinned clinopyroxene, a feature noted above for isolated orthopyroxene crystals.

3.3.4. Sandstone inclusions

Sandstone inclusions were found in the lavas on the western slopes of La Grille, and also in the basanitic inclusions of the Dinde tuff cone (Plate 20), but none have been detected in the lavas of Kartala.   They are white, friable, and always less than 1 cm. across. Although they were too small for thin-sectioning, quartz, microcline, and albite were identified by X-ray diffraction and confirmed by oil immersion techniques.   These inclusions may thus be described as arkosic, similar to those of Moheli and Anjouan.

3.4. SUMMARY

The lavas of each volcano, Kartala and La Grille, are distinct and conveniently separable on the basis of normative nepheline content. The Kartala lavas are classed as alkali basaltic, with an average of 3·7% normative nepheline. The La Grille lavas are classed as basanitic, with an average of 11·5% normative nepheline.

The Kartala lavas contain olivine, clinopyroxene, and in some instances plagioclase, as phenocrysts. The La Grille lavas invariably contain olivine phenocrysts, and rarely subordinate amounts of titanaugite as phenocrysts.

The Badjini lavas are petrographically allied to both the Kartala and La Grille lavas.

Ultramafic inclusions are rare in Kartala and Badjini lavas, but are abundant in some of those of La Grille. Sandstone inclusions are found only in the La Grille lavas.

4. MINERALOGY

4.1. MINERALOGY OF THE KARTALA LAVAS

4.1.1. Introduction

The compositions of fifteen olivines, twelve clinopyroxenes, and fifteen feldspars have been estimated, using optical, X-ray diffraction, X-ray fluorescence, and electron microprobe methods, as described in Appendix A. Because of the large amounts of data involved, the microprobe analyses are only summarized in this chapter, and are presented in detail in Appendix E.

4.1.2. Olivine

The olivine phenocrysts of Kartala, with the exception of those in the feldspar-phyric basalt (No. 30), are within the composition limits Fo-80 to Fo-87 (Tables 4 and 5). In contrast, olivine from the alkali dolerite (No. 44) is more fayalitic, and zoned from Fo-57 to Fo-32, although the bulk chemistry of the rock is similar to that of the lavas. The groundmass olivines are more fayalitic than the phenocrysts, ranging from Fo-80 to Fo-65 in the basalts and Fo-38 in the alkali dolerite. Neither the groundmass nor phenocryst olivines show any obvious correlation with the bulk composition of their host rocks.

4.1.3. Clinopyroxene

All analysed clinopyroxenes in the lavas can be described as augites, with an average composition of $Ca_{42}Mg_{48}Fe_{10}$ indicated by X-ray fluorescence analysis of separated phenocrysts (Table 6).

Table 4.

Chemical composition of Kartala olivines

wt.%	18	19	21
SiO_2	39·08	39·77	39·27
TiO_2	·07	·07	·08
Al_2O_3	·48	·53	·48
Fe_2O_3	1·69	1·16	2·12
Cr_2O_3	·20	·20	·15
FeO	13·04	13·21	13·48
MnO	·22	·22	·24
MgO	43·72	44·41	43·18
NiO	·22	·23	·21
CaO	·48	·57	·48
Na_2O	·01	·00	·01
K_2O	·01	·01	·00
H_2O	·21	·10	·09
P_2O_5	·02	·02	·01
Total	99·45	100·72	99·79

ppm			
Cu	22	23	33
Zn	102	103	117
Zr	17	17	17
Fo mol %	84·4	84·7	83·3

Table 5.

Composition of Kartala olivines

Rock No.	Separated Bulk Phenocrysts XRF	XRD	Microprobe Analyses Phenocrysts Core	RIM	Ground-Mass	Normative
1	-	87	86·4	83·9	64·5	73
2	-	86	86·0	77·3	70·0	-
3	-	86	-	-	-	-
8	-	84	-	-	-	72
18	84·4	84	-	-	-	83
19*	84·7	84	-	-	-	82
21	83·3	-	-	-	-	72
22	-	87	-	-	-	67
26	-	-	80·0	80·9	77·7	71
31	-	-	82·8	80·7	80·4	81
41	-	81	84·7	81·5	-	75
Mean	84·1	85	84·2	80·8	73·2	70**
16	-	87	-	-	-	90
30	-	-	69·8	66·2	66·1	67
44	-	-	57·5	31·9	38·4	59

* $\beta_{R.I.} \implies Fo ·84$

** Normative mean includes all Kartala lavas.

All data expressed in mol % Fo.

XRF = X-ray fluorescence

XRD = X-ray diffraction

Table 6

X-ray fluorescence analysis of Kartala clinopyroxenes

Wt.%	1	13	18	21	23	30	31	42
SiO_2	51·19	50·84	50·87	50·46	49·41	48·41	51·18	44·99
TiO_2	1·08	0·88	0·71	0·76	1·11	2·24	0·99	3·96
Cr_2O_3	0·27	0·44	0·36	0·38	0·41	0·05	0·46	-
Al_2O_3	4·68	3·99	2·92	3·67	4·42	6·45	4·47	4·89
Fe_2O_3	0·47	1·30	0·53	0·92	0·60	2·30	0·07	2·21
FeO	5·55	3·85	5·58	4·92	6·20	5·82	5·47	14·70
MnO	0·11	0·10	0·11	0·10	0·11	0·15	0·07	0·18
MgO	15·49	15·70	19·96	17·41	16·50	12·31	15·64	10·02
CaO	20·81	21·63	19·49	20·07	19·91	21·03	21·76	17·62
Na_2O	0·55	0·34	0·26	0·49	0·45	0·61	0·38	0·97
K_2O	0·11	0·02	0·01	0·03	0·04	0·05	0·04	0·32
P_2O_5	0·11	0·10	0·08	0·08	0·13	0·10	0·09	0·37
H_2O	0·15	0·09	0·13	0·20	0·14	0·14	0·20	0·34
Total	99·77	99·28	101·01	99·49	100·16	99·66	101·42	100·57

[Contd.

Table 6 [Contd.]

Wt.%	1	13	18	21	23	30	31	42
Or	0·65	0·12	0·06	0·18	0·24	0·30	0·24	1·89
Ab	4·35	2·91	2·19	4·10	2·61	3·21	1·72	3·69
An	9·96	9·42	6·74	7·81	10·03	14·79	10·36	8·02
Ne	0·16	-	-	0·05	0·67	1·07	0·81	2·44
Di	73·39	77·68	70·43	73·04	70·75	70·81	76·99	62·94
Hy	-	1·57	1·88	-	-	-	-	-
Ol	8·50	4·46	16·41	11·82	12·37	1·95	7·77	9·45
Mt	0·68	1·91	0·76	1·35	0·88	3·35	0·01	3·20
Ilm	2·05	1·69	1·34	1·46	2·13	4·28	1·88	7·50
Ap	0·26	0·24	0·19	0·19	0·31	0·24	0·21	0·87
ppm								
Cu	18	13	16	48	27	10	22	83
Sr	74	50	40	92	97	201	53	109
Ba	45	72	50	-	50	100	50	40
Zn	44	36	45	51	45	45	41	103
Zr	67	44	35	40	62	227	55	226
Cr	1850	3020	2430	2610	2820	350	3140	20
Ni	360	200	630	390	245	80	240	22
Ca	43·79	45·51	37·29	40·96	41·20	47·24	45·32	47·62
Mg	46·15	46·24	53·48	49·77	47·80	38·69	45·60	27·00
ΣFe^{*}	10·05	8·38	9·22	9·27	11·00	14·07	9·08	25·38

$^{*}\Sigma Fe = Fe^{2+} + Fe^{3+} + Mn.$

The gabbroic augite (No. 42) is richer in iron, at $Ca_{48}Mg_{27}Fe_{25}$, and that of the feldspar-phyric basalt (No. 30) lies between these extremes at $Ca_{47}Mg_{39}Fe_{14}$. A plot of these compositions in the "pyroxene quadrilateral" (i.e. the mol. proportions of $Ca-Mg-Fe^{++}$) shows them to be less calcic than the augites from other alkaline basaltic magmas (Fig. 11a). This almost certainly results from contamination with olivine, which is also suggested by the high Ni concentrations and the substantial content of normative ol (Table 6).

The electron microprobe data for Kartala augites (Table 7) have been selected from the original data (Appendix E) to show the most iron-poor cores and iron-rich rims of phenocrysts and the most iron-rich groundmass compositions. The average phenocryst composition calculated from these data, $Ca_{45}Mg_{46}Fe_9$, is more diopsidic than that indicated by X-ray fluorescence analyses, further supporting the suggestion that the latter may reflect slight olivine contamination. There is a general trend of iron-enrichment from the cores to rims of phenocrysts which continues into the groundmass augites (Fig. 11b). The doleritic augite (No. 44) appears to resemble tholeiitic augites in its low calcium content (Fig. 11b), although the bulk rock contains 6% normative nepheline.

The composition of Kartala augites, like that of the olivines, shows no apparent correlation with bulk rock composition, implying a lack of equilibrium between crystals and melt, although only very minor resorption textures are seen in thin-section (Chapter 3). To obtain some idea of the relations between the minerals themselves, they have been plotted in the pyroxene quadrilateral, with tie-lines

Table 7

Electron microprobe analysis of Kartala augites

	CORE			RIM			GROUNDMASS		
	Ca	Mg	ΣFe	Ca	Mg	ΣFe	Ca	Mg	ΣFe
1	44·4	48·9	6·7	45·4	41·8	12·8	46·1	41·4	12·5
2	44·4	48·9	6·7	44·8	44·8	10·4	52·8	26·4	20·6
26	47·1	44·7	8·2	46·5	44·1	9·5	44·2	44·2	13·5
*30	47·5	42·6	10·0	44·4	42·1	13·5	48·3	38·0	13·8
31	45·4	46·9	7·7	44·5	46·0	9·6	43·7	47·0	8·3
41	48·3	45·4	5·9	43·0	47·7	9·3	42·4	45·8	11·8
*44	40·3	50·7	9·0	36·3	43·7	20·0	-	-	-
Mean	45·9	47·0	7·1	44·8	44·9	10·3	45·8	41·0	13·2

ΣFe = Fe^{+2} + Fe^{+3} + Mn^{+2}

* excluded from calculation of the mean.

Fig. 11.

Plot of Ca:Mg: ΣFe ratios of Kartala clinopyroxenes
(ΣFe = Fe^{+2} + Fe^{+3} + Mn)

    a. X-ray fluorescence analyses

        ● = data
        1 = Black Jack sill
        2 = Garbh Eilean sill
        3 = Skaergard intrusion

    b. Electron microprobe analyses

       ▼ = core

       ▽ = groundmass

(cross-hatched area in insert shows area of main diagram)
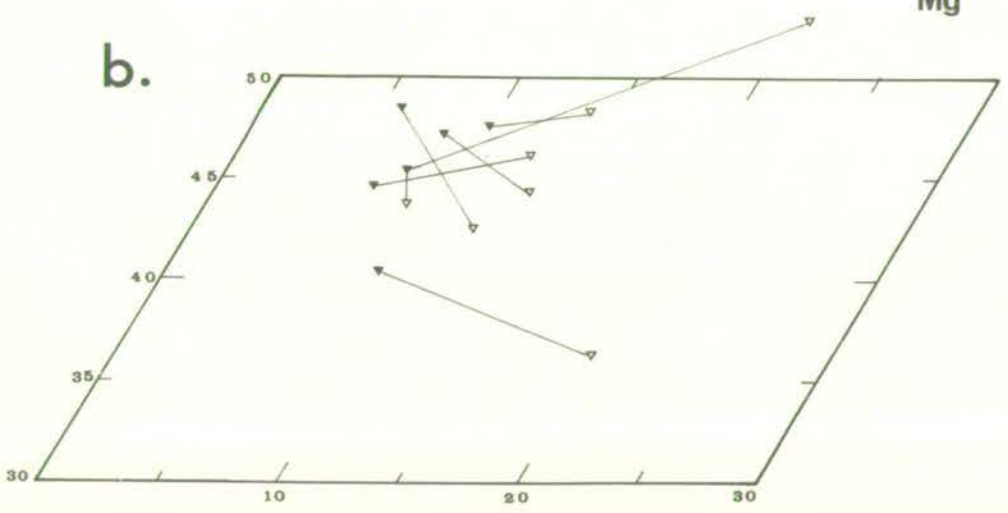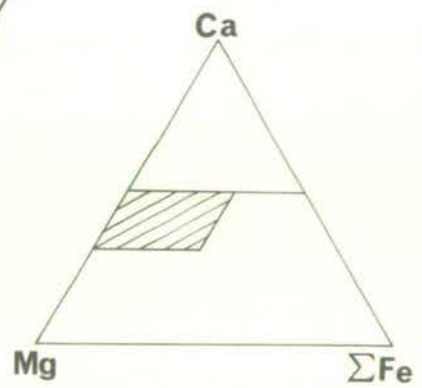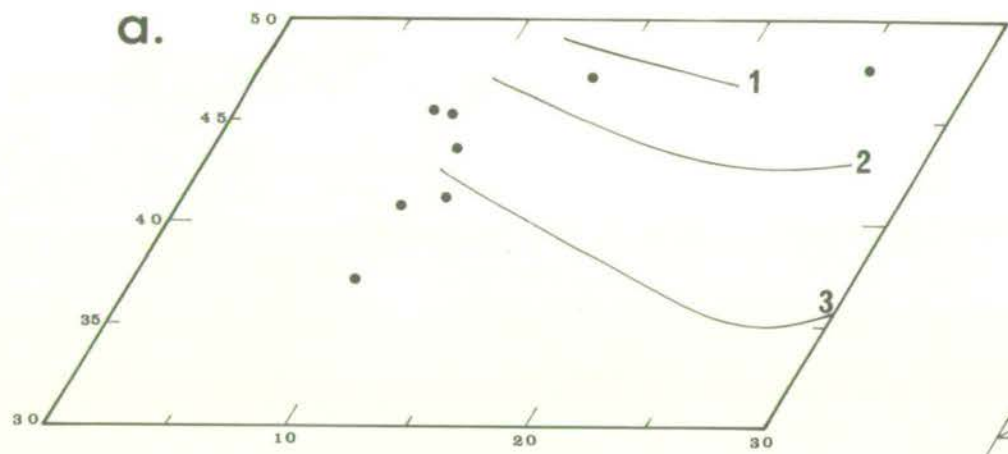
drawn between coexisting olivine and augite phenocrysts (Fig. 12a).
The consistent orientation of these tie-lines suggests that these
phases could have crystallized in equilibrium with one another. It
is uncertain, however, just what should be the orientation of
equilibrium tie-lines between olivine and augite since, for example,
those of the Garbh Eilean sill (Murray, 1954), the Black Jack sill
(Wilkinson, 1956), and the Nandewar volcano (Abbott, 1969) all show
tie-lines of different orientation (Fig. 12b).   If the Kartala
olivine and augite are in equilibrium with one another but not with
the liquid, as these data suggest, one must suppose that they remained
together during movement from the source of crystallization.

4.1.4. Plagioclase

As plagioclase phenocrysts occur in only six of the analysed
Kartala lavas (Chapter 3; Appendix B), they were of relatively minor
interest to the present study.   However, analyses of plagioclase
from one lava flow (No. 30) and one gabbroic block (No. 42) are given
in Table 8.

The anorthite contents of microphenocrysts and groundmass
feldspars from a range of Kartala lavas, as determined by optical
methods (Appendix A), are given in Table 9.   These show slight
variation about a mean of An-65 for the microphenocrysts and An-54
for the groundmass feldspars, corresponding with the average normative
composition of An-54.

4.1.5. Other Minerals

Opaque oxides are the only visible crystalline phase, other
than olivine, augite, and plagioclase, in the lavas.   These consist

Fig. 12.

Augite - olivine tie-lines in

Ca:Mg:$\sum$Fe   diagram.

      a.   Kartala data

      b.   Data from other studies

   ▼   = (Murray, 1954)

   ●   = (Wilkinson, 1956)

   ■   = (Abbott, 1969)

Areas of diagram shown in insert.

olivines

a.

b.

Ca

Mg   ∑Fe
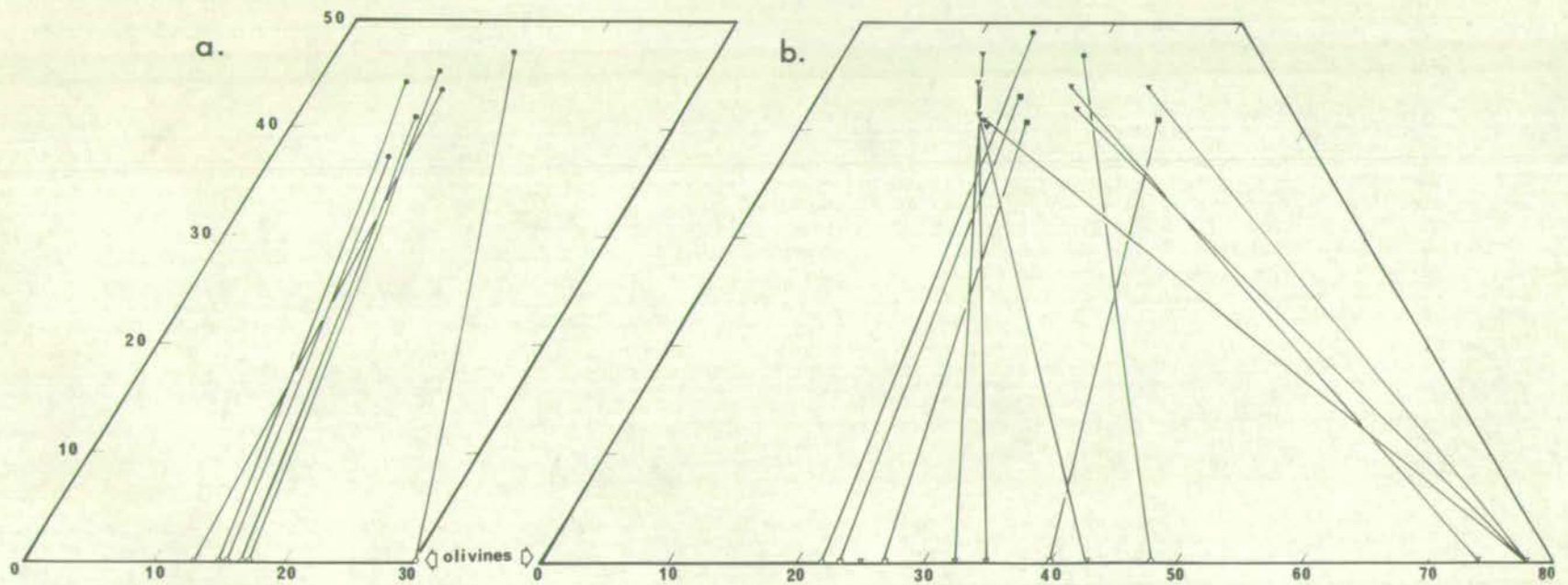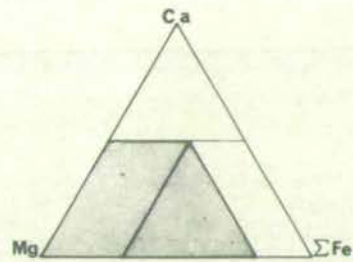
primarily of magnetite, generally homogeneous but rarely with hematite lamellae, occurring as octahedral microphenocrysts or skeletal groundmass crystals. Less commonly, tabular ilmenite-hematite intergrowths are seen, as well as very scarce specks of sulphide, probably pyrite.

Nepheline has been detected in some of the coarser-grained lavas (e.g. No. 22, Tables B-1 and C-1) by X-ray diffraction, but it is not identifiable under the microscope. It does not occur in the more glassy lavas. As shown in Chapter 3, the yellow-brown groundmass glass of the lavas has refractive indices between 1·606 and 1·610, corresponding to 47·0 and 46·4% SiO_2 respectively (using the curves for Gough Island given by Yoder and Tilley, 1962, Fig. 9).

4.2. MINERALOGY OF THE LA GRILLE LAVAS

4.2.1. Olivine phenocrysts

As described in Chapter 3, olivine is the dominant phenocryst phase in all the analysed lavas of La Grille, and it is the only phenocryst phase in 70% of them. The forsterite contents of olivine phenocrysts from eight of the La Grille lavas and from one lherzolite inclusion are given in Table 10. An outstanding feature of these olivines is their high forsterite content, averaging Fo-90. These are more forsteritic than those of Kartala lavas, at Fo-84, and even the lherzolite olivine, at Fo-86. In fact, olivines of this composition are only very rarely found in lavas (cf. Brown, 1967). Although one can only tentatively accept these compositions until more accurate data are available, the consistency of the two methods of

Table 8

Chemical composition of Kartala plagioclases

wt.%	30	42
SiO_2	52·76	57·93
TiO_2	0·17	0·14
Al_2O_3	29·35	24·72
Fe_2O_3*	0·67	1·00
MnO	0·00	0·00
MgO	0·45	0·04
CaO	12·41	7·26
Na_2O	3·91	6·20
K_2O	0·46	2·34
P_2O_5	0·08	0·35
H_2O	0·12	0·11
Total	100·33	100·00
Q	0·84	-
Cor	0·05	-
Or	2·71	13·84
Ab	33·02	48·37
An	60·93	32·75
Ne	-	2·25
Di	-	0·90
Hy	1·94	-
Ol	-	0·79
Ilm	0·32	0·27
Ap	0·19	0·83
Rb	-	45
Cu	10	39
Sr	2590	1120
Ba	535	770
Zn	10	7
Zr	-	6

	Or	Ab	An	Or	Ab	An
	2·8	34·2	63	14·6	51	34·4

* Fe_2O_3 = total iron as Fe_2O_3.

Table 9

Anorthite contents* of Kartala plagioclases

Rock No.	Microphenocrysts	Groundmass	Normative
1	-	48	54
3	72	55	-
4	60	-	55
5	65	55	-
13	-	55	57
17	60-65	44-52	57
22	-	58	52
25	60	-	49
26	-	55	53
28	68	55	52
32	-	55	52
45	-	54	-
50	-	58	-
Mean	65	54	54

* Optically determined (see Appendix A).

determination, already confirmed for the Kartala lavas, suggests that they are reliable. Some further support for this assumption may be derived from the bulk rock normative olivine compositions, which at an average of Fo-79 are more basic than the Kartala normative olivines with an average of Fo-70.

4.2.2. Clinopyroxene phenocrysts

None of the scarce clinopyroxenes of La Grille lavas were chemically analysed, but their optical properties suggested they are titanaugites, some_times showing pale green cores, possibly diopsidic. The possibility that these clinopyroxenes are xenocrysts derived from the lherzolites cannot be discounted.

Pale green chrome diopside was separated from a lherzolite inclusion (No. 35, Tables B-3 and C-3), and its composition is given in Table 11.

4.2.3. Groundmass minerals

The groundmass of La Grille lavas consists of forsteritic olivine, augite, opaque oxides, plagioclase and apatite in some cases, nepheline in the coarser rocks, and brown glass in most. Groundmass augites are distinctly brown in colour, as compared to the grey-purple colour of the phenocrysts. An outstanding example of these are found in the basanite No. 10 (Tables B-2 and C-2) where there is an abrupt deepening of the brown colour around the margins of vesicles and in residual liquid which lines the vesicles (cf. Smith, 1968).

The opaque minerals in La Grille lavas are magnetite, sometimes

Table 10

Forsterite contents of La Grille Olivines

Rock No.	XRD ± 4%	βRI ± 2%	Normative[*]	
9	90·9	88	77	
36	92·3	88	84	
37(2)	90·6	90	85	
52	-	83	83	
53	-	84	80	
54	94·1	88	76	
165	-	88	88	
171	-	87	82	
Mean	92·0	87	79[*]	
				Probe
35	84·7	86	90	86·2

[*] Normative mean = mean of all 19 La Grille lavas.

Table 11

Chemical composition of clinopyroxene from lherzolite (No. 35)

wt.%	
SiO_2	52·53
TiO_2	0·59
Al_2O_3	4·53
Fe_2O_3	0·03
Cr_2O_3	1·06
FeO	3·71
MnO	0·11
MgO	18·07
CaO	18·21
Na_2O	0·25
K_2O	0·02
H_2O	0·19
P_2O_5	0·09
Total	99·80
ppm	
Cu	42
Sr	138
Zn	31
Zr	72
Cr	7246
Ni	580
Ca	39·2
Mg	54·4
Σ Fe	6·4

with hematite lamellae, or ilmenite-hematite intergrowths, all
apparently similar to those of Kartala lavas.   The groundmass
plagioclase was generally too small for reliable estimates of
composition, but determinations on three rocks gave an average of
An-54, similar to those of Kartala.   Nepheline was identified by
X-ray diffraction, but although apparently visible microscopically
it could not be reliably identified.

4.3.   SUMMARY

The Kartala lavas are made up of forsteritic olivine, diopsidic
augite, and scarce calcic plagioclase phenocrysts in a commonly
glassy matrix of sodic labradorite, olivine, augite, magnetite, and
rare nepheline.   The La Grille lavas consist of forsteritic olivine
and scarce titanaugite phenocrysts in a glassy groundmass of olivine,
augite, nepheline, magnetite, sometimes plagioclase, and very rarely
apatite.

5. PETROCHEMISTRY

5.1. INTRODUCTION

Eighty new chemical analyses and C.I.P.W. norms of rocks from Grande Comore are presented in Appendix C.   The analysed rocks have the following distribution:

Kartala lavas	46
La Grille lavas	19
Badjini lavas	5
Kartala intrusive rocks	5
Other miscellaneous rocks	5

The apparent bias of sampling towards Kartala lavas reflects the greater size of this volcano (cf. Figs. 3 and 5).

Rocks were chosen for analysis in order to maintain an even distribution over the whole island (see Fig. 5), and to cover as wide as possible a range of chemical variation.   This variation was predicted to some extent from phenocryst content of the rocks, although a large number of aphyric rocks were analysed in order to detect any variation not predictable from petrography.   No analysed lavas from Grande Comore show any significant indication of chemical weathering or other secondary alteration, except for No. 38A, which is excluded from any petrological interpretations.

The methods of chemical analysis are described in Appendix A.

Chemical analyses of five rocks from Grande Comore were given by Lacroix (1922), and these are shown in Table 12, along with C.I.P.W. norms calculated in the present study.   Because of differences in analytical methods, and the imprecise location of the rocks,

Table 12

Chemical analyses of rocks from Grande Comore given by Lacroix (1922)

wt %	4	7	8	15	18
SiO_2	48·76	47·36	46·50	45·84	42·00
TiO_2	3·16	2·87	2·29	3·00	1·83
Al_2O_3	12·31	12·50	14·66	7·45	11·04
Fe_2O_3	2·54	2·26	3·69	1·66	3·94
FeO	10·58	10·51	9·32	9·64	7·71
MnO	-	-	-	-	-
MgO	5·43	7·05	6·04	16·76	16·38
CaO	12·32	13·24	12·00	12·64	12·50
Na_2O	3·44	2·25	3·33	1·38	2·30
K_2O	1·27	1·37	1·38	·99	1·65
P_2O_5	·39	·44	·41	·42	·53
H_2O^+	·11	·09	·16	·32	·37
H_2O^-	-	·18	·10	·10	·04
Total	100·31	100·12	99·88	100·20	100·31
Or	7·49	8·11	8·18	5·86	Lc. 7·65
Ab	21·54	15·52	15·84	8·00	Cs. 1·84
An	14·37	19·99	21·05	11·23	14·85
Ne	4·07	1·92	6·74	2·01	10·64
Di	36·34	35·13	29·43	38·98	29·98
Ol	5·62	9·56	8·05	24·80	24·58
Mt	3·67	3·28	5·37	2·41	5·72
Ilm	5·99	5·46	4·36	5·71	3·48
Ap	·92	1·04	·97	1·00	1·26
D.I.	33·09	25·55	30·76	15·87	18·29

D.I. = Differentiation index (Thornton and Tuttle, 1960).

4. "Basalte andesitique", 1918 eruption, Kartala (compact, sparse olivine phenocrysts).

7. "Basalte labradorique", Oussivo, Kartala volcano (corded vitreous flow).

8. "Basalte labradorique", 1860 eruption, Kartala (transitional to basanitoide).

15. Ankaramite, Iconi, Kartala (equally abundant olivine and augite phenocrysts).

18. "Ankaratrite limburgitic", Bangoi-Kouni, La Grille (Olivine rich in spinel, brown glass).

these analyses are of limited value to the present study.   They
do, however, indicate the undersaturated nature of the Grande
Comore lavas, and No. 18 (Table 12), with 1·84% normative larnite
(cs), displays a degree of silica-undersaturation unmatched in
any rocks analysed in the present study.

In the following description of the petrochemistry, the
Kartala and La Grille lavas are compared and contrasted.   Following
a brief discussion of the other analysed rocks, a statistical
comparison of the two groups of lavas is made by means of dis-
criminant function analysis.

5.2. MAJOR ELEMENT CHEMISTRY OF THE LAVAS

5.2.1. Introduction

The chemical characteristics of groups of related rocks are
often represented by means of an average of a number of analyses.
Averages, in general, can be misleading, however, as they give no
information about the type of distribution, and they can be repre-
sentative of a whole population only when its distribution is
normal and when it has been representatively sampled.   Averages
of chemical analyses can be especially misleading, since each
element has a characteristic distribution which may vary indepen-
dently of the other elements.   Although these drawbacks can be
minimized by calculating separate averages for each rock type, this
should be done only when the rock classification has a chemical
basis.   This procedure cannot be followed in the present study
because the rock classification adopted is both petrographic and
chemical.   Because of these considerations it is felt that a clearer

picture of the rock chemistry can be obtained by means of histograms.

5.2.2. Histograms

The chemical characteristics of lavas from Kartala and La Grille are summarized in the form of histograms in Fig. 13. Also included in Fig. 13 are the distributions (scaled down to one tenth) of major elements in 414 "nepheline basalts" given by Manson (1967, Table XIII). Some general comments on these distributions are made below, and the reader is referred to particular histograms for more precise information and for comparison with the data of Manson.

1. The modes of SiO_2, TiO_2, and Al_2O_3 are generally lower in the La Grille lavas than in those of Kartala. Conversely, the modes of CaO, MgO, P_2O_5, MnO, and H_2O are higher in the La Grille than in the Kartala lavas. K_2O, Na_2O, Fe_2O_3, and FeO have essentially similar distributions in each group.

2. All distributions are closer to normal in La Grille than Kartala lavas. This is especially so for the important variable MgO, which has a positively skewed distribution in Kartala lavas.

3. Distribution of the La Grille differentiation indices (of Thornton and Tuttle, 1960) are normal, with a mode at 20, while that of Kartala is negatively skewed with a mode at 33.

5.2.3. Variation diagrams

An analysis of variance and correlation matrices for the La Grille and Kartala lavas are given in Appendix D, showing that the

Fig. 13.

Histograms of major element distributions in
(a) La Grille and (b) Kartala lavas.
Stippled areas represent data of Manson (1967,
Table XIII) scaled down to one tenth.

FREQUENCY (in units of 2)

Wt. percent
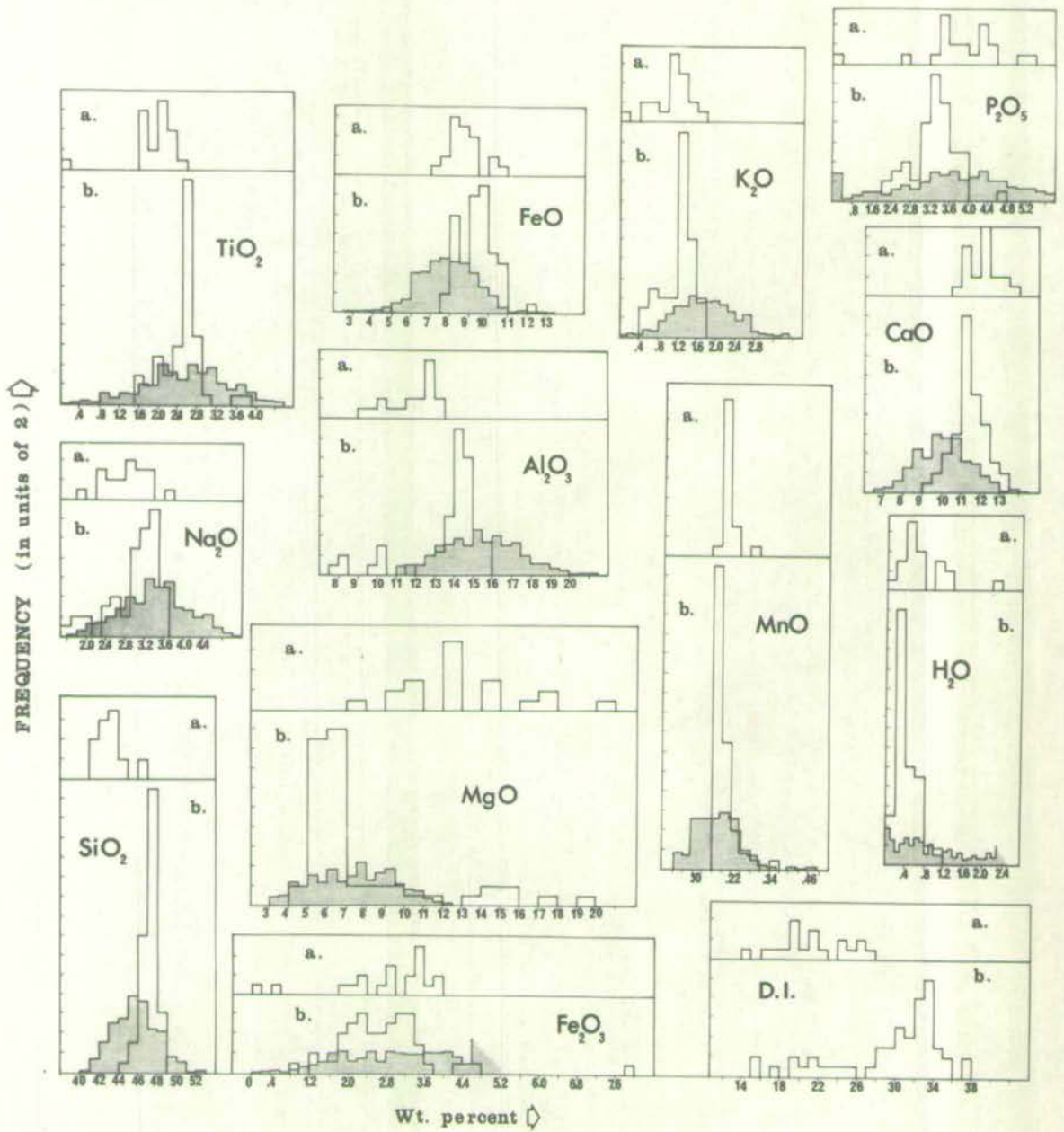
variance of MgO makes the largest single contribution to the total variance of both Kartala and La Grille analyses. Consequently, the overall chemical variation is best illustrated by means of the MgO variation diagrams, as shown in Figs. 14 and 15. It can be seen from Fig. 14 that Kartala lavas with more than about 7·0% MgO form a linear trend which intersects the olivine-augite tie-line very close to a point representing the average olivine/augite ratio of phenocrysts in these lavas. The Kartala lavas with less than 7·0% MgO show a less clearly defined trend which extends towards the composition of augite phenocrysts in the lavas.

Variation trends for the La Grille lavas (Fig. 15) are much more poorly defined than those of Kartala, with cloudy distributions for most elements, as one would expect from the correlation coefficients given in Appendix D. As olivine is the only phenocryst phase in these lavas, control lines have been drawn from olivine through the clouds of points (Fig. 15). However, the major axis of any cloud of points is not parallel to any olivine control line.

Other relations between these two groups of lavas are illustrated in two commonly used variation diagrams in Figs. 16 and 17, where they are also put in a broader context by comparison with Hawaiian lava. From the alkali-silica diagram (Fig. 16) it is seen that all lavas of Grande Comore fall on the alkalic side of the dividing line between Hawaiian tholeiitic and alkalic basalts. The Kartala lavas fall in the field of Hawaiian alkali olivine basalts, and the La Grille lavas show affinities with the Hawaiian "nephelinic series" (cf. Macdonald, 1968a).

Fig. 14.

Variation diagrams for major elements in the
Kartala lavas.

Light solid lines are olivine-augite tie-lines.
Heavy dashed lines are "control lines" from
average olivine/augite phenocryst ratio in
cumulus-enriched lavas.

Oxides in weight percent.

FeO = total iron as ferrous iron.

O   = Kartala lavas

▼   = augite (No. 21, Table 6).

▽   = olivine (No. 21, Table 4).
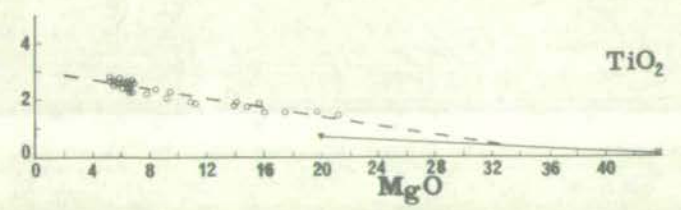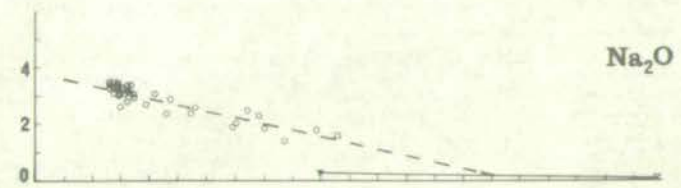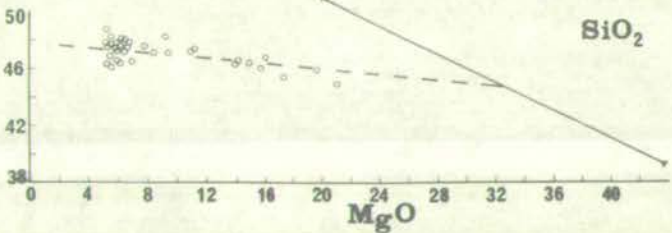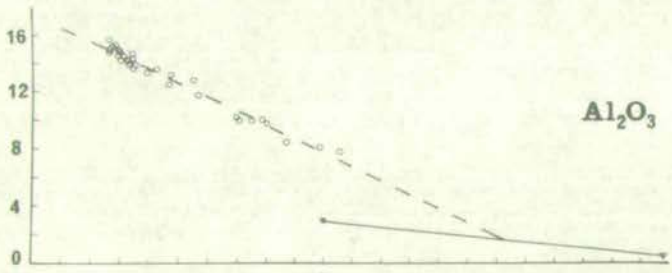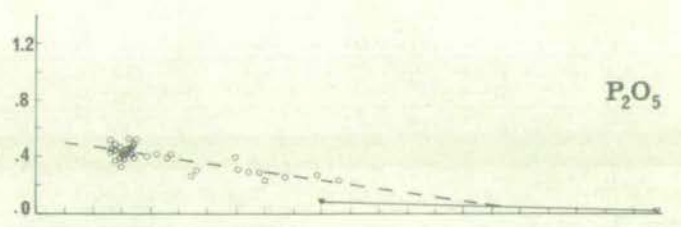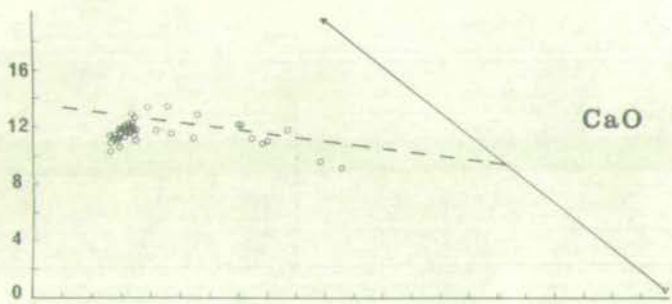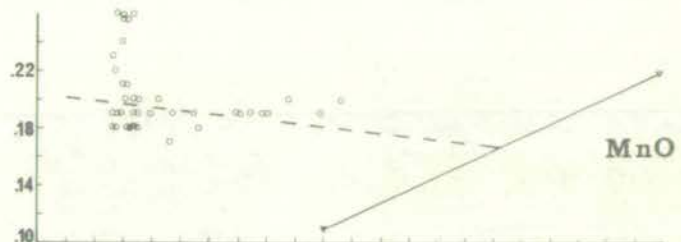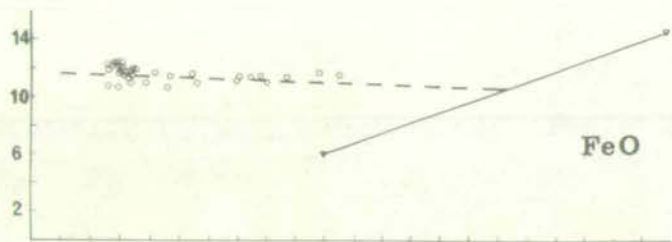
Fig. 15.

Variation diagrams for major elements in
La Grille lavas.

Oxides in weight percent.

FeO = total iron as ferrous iron.

Areas inside dashed line are fields of Kartala lavas.

Solid lines are olivine "control lines".

●   = La Grille lavas

∇   = olivine (No. 21, Table 4).
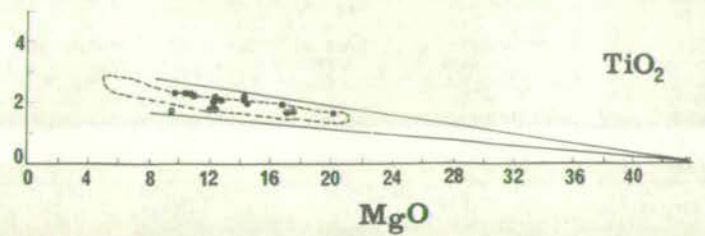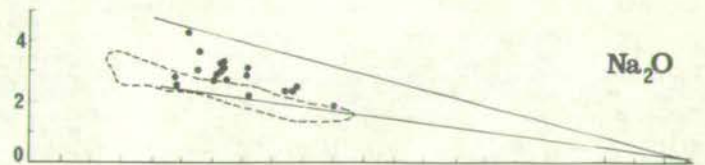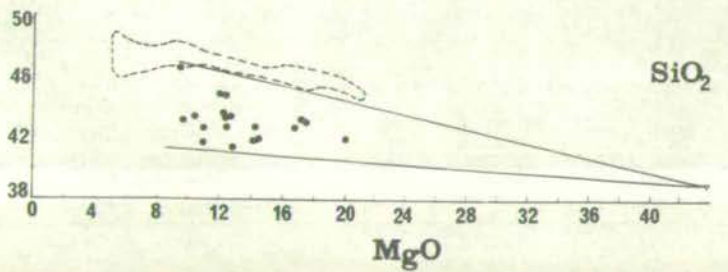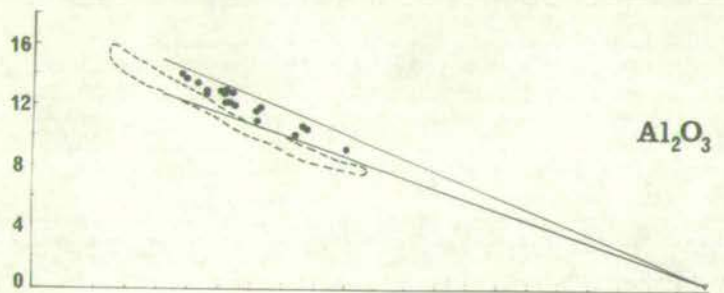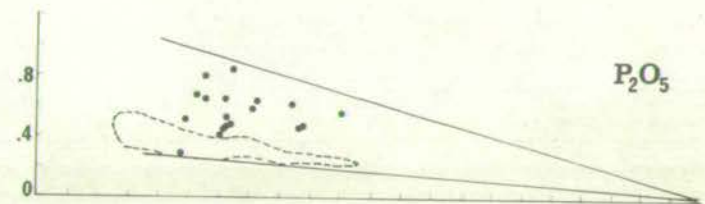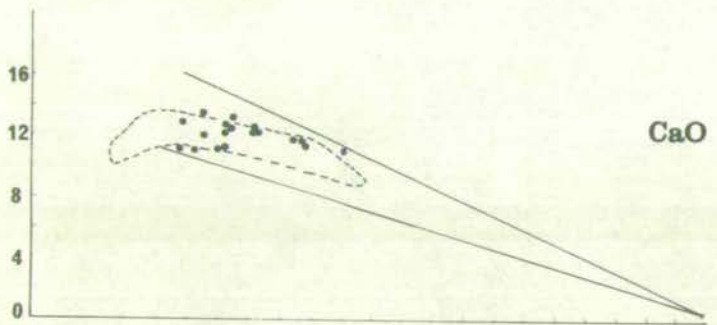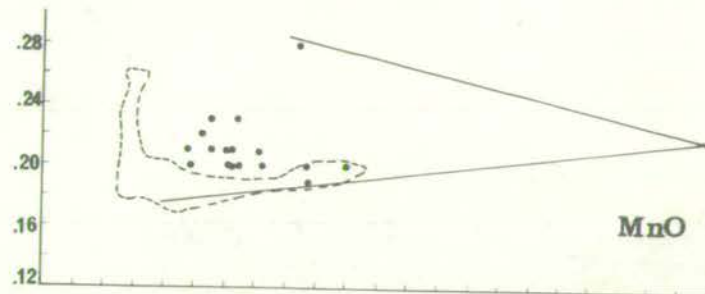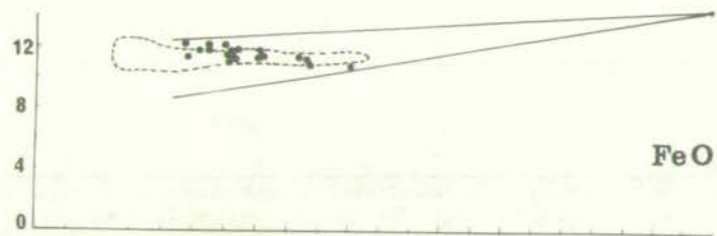
Fig. 17 is an "F.M.A." diagram, on which is plotted the alkali basalt variation trend of Hawaiian basalts (Macdonald and Katsura, 1964). This diagram shows that Kartala lavas fall on the trend of Hawaiian alkali basalts, while the La Grille lavas are generally less iron-enriched. The Kartala lavas show a trend away from the olivine and augite phenocrysts which they contain, while the La Grille lavas are more scattered.

5.3. C.I.P.W. NORMS OF LAVAS

The effects of oxidation on the norm of four Kartala lavas and two Badjini lavas (Tables C-1 and C-3) were eliminated by recalculating the iron to $2 \cdot 00$ wt % Fe_2O_3. The value of $2 \cdot 00\%$ Fe_2O_3 was used instead of the $1 \cdot 5\%$ recommended by Coombs (1963) because even the very fresh historic lavas of Grande Comore generally contain more than $2 \cdot 00\%$ Fe_2O_3, indicating that at least this much is possible as a primary feature of the magmas.

The following aspects of the norms should be noted:

1. All analysed lava flows from Grande Comore contain normative nepheline, and those of La Grille more than three times as much as those from Kartala (Table 13). This was summarized in Fig. 8 (Section 3.2.1.), and the separate positions of Kartala and La Grille lavas in this diagram form the basis for calling them alkali basalt and basanite groups respectively (after Coombs, 1963).

2. Normative leucite replaces normative albite in seven (37%) of the La Grille lavas (the nepheline basalts), but never in the Kartala lavas (see Table 13). The normative feldspars

Fig. 16.

$Na_2O + K_2O$ vs. SiO_2 in Kartala and La Grille lavas.

The line separates Hawaiian tholeiitic from alkali basalts
(after Macdonald and Katsura, 1964).
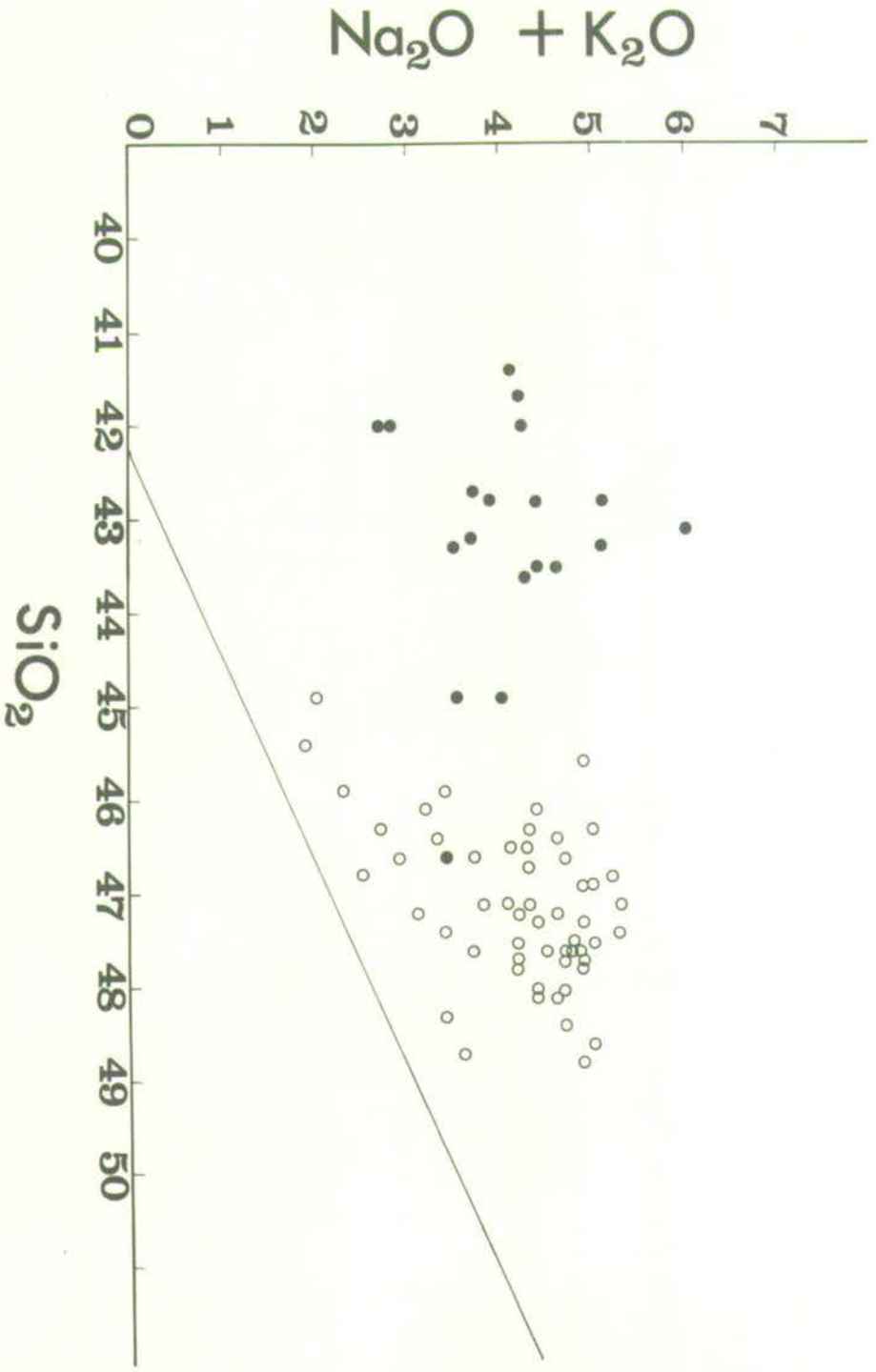
○   = Kartala
●   = La Grille

Fig. 17.

"F.M.A." diagram for Kartala and La Grille lavas (wt.%)

F. = total iron as FeO

M. = MgO

A. = $Na_2O + K_2O$

Insert shows area (stippled) of the main diagram.

Dashed line shows the Hawaiian alkalic trend (after

Macdonald and Katsura, 1964).

○ = Kartala

● = La Grille

▽ = Kartala olivines (Table 4)

▼ = Kartala augites (Table 6).
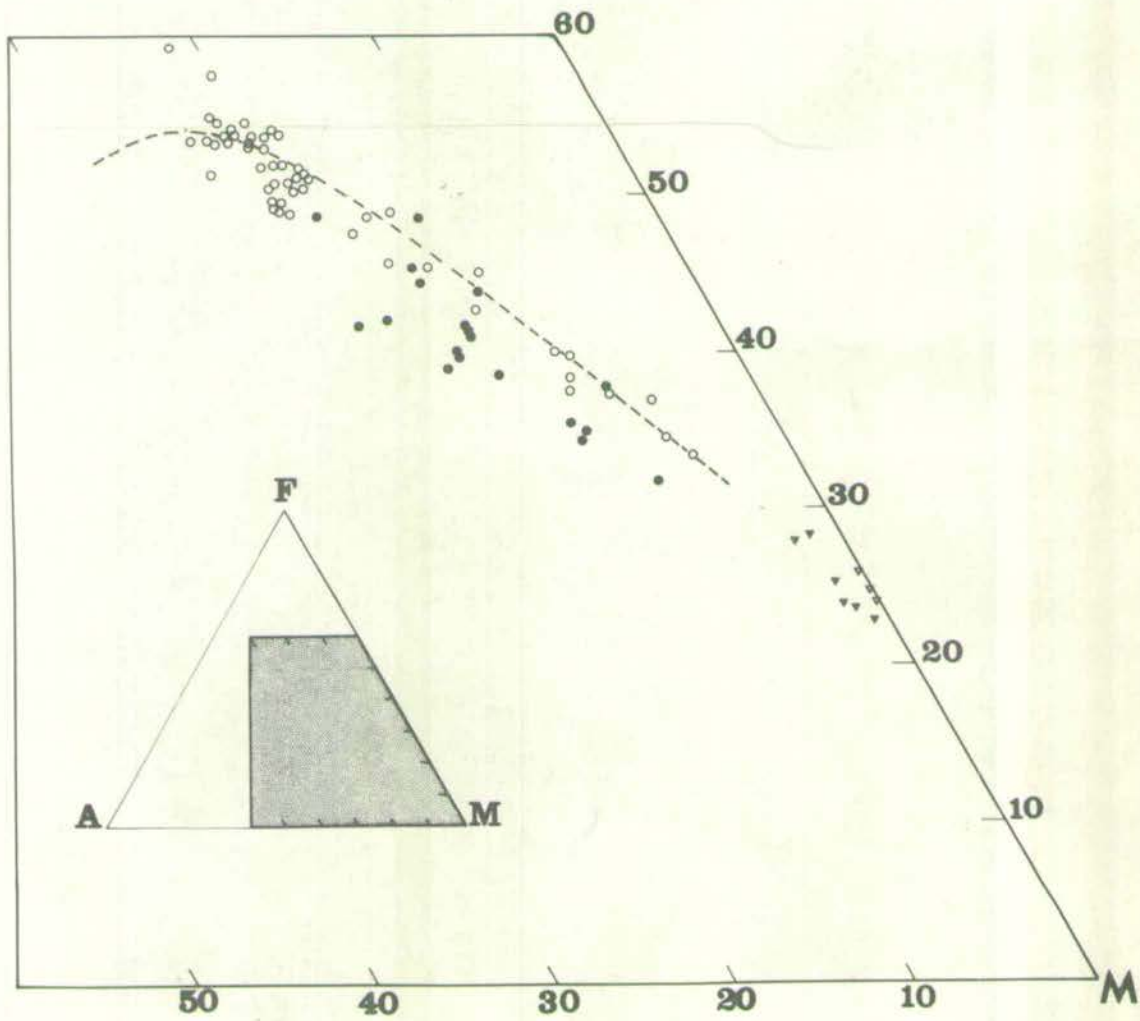
of La Grille basanites are consistently richer in An than
those of the Kartala alkali basalts, with much variation
in Ab/Or ratios, as shown in Fig. 18.   The Kartala normative
feldspars vary only slightly between An-40 to 50 and Or-10 to
20 (Fig. 18), which may be taken as a reflection of the homo-
geneity of the groundmass of these rocks, since the pheno-
crysts contribute relatively little to normative feldspar
compositions (cf. Table 6).

Table 13.

Relative silica-undersaturation in the lavas of Grande Comore,
as indicated by normative mineralogy.

		nepheline	leucite
Kartala	average	3·72	-
	low	0·31	-
	high	6·85	-
	number of rocks	46	-
La Grille	average	11·50	3·21
	low	2·26	0·10
	high	18·74	6·12
	number of rocks	19	7

The variation of normative components in the "simple basalt
tetrahedron" (Yoder and Tilley, 1962) is shown in Fig. 19, in which
projections are made onto each face of the normative tetrahedron

Fig. 18.

Normative feldspar compositions in the
system albite-anorthite-orthoclase.

○   = Kartala

●   = La Grille
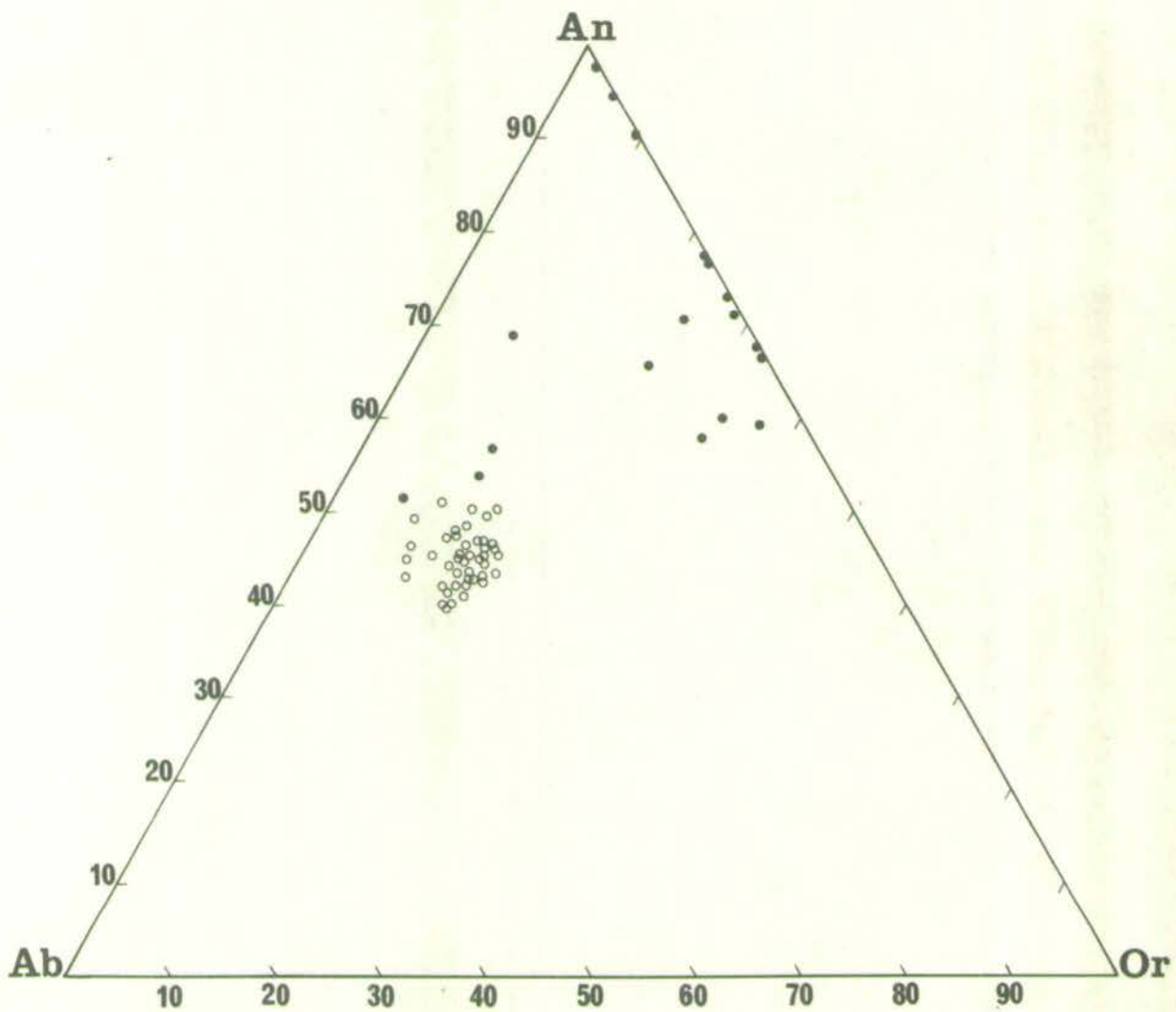
nepheline-olivine-plagioclase-diopside. Also plotted are tie-lines between olivine and augite, showing that, as in the simpler variation diagrams (Fig. 14), the normative trend falls on control lines from the average ratio of olivine to augite phenocrysts on this tie-line.

A similar projection of the La Grille lavas (Fig. 20) shows no clearly defined or consistent trends. In the nepheline and plagioclase projections there is some suggestion of a trend away from the olivine-diopside join, but in the other two projections it is not away from either of these components. This means that the La Grille trends are controlled by neither olivine nor clinopyroxene. Neither the elbow-shaped cloud in the diopside projection nor any of the patterns in other projections are simply explicable as resulting from fractionation of the phases common in basaltic magmas.

5.4. TRACE ELEMENT CHEMISTRY OF THE LAVAS

5.4.1. Introduction

In terms of basalt petrogenesis, an important crystal-chemical control of trace element behaviour is that of excluding particular elements from stable crystal lattices, thus restricting them to a purely passive role of dilution or concentration in the liquid, as governed by an increase or decrease in liquid volume. Elements which behave in this way are termed "incompatible elements" in this study (after Green and Ringwood, 1967). The incompatibility or otherwise of a particular element is only dependent upon the particular phases stable. For example, Sr can be thought of as incompatible under upper mantle conditions but as compatible under

Fig. 19.

Projections of norms of Kartala lavas in the silica-
undersaturated part of the "simple basalt tetrahedron"
nepheline-olivine-plagioclase-diopside.
Insert shows planes of projection.
Scale, in weight percent, is shown on the
nepheline-diopside join.
Dashed line is the "control line" from a point on the
olivine-augite tie-line representing the average ratio
of olivine to augite phenocrysts in the lavas.

O   = lavas

∇   = olivine (No. 21, Table 4).

▼   = augite (No. 21, Table 6).
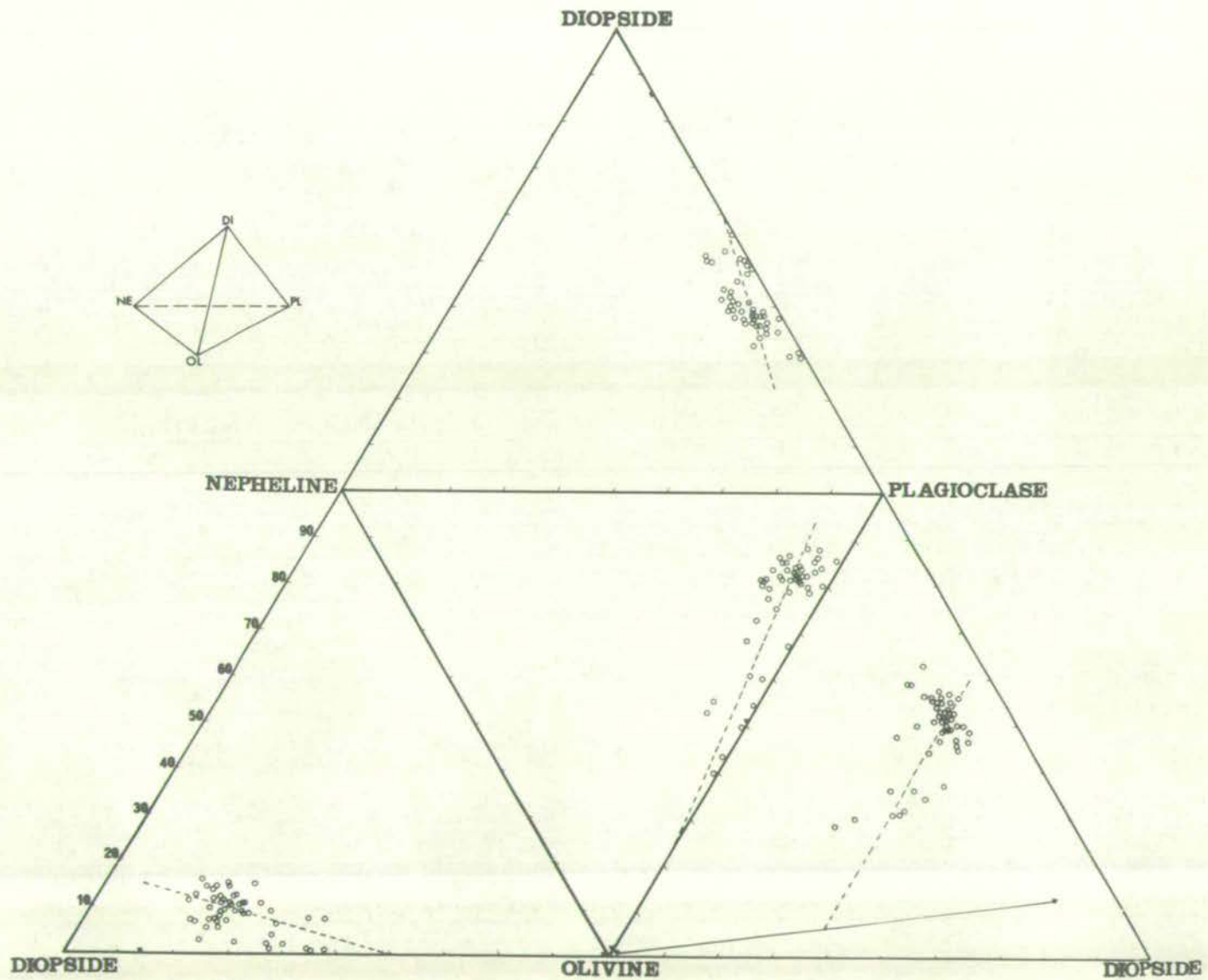
Fig. 20.

Projections of norms of La Grille lavas, as for
Fig. 19.

Areas inside dashed line represent Kartala lavas.

Solid lines are olivine "control lines".

DIOPSIDE

DI

NE .... PL

OL

NEPHELINE   PLAGIOCLASE

90
80
70
60
50
40
30
20
10

DIOPSIDE   OLIVINE   DIOPSIDE
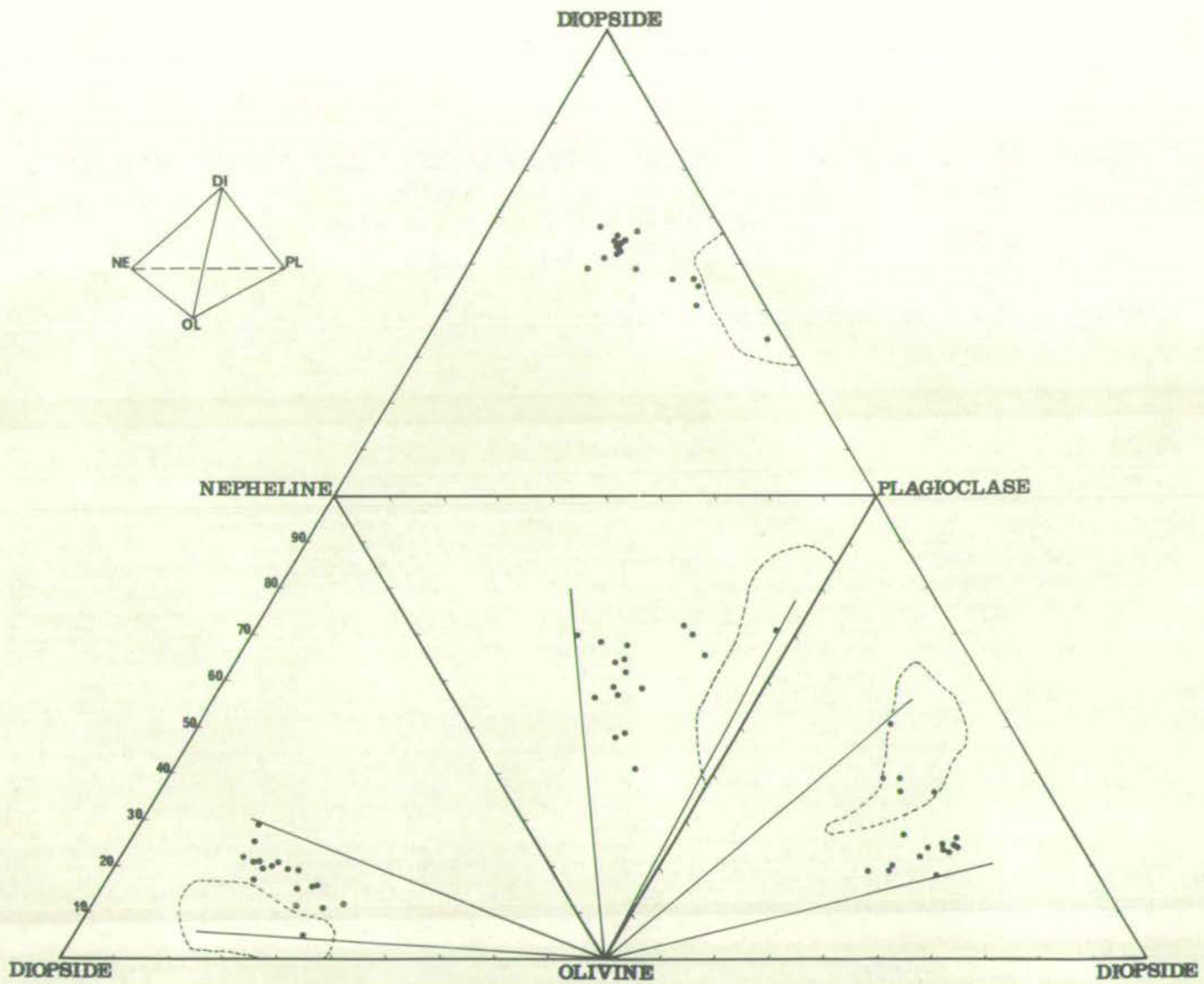
crustal conditions where plagioclase is stable (Green and Ringwood, 1967). This concept of "residual" or "incompatible" elements has been crucial to the hypotheses of basalt petrogenesis expounded by Harris (1957, 1967) and Green and Ringwood (1967).

Because of the passive behavior of incompatible elements, the concentrations of all such elements in the liquid phase will maintain linear relations to one another during processes such as partial melting and fractional crystallization. Those which deviate from linearity are not truly incompatible, and thus give important clues as to which phases may have been stable during the development of the liquids. The relative and absolute concentrations of a variety of trace elements in basaltic liquids are thus sensitive and easily interpreted indications of the petrogenetic history of these liquids.

The trace elements determined in the present study were chosen to represent a range of both compatible and incompatible elements common in basaltic magmas.

5.4.2. Histograms

The distributions of trace elements in the lavas of Grande Comore are shown as histograms in Fig. 21, along with those for "nepheline-normative alkali basalts" compiled by Prinz (1967, p. 281, Fig. 1). The following general features are noteworthy.

1. As noted for major elements, the La Grille trace element distribution patterns are closer to normal than those of Kartala.
2. The range of concentration is greater in La Grille than in Kartala lavas for all elements except Cu, which has a strikingly narrow range.

Fig. 21.

Histograms of trace element distributions in
(a) La Grille and (b) Kartala lavas.
Stippled areas represent data compiled by
Prinz (1967, Fig. 1), scaled down to
one tenth.

FREQUENCY (in units of 2)
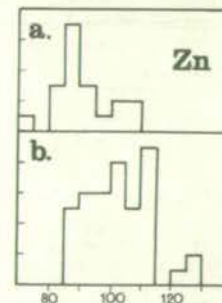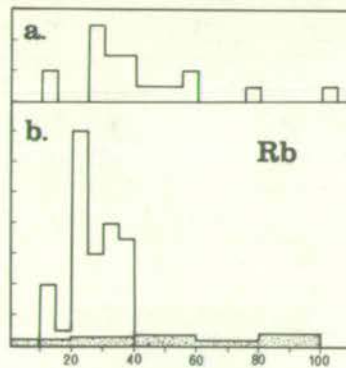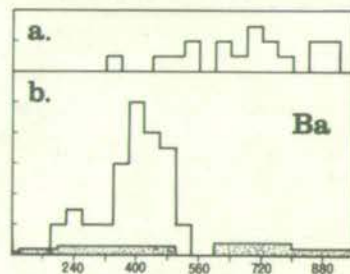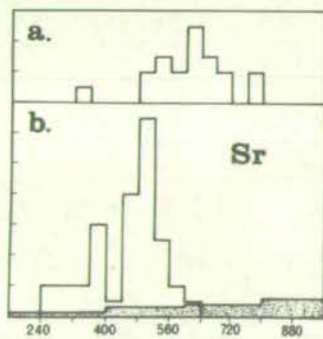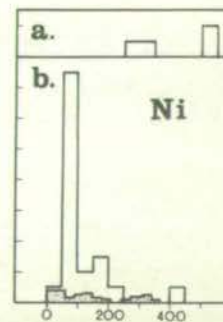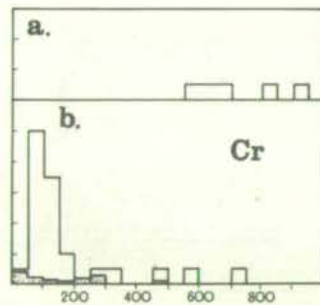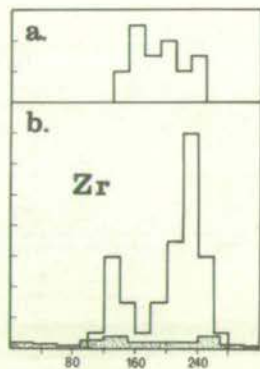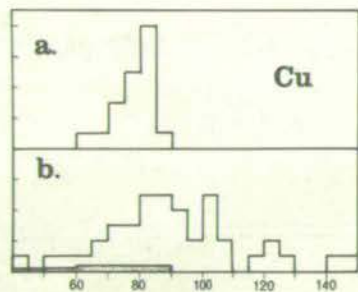
P.P.M.

3. Relative to Kartala, the La Grille lavas are enriched in
all elements except Cu and Zn, the concentrations of which
are lower.

5.4.3. Variation diagrams

The variation of trace elements with respect to MgO is shown
for Kartala and La Grille lavas in Figs. 22 and 23, respectively.
As was done for the major element variation diagrams (Fig. 14), the
olivine-augite control lines are drawn for Kartala lavas, and it is
clear that, except for Cu and Zn, the trace element concentrations
are likewise controlled by these phases.

The variation of trace elements in La Grille lavas (Fig. 23)
is much more haphazard than in those of Kartala.   For example, Rb
can be seen to vary by as much as 100% at constant MgO content.

The K/Rb ratios of igneous rocks, regarded by many workers as
sensitive indicators of their "primitiveness" or degree of differ-
entiation from the mantle (e.g. Shaw, 1968; Gast, 1965, 1968),
are shown in Fig. 24.   It can be seen from Fig. 24 that the Kartala
lavas have K/Rb ratios between 300 and 600, similar to alkali basalts
in general (Gast, 1968).   The La Grille K/Rb ratios are mostly
between 150 and 350, but reach as low as 35 (No. 165, Table C-2).

5.5. RARE-EARTH ELEMENTS

Rare-earth elements have been determined for one rock each
from Kartala and La Grille (Table 14).   The La Grille rare-earth
concentrations are consistently higher than those of Kartala, by
an average factor of 1·7.   This factor is higher than that for
other incompatible elements (cf. Table 16), but it is probable that

Fig. 22.

Variation of trace elements with MgO in Kartala lavas.

MgO in weight percent, trace elements in ppm.

Symbols and lines as for Fig. 14.
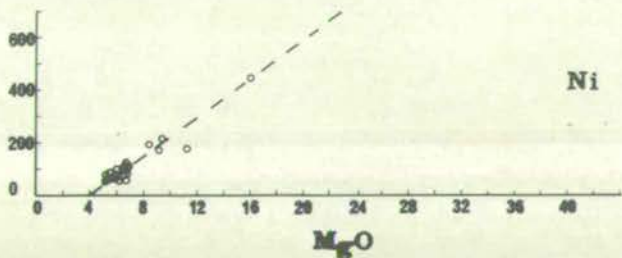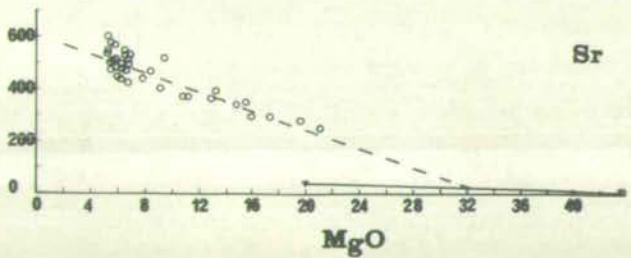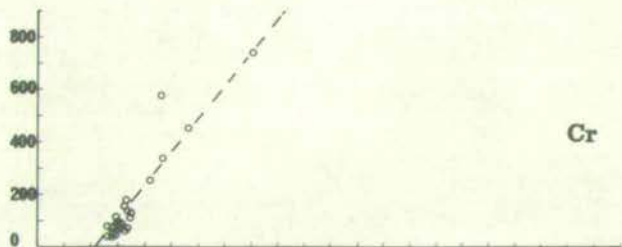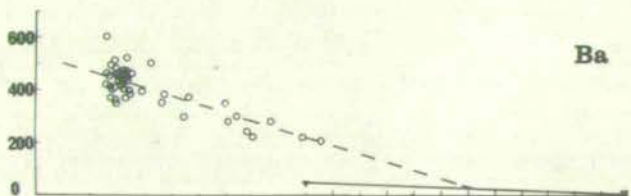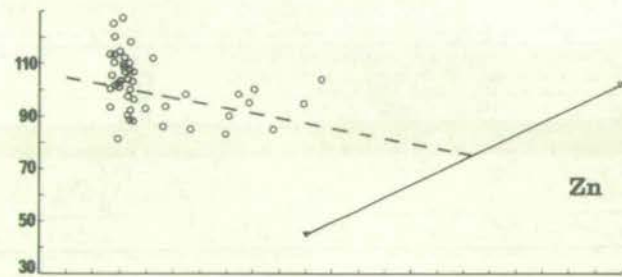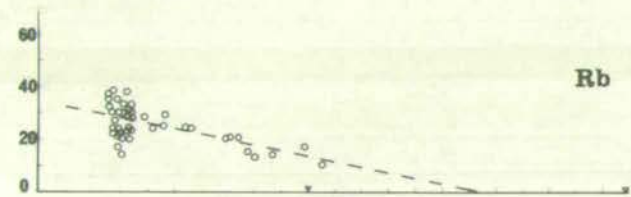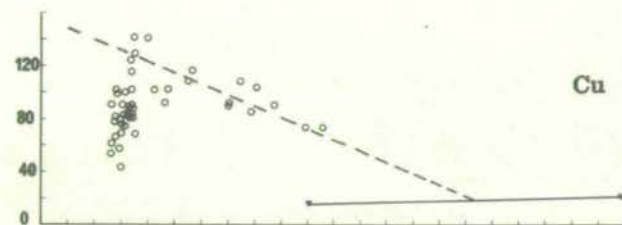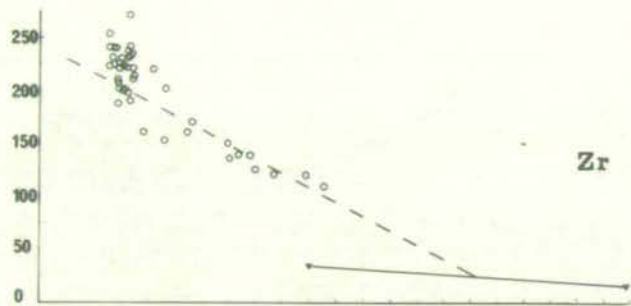
Fig. 23.

Variation of trace elements with MgO in
La Grille lavas.

MgO in weight percent, trace elements in ppm.

Symbols and lines as for Fig. 15.
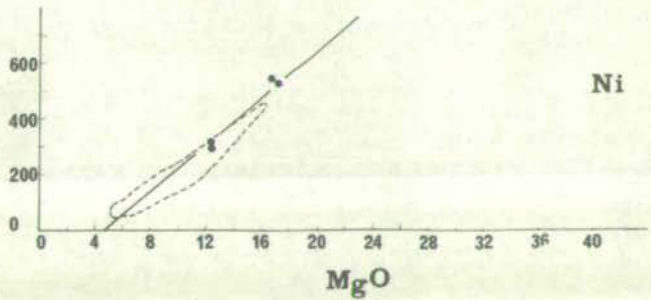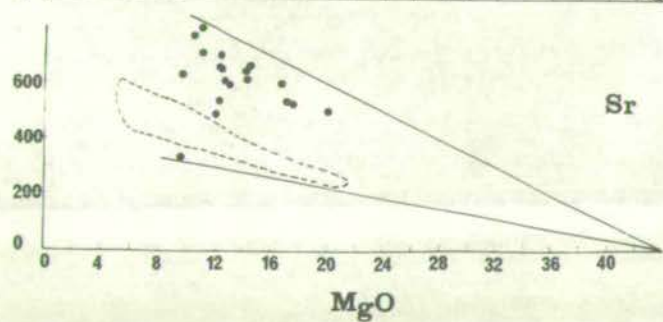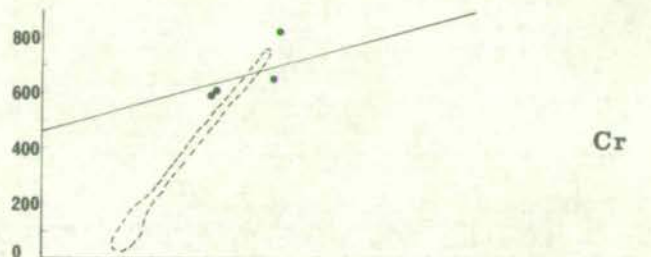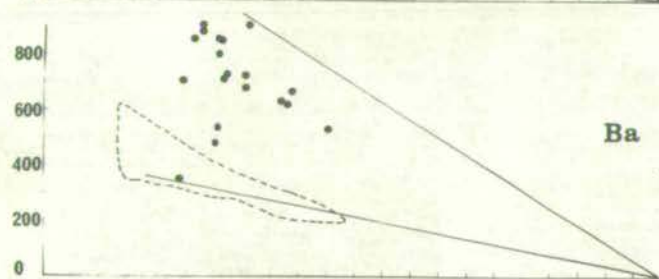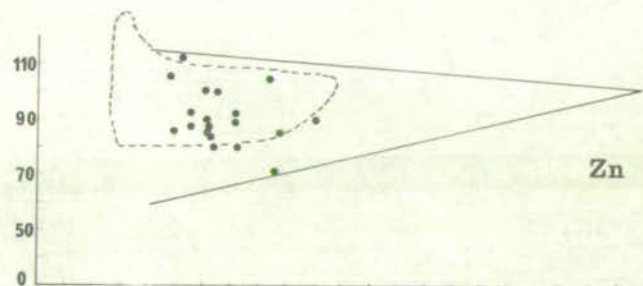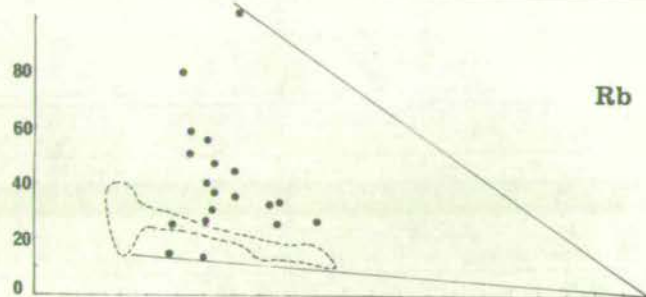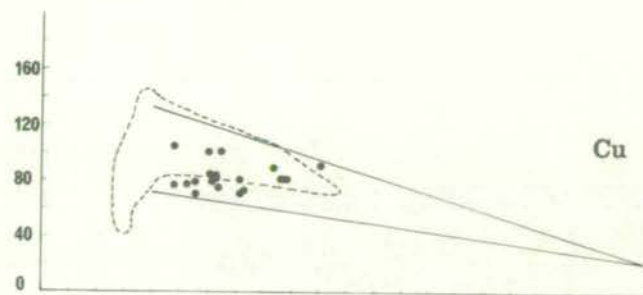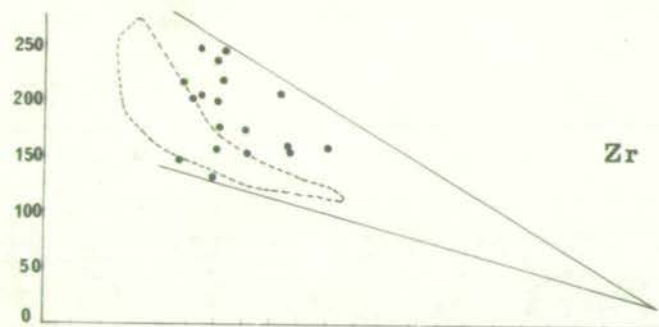
these two rocks are not quantitatively representative of the volcanoes as a whole. The patterns of distribution of the rare-earth elements (Fig. 25) are comparable to those for similar rocks elsewhere (cf. Schilling and Winchester, 1967, 1969).

5.6. CHEMISTRY OF OTHER ANALYSED ROCKS

5.6.1. Badjini lavas

The Badjini lavas (Table C-3) are chemically similar to those of Kartala, except for Nos. 156 and 158. The higher MgO and Ba contents of these two lavas suggest an affinity with those of La Grille, as was indicated by petrographic features.

5.6.2. Intrusive rocks

The three basaltic dykes from the Kartala caldera (Nos. 105, 107, and 110, Table C-4) have higher Al_2O_3 and K_2O than most other Kartala rocks, and are also more differentiated, with differentiation indices from 32·7 to 37·5. The two coarse-grained blocks from the caldera floor (Nos. 42 and 44, Table C-4) have higher total iron, TiO_2, and K_2O, and lower MgO, and are also more differentiated than most of the Kartala lavas.

5.6.3. Pyroclastic rocks

The vitric crystal-tuff (No. 16, Table C-5) is rich in water (5·93%) and ferric iron (5·32%). Because all water must be contained in the glass, which makes up only 73% of the rock (Table B-5), the water content of the glass must be around 8·1%. This rock might therefore be described as palagonitic.

The basanitic block No. 38A (Tables B-5 and C-5) shows petrographic indications of weathering which is chiefly reflected in the
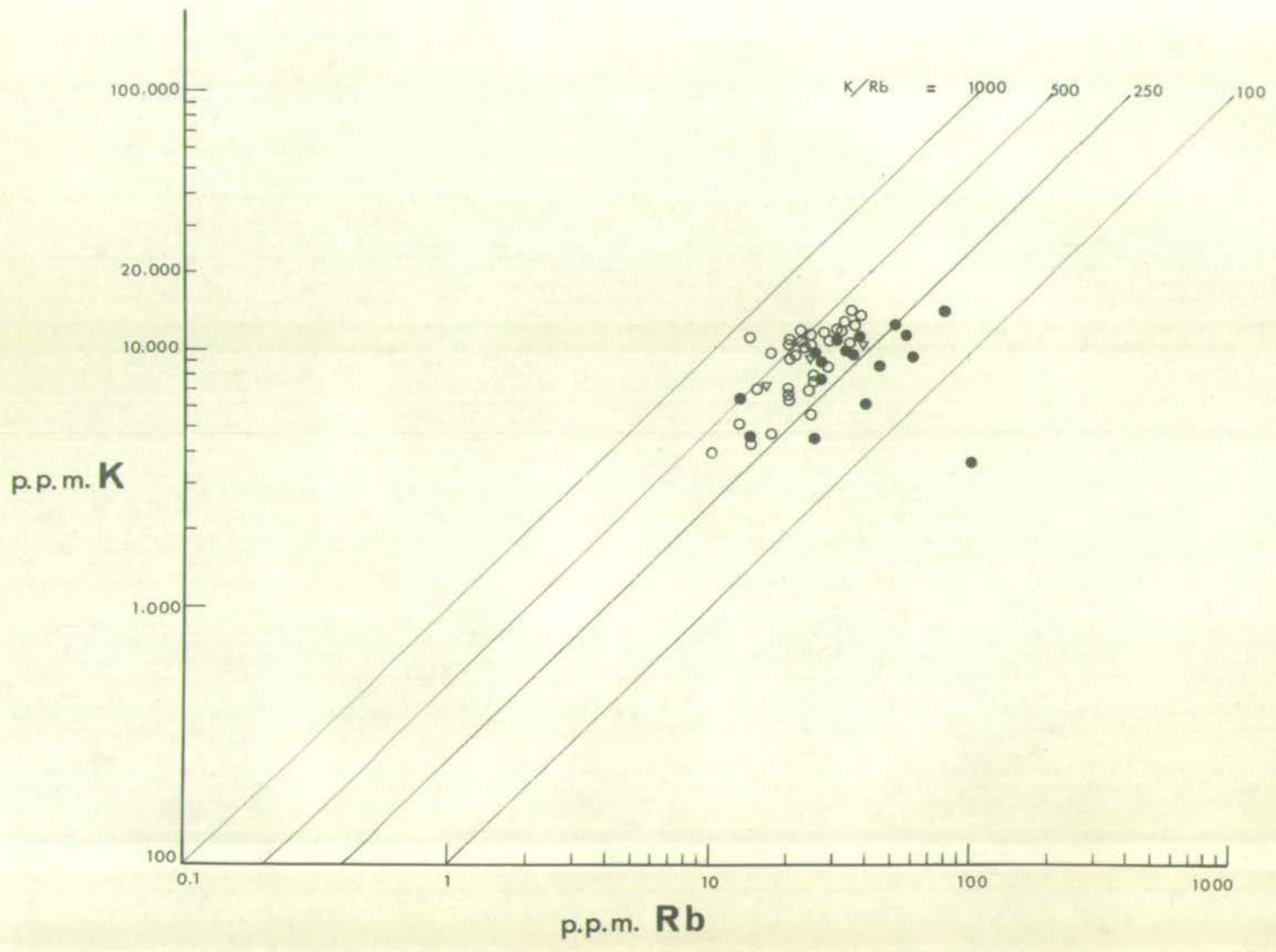
Fig. 25.

Rare-earth elements in samples No. 1 (Kartala)
and 9 (La Grille), normalized to chondritic values
given by Schmitt, et al. (1964).

○   = Kartala

●   = La Grille
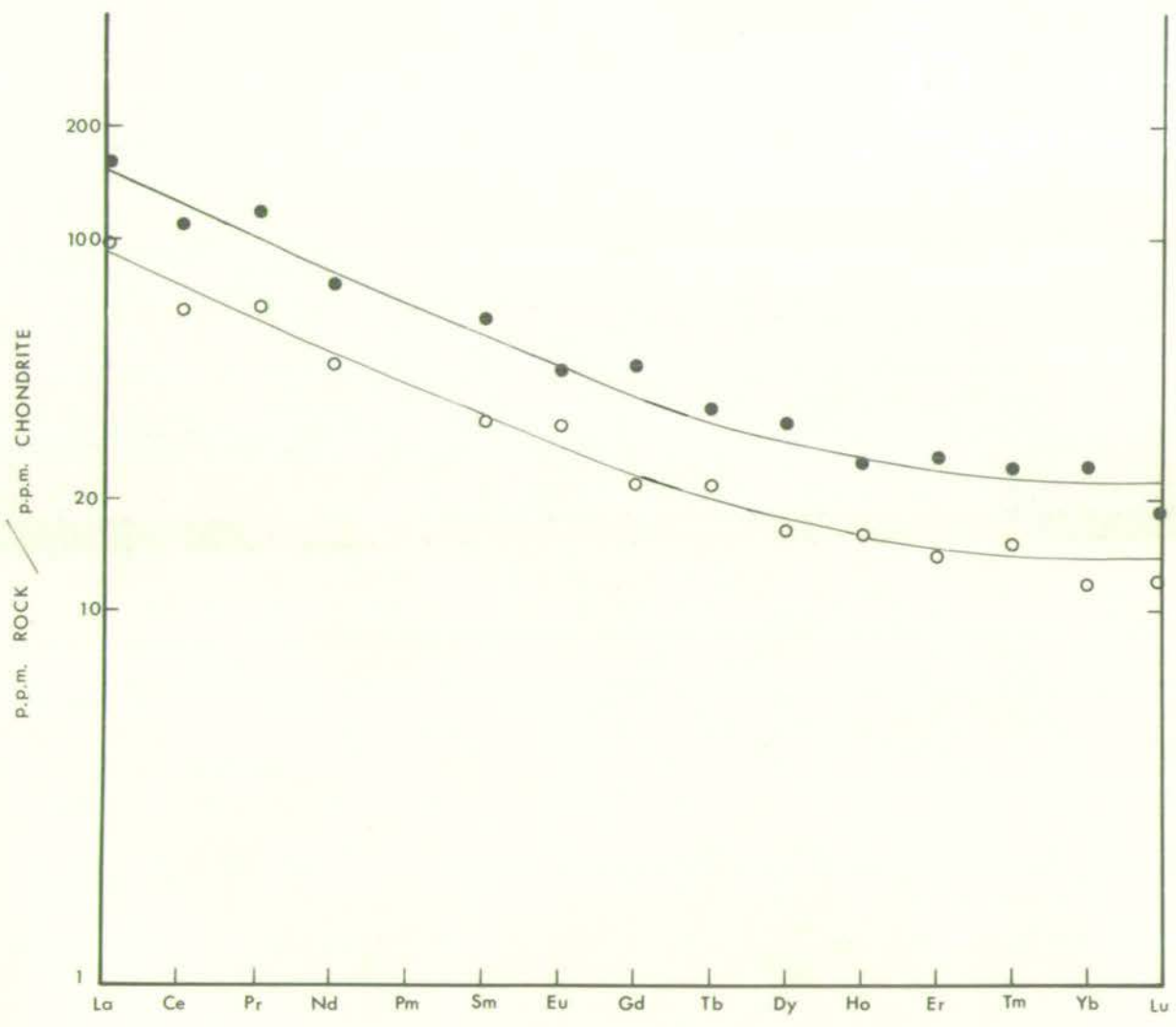
Table 14.

Rare-earth elements

ppm	Kartala (No.1)	La Grille (No.9)	La Grille/Kartala
La	29·44	48·01	1·63
Ce	54·01	90·72	1·68
Pr	7·91	14·17	1·79
Nd	26·67	43·86	1·64
Sm	7·14	12·80	1·80
Eu	2·44	3·31	1·36
Gd	7·03	14·77	2·10
Tb	1·28	2·02	1·97
Dy	5·12	10·03	1·95
Ho	1·17	1·82	1·56
Er	2·95	5·55	1·88
Tm	0·50	0·80	1·60
Yb	2·01	4·13	2·05
Lu	0·35	0·55	1·57
TOTAL	148·02	252·54	1·71

high water content (2·44%).   The high Sr concentration is almost certainly due to the abundant calcareous vesicle fillings.

5.6.4. Feldspar-phyric rocks

The feldspar-phyric basalt boulder No. 30 (Tables B-5 and C-5) is similar in most chemical aspects to the other Kartala lavas, except that its high modal feldspar is reflected in high concentrations of Na_2O, K_2O, Ba, and Sr.

The feldspar-phyric basalt found as beach cobbles (No. 130, Tables B-5 and C-5) is the only unoxidized basalt with normative hypersthene found on Grande Comore.   As such, it is the only

indication that tholeiitic rocks (using the definition of Yoder and Tilley, 1962) may occur there.

5.7. STATISTICAL ANALYSIS OF LAVA CHEMISTRY

5.7.1. Introduction

It is clear that there are obvious chemical differences between Kartala and La Grille lavas, and that almost any element determined in this study can be used to distinguish between these two groups of lavas. The overlap in distribution of most elements, however, makes it difficult to assign some samples to one group or another. This might be better accomplished by some combination of the elements instead of any one alone.

The C.I.P.W. norm is a conventional method of expressing a combination of the major elements, and it has been shown in Fig. 8 that these are largely successful in separating the lavas of each volcano. However, this method of discrimination still results in some overlap between the two groups, so that problems may still arise in classifying some specimens.

In an attempt to refine the classification of samples on the basis of bulk chemistry, the statistical method of discriminant function analysis has been employed. This method is described in standard statistical textbooks (e.g. see Goulden, 1952; Hope, 1968), and some of its geological applications are discussed by Krumbein and Graybill (1965). It has been summarized in Appendix D.

5.7.2. Discriminant function analysis

To calculate the discriminant functions (see Appendix D), samples were carefully selected on geographic and geomorphological

grounds as definitely belonging to one or the other volcano. 38 analyses were from Kartala and 14 from La Grille, and those collected in zones of uncertain derivation, between the volcanic centres, were treated as unknowns. The characteristic numbers and deciding discriminant functions so calculated are given in Table D-1 so that any future analyses of lavas from Grande Comore may be objectively compared to those from each volcano, and assigned to one or the other if its origin is unknown.

Results of the discriminant function analysis are shown diagrammatically in Figs. 26 and 27. On the basis of trace element concentrations alone, (Fig. 26), the Kartala and La Grille lavas can be separated at a significance level of 0·1%; i.e. there is a 0·1% chance of error in assuming that they are different. Using trace elements only (Fig. 26), the Badjini lavas 156 and 158 appear to be more closely related to the La Grille lavas than those of Kartala, as predicted on petrographic grounds. One sample from La Grille, No. 57, was incorrectly assigned to the Kartala group; this sample plots in the field of Kartala lavas in all diagrams used in this study.

Although the statistical significance of the major element discrimination could not be estimated due to their non-normal distribution (see Appendix D), it can be seen from Fig. 27 that the separation of the two groups of lavas using major elements is just as distinct as that obtained using trace elements. However, the Badjini lavas 156 and 158 are now assigned to the Kartala group and 147 to the La Grille group, contrary to that expected on petrographic grounds.

Fig. 26.

Discriminant functions calculated from
trace element concentrations.
Vertical scale gives value of discriminant
function.
Significance of discrimination = 0·1%.

UNKNOWNS LA GRILLE KARTALA

DECIDING DISCRIMINANT FUNCTION

MEAN

- 5
- 10
- 15
- 20
- 25
- 30
- 35
- 40
- 45
- 50

UNKNOWNS: 384, 52, 192, 156, 158, 6, 23, 142, 133, 35, 190, 23, 16

LA GRILLE: 172, 178, MEAN, 56, 57

KARTALA: 119, MEAN, 30, 44
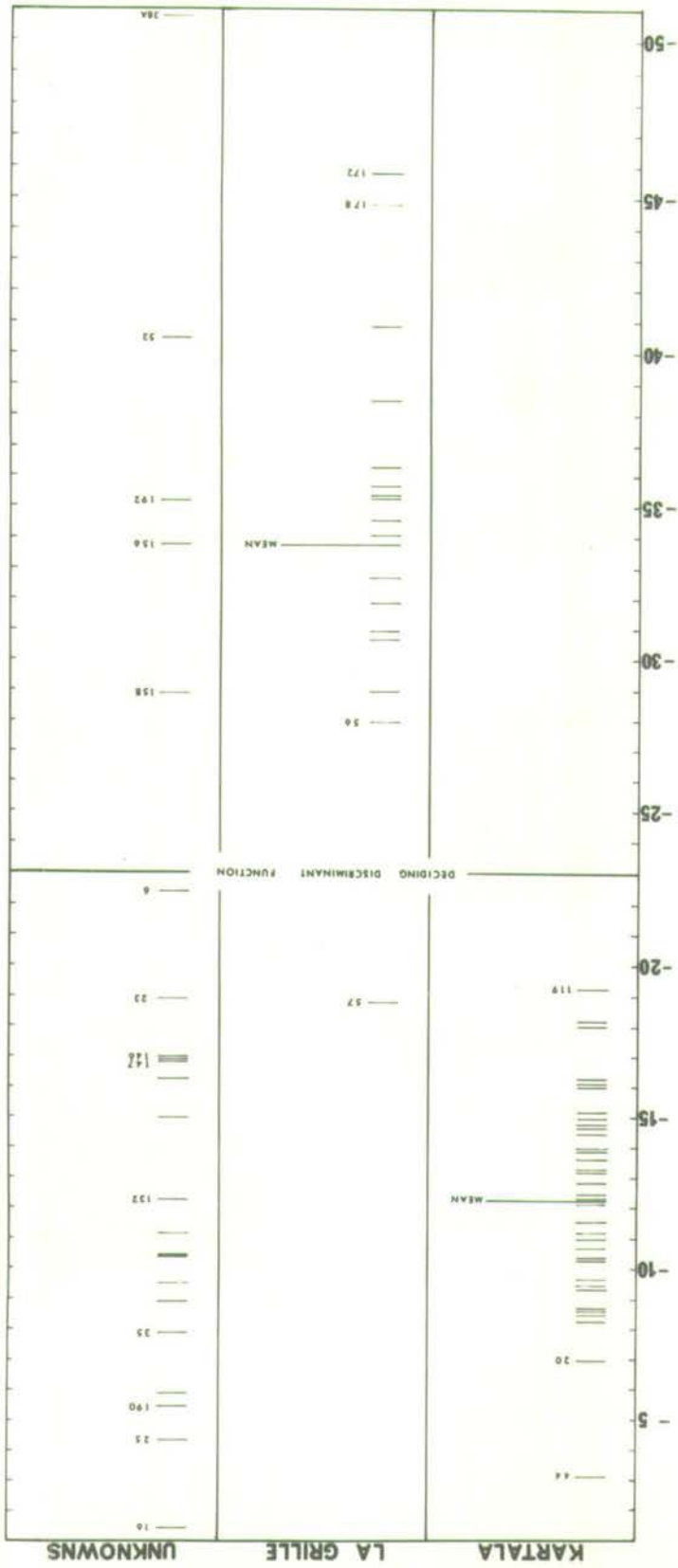
Fig. 27.

Discriminant functions calculated from
major element concentrations.

Vertical scale gives value of discriminant function.

Significance of discrimination not calculated (see text).

KARTALA   LA GRILLE   UNKNOWNS

75

70 — MEAN

65

60

DECIDING DISCRIMINANT FUNCTION

55

50

45

40

35
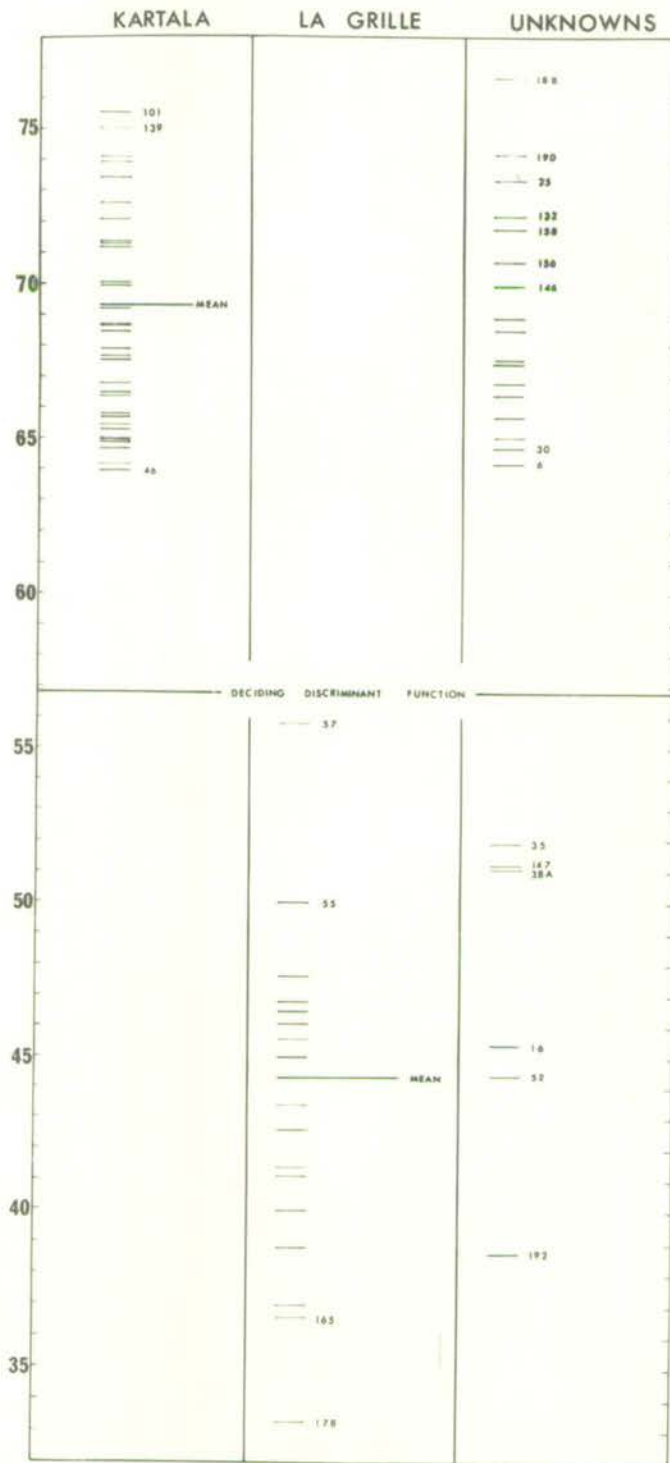
In summary, the discriminant function analysis has shown that a) there are highly significant trace element (and possibly major element) differences between the lavas of each volcano; b) the geochemical boundaries coincide with the geographic and geomorphological boundaries (cf. Figs. 3 and 5); and c) the petrographic classification of Badjini lavas is supported by the trace element discriminant functions.

5.8. SUMMARY

Lavas of the two volcanoes of Grande Comore form two distinct chemical groups. Geochemical boundaries can be drawn on a locality map of analysed specimens, and these boundaries coincide with the geomorphological boundaries between each volcano as proposed in Chapter 2.

The lavas of La Grille are more silica-undersaturated than those of Kartala, with an average of three times as much normative nepheline; and they commonly contain normative leucite, which is absent from the Kartala lavas.

The patterns of distribution of both major and trace elements are more normal for the La Grille lavas than for those of Kartala. The Kartala variation trends, in both MgO variation diagrams and normative projections, fall on control lines to olivine and augite in the average proportions in which they are present as phenocrysts. The La Grille lavas do not have clearly defined variation trends, and do not fall on control lines to any common basaltic crystalline phase or combination of phases.

6. DIFFERENTIATION OF THE LAVAS

6.1. INTRODUCTION

It was shown in the preceding chapters that, although the Kartala and La Grille lavas were simultaneously active in the same geological setting, each has its own distinctive lava chemistry. The origin of these chemical differences will be discussed in Chapter 7, and the purpose of the present chapter is to examine possible causes of variation within each group of lavas. Before discussing these variations specifically, it is convenient at this point to consider possible effects of contamination from the silicic rocks through which these lavas must have passed.

The sandstone inclusions in the lavas show petrographic indications of reaction with the lavas (Chapter 2), and this presumably has some effect on the lava chemistry. Such effects must be minor, however, since the trace element concentrations in an arkosic sandstone from Moheli (Table C-5) do not show any consistent relation to those of either the Kartala or La Grille lavas, nor do the Rb/Sr or K/Sr ratios (cf. Green and Ringwood, 1967, Table 21) show any indications of crustal contamination (Table 15). Furthermore, the concentrations of rare-earth elements (Fig. 25) appear to be higher in La Grille than Kartala lavas and have similar distributions in both. This is contrary to what should result from crustal contamination (cf. Haskin and Gehl, 1962). Crustal contamination is consequently dismissed as unimportant as a cause of the chemical variations in the lavas of Grande Comore.

Table 15

Average K/Sr and Rb/Sr in Kartala and La Grille lavas

	K/Sr	Rb/Sr
Kartala lavas	21	0·056
La Grille lavas	16	0·067
* Crust-contaminated lavas	31 - 88	0·12 - 0·4
* Mantle-contaminated lavas	10 - 22	0·015 - 0·07

* Green and Ringwood (1967, Table 21).

6.2. DIFFERENTIATION OF THE KARTALA LAVAS

The phenocryst assemblages in the Kartala lavas (Table B-1) are as follows:

olivine

olivine + augite

olivine + augite + plagioclase

olivine + plagioclase

augite + plagioclase

These are set in a groundmass of olivine + augite ± plagioclase ± glass + opaque oxides. The order of crystallization appears to have been olivine → augite → plagioclase → opaque oxides, and the ubiquitous presence of groundmass olivine shows that it is not involved in any reaction relation - as the phenocryst assemblage augite + plagioclase might suggest. The abundance of olivine and augite phenocrysts in many of the lavas makes these phases important contributors to the overall chemical variation.

The most basic analysed aphyric lava from Kartala is glassy spatter from the Haboho cinder cone (No. 142, Table C-1), containing 7·0% MgO. Lavas with higher MgO contents show a continuous increase in ferromagnesian phenocryst content with rising MgO. This can be seen from the histogram of phenocryst content versus MgO (Fig. 28b) or the plot of olivine phenocryst content against normative olivine (Fig. 29b). It has also been shown (Section 5.2.3.) that the variation trends for all elements in these lavas fall on what are inferred to be "control lines" from points on the olivine-augite join.

A reasonable explanation of these features is that they result from crystal-liquid fractionation, a process well-established for at least one other volcano (Murata and Richter, 1966a, b). It is hereafter considered that those lavas more basic than No. 142 have been enriched in variable amounts of cumulus olivine and augite, and that the less basic magmas were impoverished in these phases. The faintly linear trends in these less basic lavas appear to result from augite fractionation.

In order to estimate the physical conditions under which fractional crystallization of the Kartala lavas took place, their compositions have been projected on planes within the "C.M.A.S. system" (Fig. 30), as described by O'Hara (1968) and Jamieson (1969, 1970). These diagrams have a considerable advantage over other diagrams in that most components of a rock analysis are used in the projections. Although there is a slight disadvantage that variations in ratios such as FeO/MgO or Na_2O/CaO are lost, this can be remedied by contouring the diagrams with any such parameter which may be important.

Fig. 28.

Histogram of phenocryst distribution as a function
of MgO content in (a) La Grille and (b) Kartala lavas.

■ = Olivine

▨ = augite

☐ = plagioclase
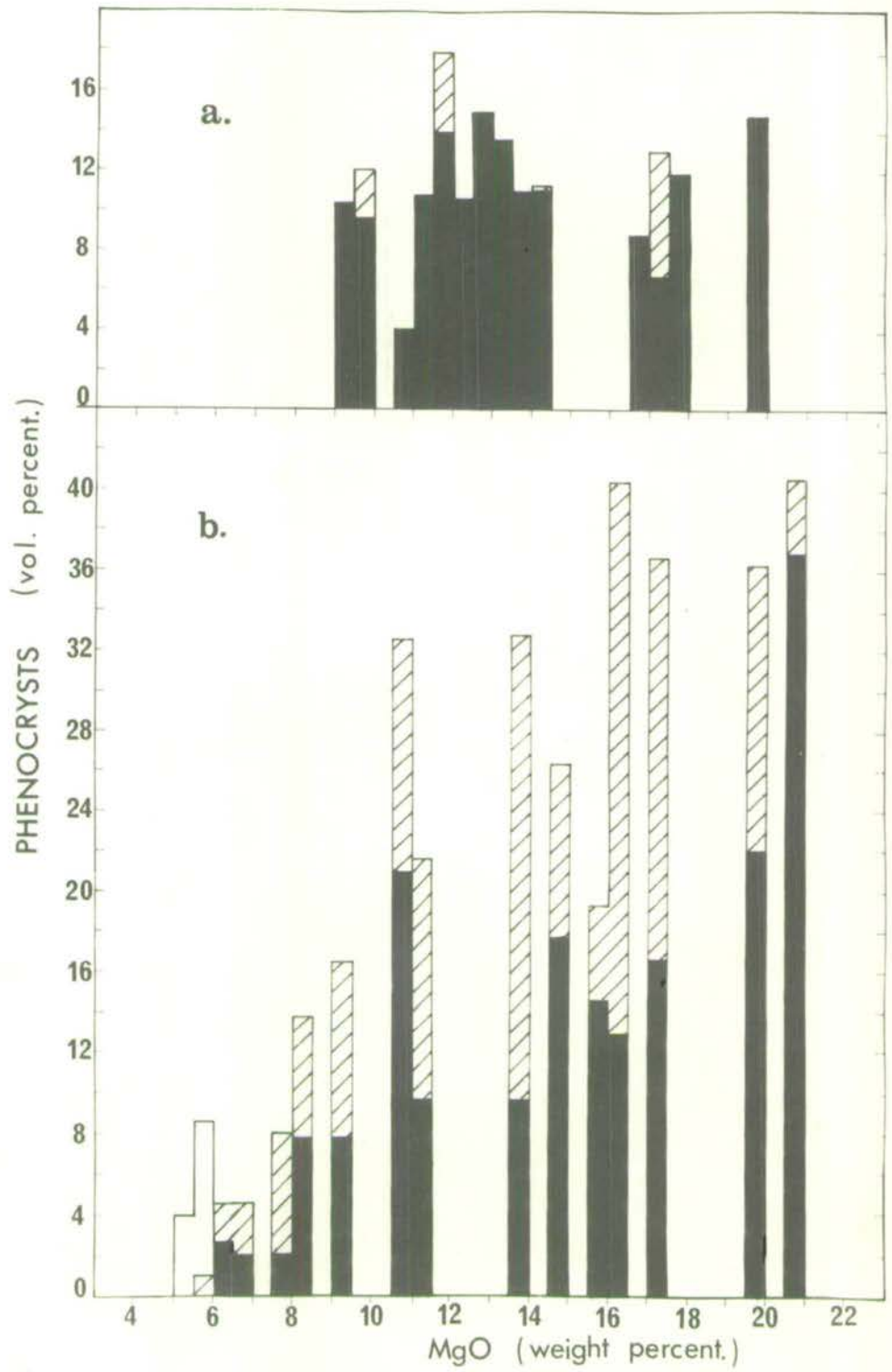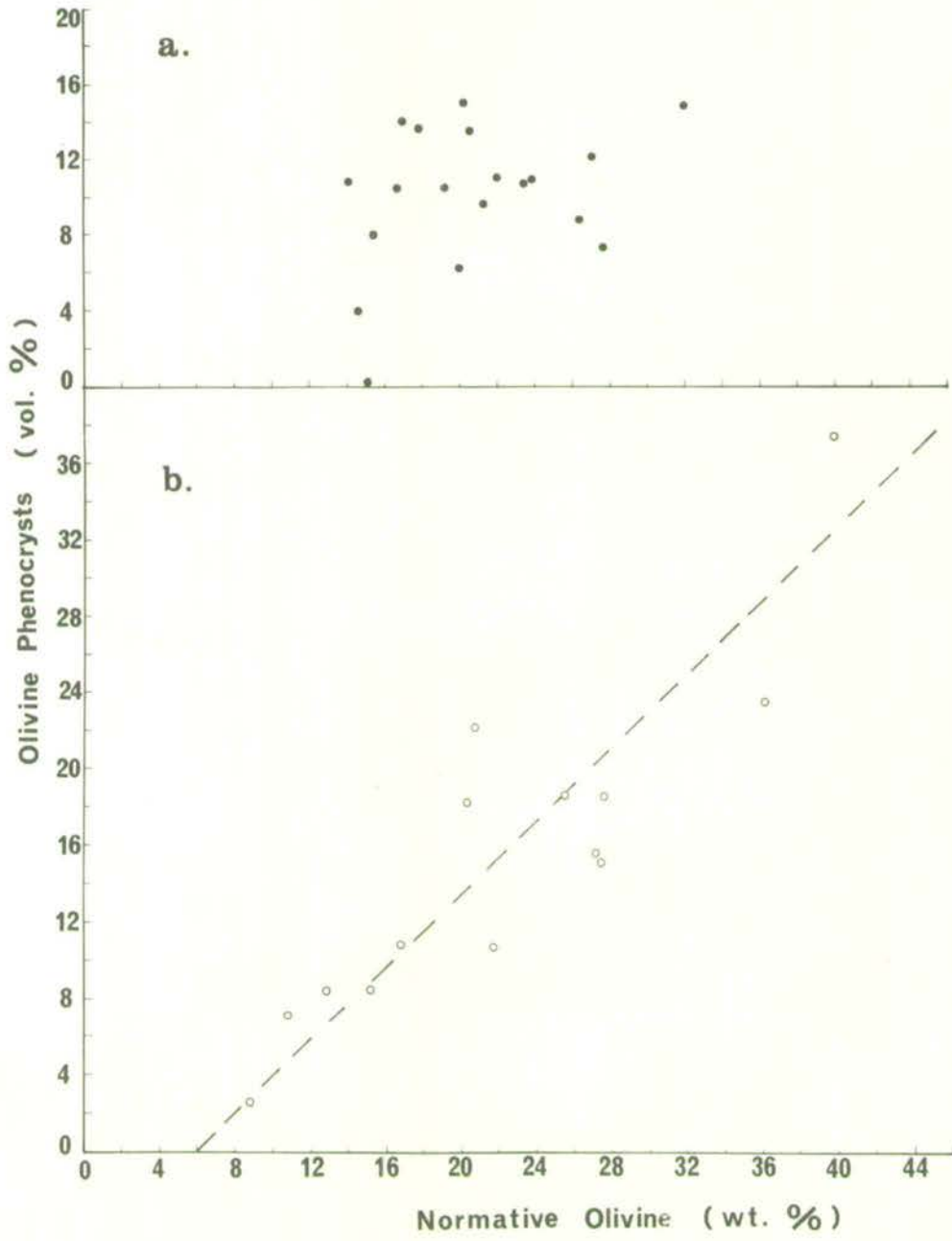
The phase boundaries shown in Fig. 30, and subsequent diagrams, were constructed by O'Hara (1968, Figs. 4 to 6) from melting experiments on natural and complex synthetic compositions. These phase boundaries are accepted by the present writer as essentially correct, since it seems unlikely that such consistent results could otherwise be obtained from so many independent workers (see O'Hara, 1968, p. 85).

From the correspondence between the aphyric lava compositions and the atmospheric pressure cotectics in Fig. 30, it is concluded that crystallization of these lavas has taken place at very shallow depths, probably less than 10 km. This agrees with the suggestion from structural considerations (Section 2.7.2.) that the Kartala caldera resulted from stresses applied (at the tops of magma chambers) at depths of 5 km or less. One might visualize the collection and crystallization of magma similar to No. 142 in a plexus of shallow magma chambers beneath Kartala, similar to the situation outlined for Kilauea by Fiske and Kinoshita (1969).

Although it is unlikely that the full range of Kartala lavas were formed by the fractional crystallization of one unique "parent magma" (cf. O'Hara, 1965), it will be assumed in further discussions that the range of "parent magmas" that ascended into shallow magma chambers can be adequately represented by the most basic liquid, No. 142. This assumption at least avoids the errors inherent in calculating an average, although the reader may want to refer to the average composition of Kartala lavas given in Appendix D. The composition of No. 142, recalculated water-free, is given in Table 16.

Fig. 30.

Projections of Kartala lava compositions in the C.M.A.S. pseudo-quaternary system (after O'Hara, 1968; Jamieson, 1968, 1970).

C = (mol. prop. $CaO - 3\frac{1}{3}P_2O_5 + 2Na_2O + 2K_2O$) x 56·08.

M = (mol. prop. $FeO + MnO + NiO + MgO - TiO_2$) x 40·31.

A = (mol. prop. $Al_2O_3 + Cr_2O_3 + Fe_2O_3 + Na_2O + K_2O + TiO_2$) x 101·96.

S = (mol. prop. $SiO_2 - 2Na_2O - 2K_2O$) x 60·09.

Inserts show planes of projections.

a. Projection from diopside onto C_3A - M - S (wt %).

b. Projection from olivine onto CS - MS - A (wt %).

Phase boundaries are for atmospheric pressure.

O = aphyric lavas;

■ = No. 142 (Table 16);

▽ = olivines (Table 4);

▲ = diopside-plagioclase piercing point (a), and olivine-plagioclase piercing point (b);

□ = cumulus-enriched lavas;

▼ = augites (Table 6).

a.

S

MS
M₂S
A
C — Cpx
M

MS (opx)

65

HYPERSTHENE GABBRO THERMAL DIVIDE (cpx – opx – plag)

Opx

Plag
Ol

OS

50

OLIVINE GABBRO THERMAL DIVIDE (cpx – ol – plag)

M₂S (ol)

40

C₃A
M

40
20

30
30

20
40

10
50

M

b.

S
A
CS   Di   MS
M₂S
C
M

40

OA

30

Pyrope

20

Plag
Cpx   Opx

OLIVINE GABBRO
THERMAL DIVIDE
(cpx – ol – plag)

10

MS (opx)

CS

80

60   Di

40

20
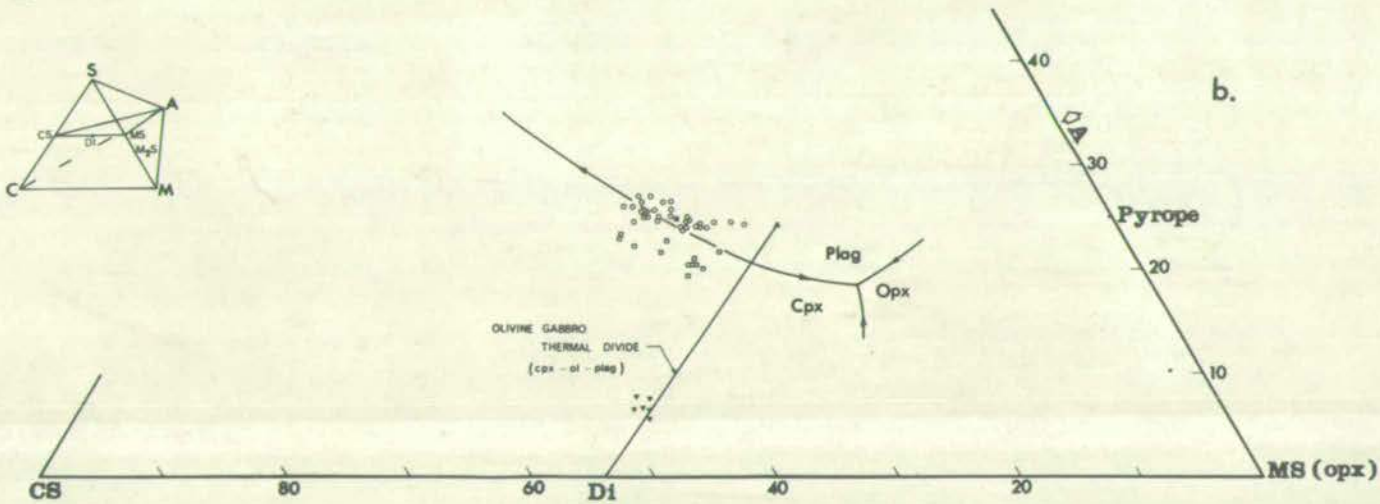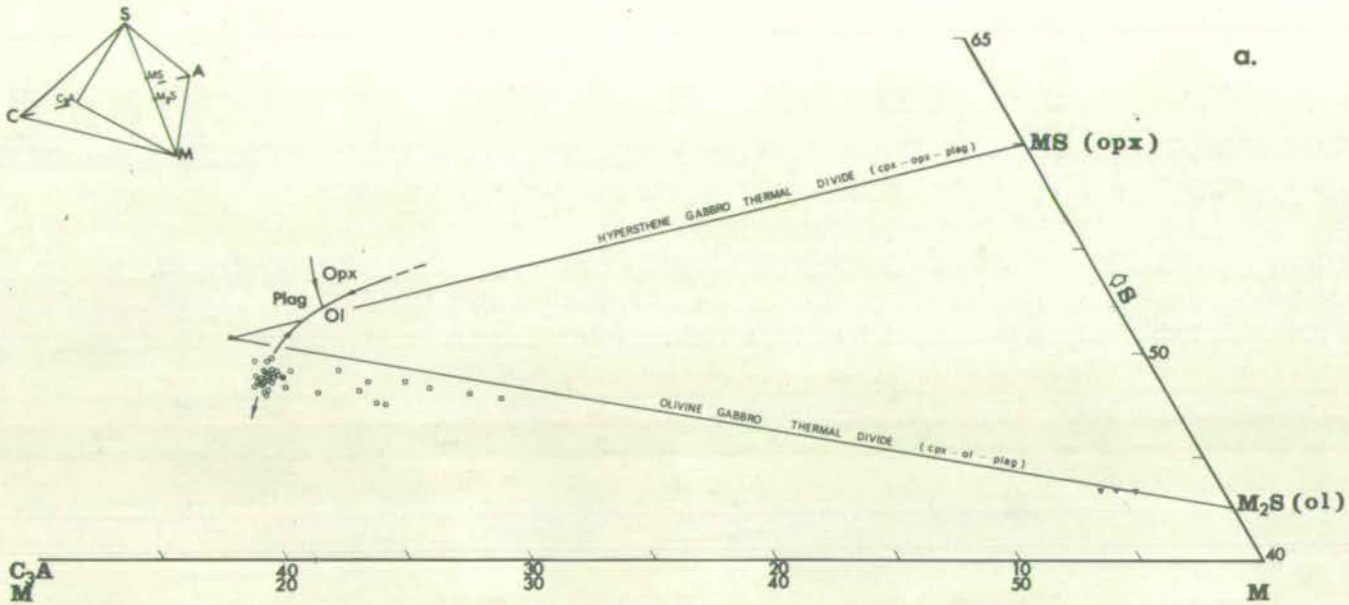
6.3. DIFFERENTIATION OF THE LA GRILLE LAVAS

The La Grille lavas, like those of Kartala, show a range of phenocryst content (0 to 19 vol. %) and MgO content (9·5 to 20·0 wt. %). It must be noted, however, that some olivine phenocrysts are skeletal and presumably crystallized from the liquid, some are xenocrystal and therefore added to the liquid, and some are euhedral and may have either or both these origins. Thus, it is difficult to evaluate the extent to which crystal-liquid fractionation has contributed to the overall chemical variation in these lavas. This is especially so because, unlike the Kartala situation, there is no obvious correlation between phenocryst and MgO content (Fig. 28a), normative olivine content (Fig. 29a) or any other chemical parameter determined in the present study. Furthermore, the La Grille chemical trends are poorly defined, with substantial scatter for most elements (see Figs. 13 and 23).

Although it is clear that the olivine phenocrysts alone do not control the chemical variation in La Grille lavas, they must nevertheless make some contribution to it. The La Grille lavas might therefore be thought of as falling on a series of olivine control lines which are offset by some additional process. If, as in the Kartala lavas, there is a simple addition-subtraction relation between phenocrysts and lava chemistry, one should be able to determine this secondary trend by recalculating the lava chemistry on a phenocryst-free basis. The results of this calculation for SiO_2/MgO are shown in Fig. 31, the cloudiness of which indicates the absence of such a simple relation. It must be concluded that a large proportion of the "phenocrysts" in La Grille lavas are non-fractionating

Table 16.

Representative lava compositions (recalculated to 100% water-free)

wt %	Kartala (No.142)	La Grille (average)	La Grille/Kartala
SiO_2	47·2	43·6	0·93
TiO_2	2·65	2·01	0·76
Al_2O_3	14·4	12·1	0·84
Fe_2O_3	1·51	3·06	2·02
FeO	10·8	8·8	0·81
MnO	·20	·21	1·05
MgO	7·1	13·4	1·89
CaO	11·2	12·1	1·08
Na_2O	2·98	2·88	0·97
K_2O	1·40	1·14	0·82
P_2O_5	·51	·56	1·10
Or	7·43	6·74	0·91
Ab	11·89	2·54	0·21
An	23·22	16·74	0·72
Ne	7·76	11·84	1·52
Di	25·55	31·78	1·24
Ol	15·39	20·77	1·35
Mt	2·28	4·44	1·95
Ilm	5·23	3·82	0·73
Ap	1·26	1·33	1·05
Rb	30	40	1·33
Cu	69	78	1·13
Sr	538	608	1·13
Ba	467	711	1·52
Zn	109	92	·84
Zr	217	188	·87

phenocrysts, and that the bulk chemistry might represent original liquid compositions.

Projections of the La Grille lavas in the C.M.A.S. system (Fig. 32) retain the cloudiness shown in the variation diagrams (esp. Fig. 32a). The elongation of the trend away from orthopyroxene in Fig. 32b has no petrological significance, being the result of distortion caused by the obliquity of the plane to the olivine projection lines (see insert in Fig. 30b). There is no correspondence between the compositions of these lavas and the low pressure cotectics, and it is concluded that the chemistry of the La Grille lavas cannot therefore be explained by any low-pressure fractionation processes. It follows that some high-pressure process must be responsible, except for the relatively insignificant effects due to near-surface fractionation of olivine phenocrysts. It will be the purpose of the following chapter to try to elucidate the nature of such processes.

Because of the lack of correlation between phenocryst content and chemical composition, one cannot assume that the most basic La Grille aphyric lava (No. 178, with 11·0% MgO) represents any unique liquid composition. For example, No. 54, recalculated as phenocryst-free, contains 13·5% MgO, and this must be taken as representative of the groundmass (liquid) composition of this rock. However, the apparently normal distribution of both chemical compositions (Figs. 13 and 21) and phenocryst contents (Fig. 9) of these rocks indicates that an average composition can probably be taken as representative of the overall chemistry. This average is given in Appendix D, and recalculated as water-free in Table 16.
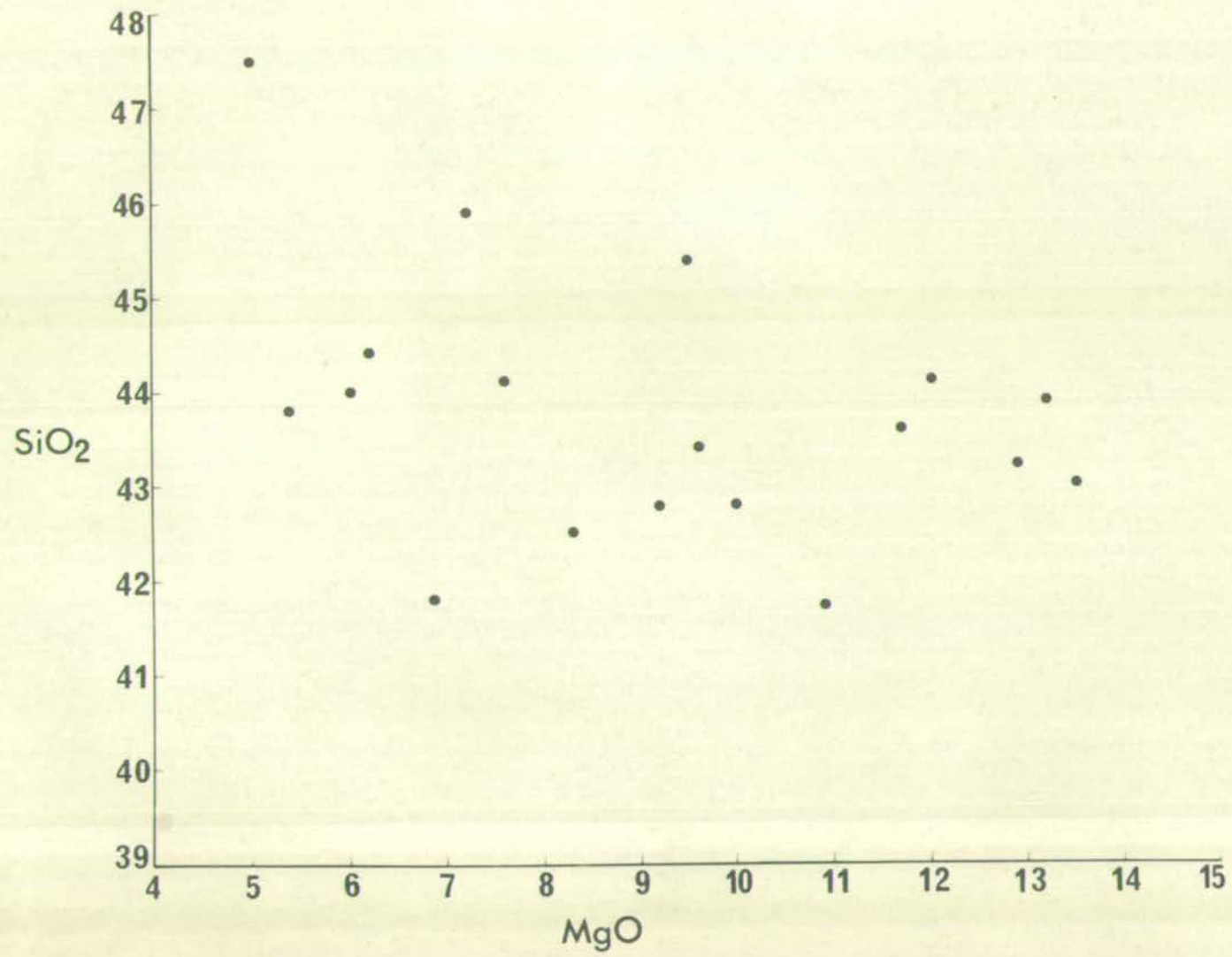
Fig. 32.

Projections of La Grille lava compositions
in the C.M.A.S. system.

See Fig. 30 for details of method.

a. projection from diopside onto C_3A-M-S (wt.%)

b. projection from olivine onto CS-MS-A (wt.%).

The thin dashed lines enclose fields of Kartala lavas.

a.

Opx

⬦B

CPX - OPX - PLAG

65

50

opx   1 ATM.

plag   ol   5 KB   15 KB   20 KB   30 KB

pl   opx

sp   gr   ol

sp

CPX   OL   PLAG

Ol

40

C₃A   40   30   20   10   M

b.

⬦A

40

Py   30

pl   sp   15 KB   20

cpx   sp   sp   ol   10

gr   30 KB

cpx   pl   1 ATM.   20

cpx   ol

CPX - OL - PLAG

10

CS   80   60   Di   40   20   MS(opx)
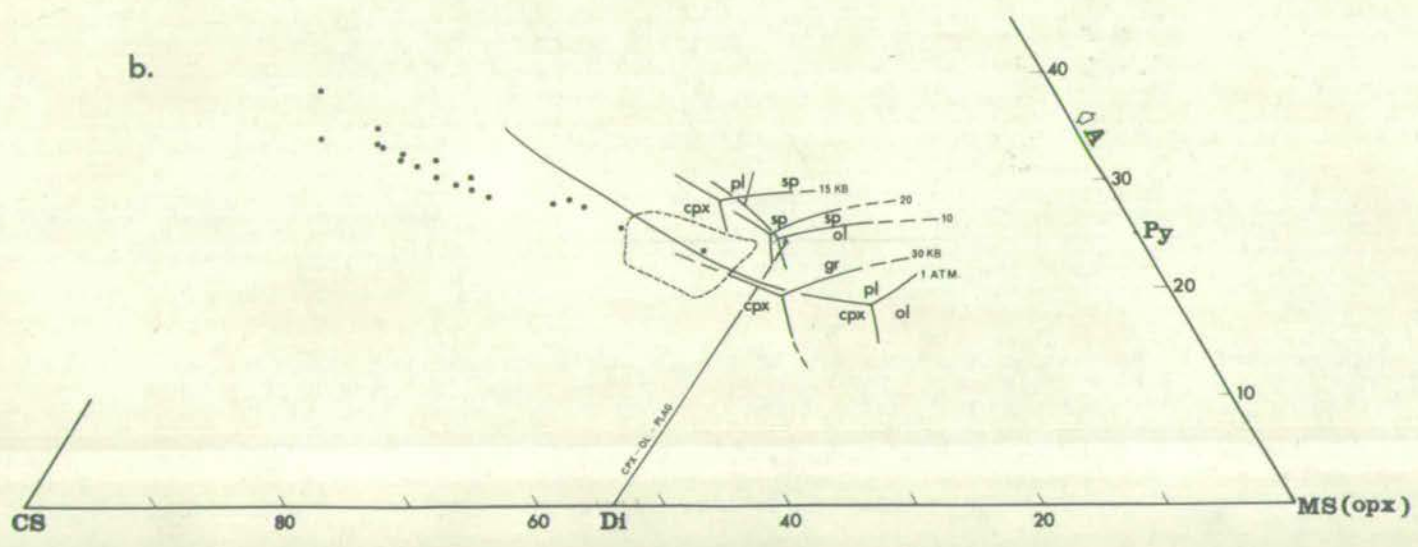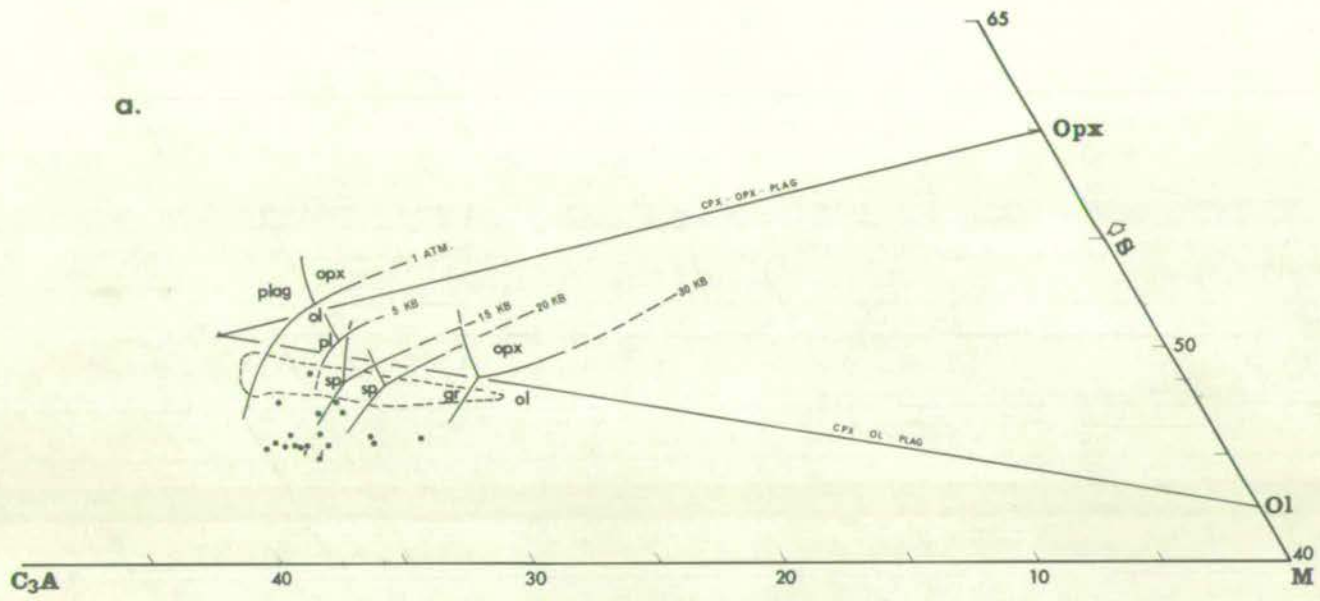
6.4. SUMMARY

Chemical variation within the Kartala lavas is directly attributable to fractional crystallization of olivine and augite in shallow magma reservoirs.

Chemical variation within the La Grille lavas is not explicable in terms of fractional crystallization of the olivine phenocrysts alone, and is thought to result from some additional process operating at high pressures.

7. FORMATION OF THE LAVAS

7.1. INTRODUCTION

Assuming that the lavas of Grande Comore originate by partial melting of the upper mantle, a knowledge of the composition and physico-chemical behaviour of the upper mantle is essential in the understanding of their petrogenesis.   The purpose of this chapter is to suggest a reasonable composition for the upper mantle, and outline means by which these lavas could have been produced from it.

7.2. UPPER MANTLE COMPOSITION

7.2.1. Major elements

It is known that various physical properties of the upper mantle are consistent with hypotheses that it consists of peridotite, eclogite, or some combination of both (e.g. Birch, 1960; Simmons, 1964).   Recent studies by Press (1969) favour the suggestion that eclogite compositions are predominant, at least in the sub-oceanic mantle.   However, experimental petrologists (e.g. Yoder and Tilley, 1962; Green and Ringwood, 1967) have argued strongly against an eclogitic upper mantle, devoting most of their attention to the experimental study of peridotite compositions.

Theoretical estimates of the upper mantle composition have also been based on terrestrial heat flow data and the cosmic abundance patterns of the elements (Macdonald, 1959; Urey, 1952; Hurley, 1957, 1968a, b; Lovering, 1958; Clark and Ringwood, 1964). However, the results of such estimates must be treated with caution, since they are entirely dependent upon the initial assumptions made.   For

example, the interpretations of terrestrial heat flow data would differ according to whether or not one assumed mantle convection. The validity of meteorite analogies depends, not only on whether representative meteorite compositions are obtainable, but more importantly on whether primitive solar abundances were maintained during earth formation.   This, in the opinion of, for example, Turekian and Clark (1969) is likely not to have been so.

Some petrologists consider the relative abundances of different ultrabasic inclusions in basic lavas and kimberlites to be indicative of their abundance at depth, and consequently a reflection of mantle composition (Harris, et al., 1967; Davidson, 1967; O'Hara, 1967, 1968; O'Hara and Yoder, 1967; Kutolin, 1970).   Such arguments, like those based on meteorite analogies, must be treated with caution. For instance, O'Hara (1967, p. 347) concludes that crystal cumulates in basalts "can be expected to occur alone and more frequently (than unmodified mantle fragments) because of their greater availability and the smaller increase in rate of flow necessary for the elutriation of such loosely attached material".   In contrast, Harris et al. (1967, p. 6361) argue that the nodules cannot be cumulates because their mineral compositions are different from those in basalts, and the nodules are similar in composition and mineralogy irrespective of the rock type in which they occur.

An alternative approach to obtaining information on mantle composition from the basaltic lavas and ultrabasic inclusions involves the determination of their phase relations under probable mantle conditions, in order to show which inclusions, if any, are capable of yielding basaltic liquids upon partial melting.   It has been shown

that basaltic liquids can be derived from a range of basic and ultra-
basic rocks, including gabbro, eclogite, pyroxenite, amphibolite,
pyroxene amphibolite (Yoder and Tilley, 1962), spinel lherzolite
(Kushiro, et al., 1968) garnet lherzolite (O'Hara and Yoder, 1967),
and a variety of synthetic peridotites (Bowen and Schairer, 1935;
Reay and Harris, 1964; Green and Ringwood, 1967).

Some of the petrogenetic hypotheses formulated as a result of
these studies appear to have exceeded the limits of what can be
deduced from the experimental data, and are consequently difficult to
evaluate until further experimental data become available. Examples
include hypotheses involving wall-rock reaction (Harris, 1957; Green
and Ringwood, 1967; Kushiro, 1968), or volatile transport (Bailey,
1964), which are to be entertained only after eliminating the re-
latively simpler hypotheses involving partial melting or fractional
crystallization.

From phase diagrams constructed in the C.M.A.S. system O'Hara
(1968, 1970) dismissed many lherzolites, including the various
"pyrolites" of Green and Ringwood (1967), as possible mantle compo-
sitions on the grounds that their Al/Ca ratios were too low to yield
the harzburgites and garnet harzburgites commonly found as inclusions
in kimberlites. He concluded that in this respect only the garnet
lherzolite inclusions found in kimberlite could be considered as
possible unmodified mantle material, a result supported by the
statistical approach of Harris, et al. (1967).

However, the arguments advanced by O'Hara for making this choice
of mantle composition are critically dependent upon the position and

orientation of the crystal-liquid control plane relating to
partial melting of a 4-phase peridotite in the phase diagrams used.
This plane shifts with pressure, with composition of the residual
crystals (orthopyroxene in particular), and with fractional melting
(cf. Presnall, 1969).   Since the extent and nature of such shifts
are not well-defined by existing data, O'Hara's conclusions cannot
be accepted in detail.   In fact, there appears to be no compelling
reason to reject any of the garnet peridotites plotted by O'Hara
(1968, Figs. 4, 5 and 6) as possible compositions of unmodified
mantle peridotite.   This being so, the average of 15 garnet perido-
tite analyses given by Carswell and Dawson (1970, Table 3) is taken
as representative of the major element composition of unmodified
mantle peridotite (see Table 17), although it is realized that this
is only a first approximation, since the upper mantle may in fact
be chemically inhomogeneous.

7.2.2. Trace elements

As the partition coefficients between crystals and liquid are
unknown for trace elements at high pressures, one can only speculate
as to their behaviour during partial melting of the upper mantle.
Gast (1968) and Griffen and Murthy (1969) have indicated that Ba,
Sr, K, and Rb are highly concentrated in the liquid phase during the
initial stages of partial melting of peridotitic compositions. This,
by definition, is true of any incompatible element.   Consequently,
any mantle fragment brought up as xenolithic material would be
severely depleted in incompatible elements if it had undergone only
very little partial melting, and any such xenoliths have little chance

of revealing true mantle concentrations.   On the other hand, there is also a chance of these inclusions being contaminated by the enclosing magma, with a resulting increase in the concentrations of incompatible elements, especially in the case of kimberlitic magmas which are highly enriched in these elements (cf. Harris and Middlemost, 1970). For example, the secondary phlogopite in many inclusions (see Nixon, et al., 1963; Carswell and Dawson, 1970) must reflect the addition of K.   Even if data existed for inclusions without secondary phlogopite, carbonate, or serpentinite, it could still not be trusted with regard to the incompatible elements which do not form a discreet phase (cf. Griffen and Murthy, 1969, pp. 1395-1396).   One is consequently left with the alternative of making some hypothetical estimate of the concentrations of incompatible elements in the upper mantle.

The concentrations of K, Rb, Sr, and Ba accepted by the present writer as representative of the upper mantle are given in Table 17. These were calculated by Griffen and Murthy (1969, Table 6) from concentrations in the individual minerals of garnet peridotite, which were combined in the proportions of olivine, 65%:clinopyroxene, 12%: orthopyroxene, 13%:garnet, 10%, as calculated for the average garnet lherzolite by Harris, et al. (1967), assuming the absence of hydrous phases such as phlogopite or amphibole.   The concentrations of Zr, Zn, and Cu (Table 17) are taken from Vinogradov (1962), and represent a variety of ultrabasic rock types.

Table 17

Hypothetical upper mantle garnet peridotite composition (after Carswell and Dawson (1970, Table 3).

wt. %	
SiO_2	46·10
TiO_2	·26
Cr_2O_3	·35
Al_2O_3	2·16
Fe_2O_3	2·42
FeO	4·40
MnO	·11
NiO	·31
MgO	41·95
CaO	1·64
Na_2O	·17
K_2O	·15
P_2O_5	·02

ppm		
K	106	*
Rb	0·48	*
Sr	15·0	*
Ba	14·0	*
Zr	30	+
Zn	30	+
Cu	20	+

* Griffen and Murthy (1969, Table 6).

+ Vinogradov (1962).

Table 18

Enrichment of minor and trace elements relative to the postulated upper mantle concentrations.

wt. %	Conc. Mantle	Kartala (No.142) Conc.	E	La Grille (mean) Conc.	E
TiO_2	0·26	2·61	10	2·00	8
P_2O_5	0·02	0·52	26	·56	28
Na_2O	0·17	2·96	17	2·86	17
ppm					
K	106	11,450	108	9,296	88
Rb	0·48	30	63	40	83
Sr	15	530	35	600	40
Ba	14	460	33	703	50
Zr	30	213	7	186	6
Zn	30	107	4	90	3
Cu	20	68	3	77	4
*Average		-	47	-	51

wt. %		Kartala (No.18)		La Grille (No.54)	
TiO_2		1·49	6	1·67	6
P_2O_5		·23	12	·55	28
Na_2O		1·56	9	1·88	11
ppm					
K		3,980	37	7,700	73
Rb		10	21	26	54
Sr		245	16	495	33
Ba		200	14	525	37
Zr		110	4	157	5
Zn		104	4	90	3
Cu		73	4	80	4
*Average		-	18	-	39

$$E = \frac{\text{concentration in lava}}{\text{concentration in mantle}} .$$

* TiO_2, Zr, Zn and Cu excluded from calculation of average E.

7.3. ENRICHMENT FACTORS

The enrichment of minor and trace elements relative to the upper mantle is shown for both Kartala and La Grille lavas in Table 18. Using the most basic liquid (No. 142) as representative of Kartala lavas, it is seen that enrichment factors (E) range from 17 (for Na_2O) to 108 (for K), with an average of 47. The enrichment factors for the average of La Grille lavas range from 17 (for Na_2O) to 88 (for K), with an average of 51. The low enrichment factors for TiO_2, Zr, Zn, and Cu (all less than 10) indicate that they cannot be considered as incompatible elements, i.e. they were retained by some solid phase or phases, during the development of these lavas.

If one assumes that the incompatible elements are perfectly incompatible, or even that they have liquid/crystal distribution coefficients greater than 10 (cf. Gast, 1968), the effect of increasing or decreasing the relative proportions of liquid to solid is merely one of dilution or concentration. For example, if the volume of liquid were doubled (by increased partial melting or crystal fractionation), the concentrations of incompatible elements would be halved; if the volume of liquid were halved (by crystal accumulation), the concentrations of incompatible elements would be doubled. These effects can be expressed by the simple equation

$$V = 100/E$$

where V is the volume of liquid remaining after a particular process, and E is the factor by which the incompatible elements are enriched during the process. This equation is used to calculate degrees of partial melting and crystal fractionation in subsequent discussions.

Some indication of the effect of low-pressure crystal accumulation on the enrichment factors of minor and trace elements are given in Table 18 for the most basic lava of each volcano. The average enrichment factor of 18 for the most basic Kartala lava (No. 18, Table 18) corresponds to an accumulation of 58% phenocrysts in a liquid with similar concentrations of incompatible elements to No. 142 (Table 18), as compared to an actual value of 40% phenocrysts in the lava. The average enrichment factor of 39 for the most basic lava of La Grille (No. 54, Table 18) corresponds to a dilution of the average La Grille lava by 25% phenocrysts, as compared to 15% phenocrysts in the lava.

7.4. ORIGIN OF THE KARTALA LAVAS

7.4.1. Introduction

The C.M.A.S. projections of Kartala lavas shown in Fig. 30 (Chapter 6) are schematically reproduced in Fig. 33. As discussed in Section 6.3., the obliquity of projection from olivine onto the plane CS-MS-A causes the projected composition fields to be distorted and elongated in a direction away from MS(orthopyroxene). Therefore, in Fig. 33b, the fields of Kartala aphyric and cumulus-enriched lavas (i.e. those with more than 7·0% MgO) are shown as circles. The diameters of these circles are taken as the width of the elongated fields that are shown in Fig. 30.

The phase boundaries shown in Fig. 33 are taken from O'Hara's (1968) Figs. 4 and 6. The hypothetical mantle composition plotted as M is that given in Table 17. The control planes for advanced partial melting of M are constructed for 15, 20, and 30 kb (Fig. 33b),

and the reader is referred to O'Hara (1970) for a detailed dis-
cussion of such planes. Unfortunately, they cannot be precisely
positioned due, in particular, to a lack of information on
appropriate orthopyroxene compositions, and may be only schematically
correct. The orthopyroxenes used in Fig. 33b to construct the 15
and 20 kb control planes are those coexisting with clinopyroxene and
liquid only (i.e. no olivine) at 13·5 kb, 1290°C and 18 kb, 1335°C,
respectively, as given by Green and Ringwood (1967, Table 9). The
control plane at 30 kb is constructed from O'Hara's (1968) Fig. 5.

7.4.2. Generation of Kartala lavas.

Because of the likelihood that basaltic magmas will fractionate
at least olivine during their ascent (Davis and Schairer, 1965; O'Hara,
1965, 1968), the Kartala magmas at depth may be assumed to have been
richer in normative olivine than any liquids which reach the surface.
Furthermore, they had probably attained their nepheline-normative
character before reaching a depth of about 25 km (equivalent to a
pressure around 8 kb), since the olivine-clinopyroxene-plagioclase
thermal divide is operative at lower pressures (Yoder and Tilley,
1962). Hence, it is reasonable to assume that the Kartala lavas
were derived from more picritic basic magmas formed at pressures
above 8 kb.

It can be seen from Fig. 33 that nepheline-normative magmas
can be produced by direct partial melting at pressures between appro-
ximately 10 and 25 kb. However, Fig. 33b shows that such magmas
will have Al/Ca ratios too high to produce the Kartala lavas without
their being modified by some additional process such as crystal

Fig. 33.

C.M.A.S. projections of the Kartala and La Grille
lava compositions, schematically reproduced from
Figs. 30 and 32.   Phase boundaries from O'Hara
(1968).

Arrows indicate directions of decreasing temperature.

▨   = Kartala aphyric lavas.

▨   = Kartala cumulus-enriched lavas.

◨   = La Grille lavas.

● A,B,etc.= see text.

————— = projections of postulated control planes for
                advanced partial melting of hypothetical upper
                mantle $\underline{M}$ at different pressures.

a.

b.
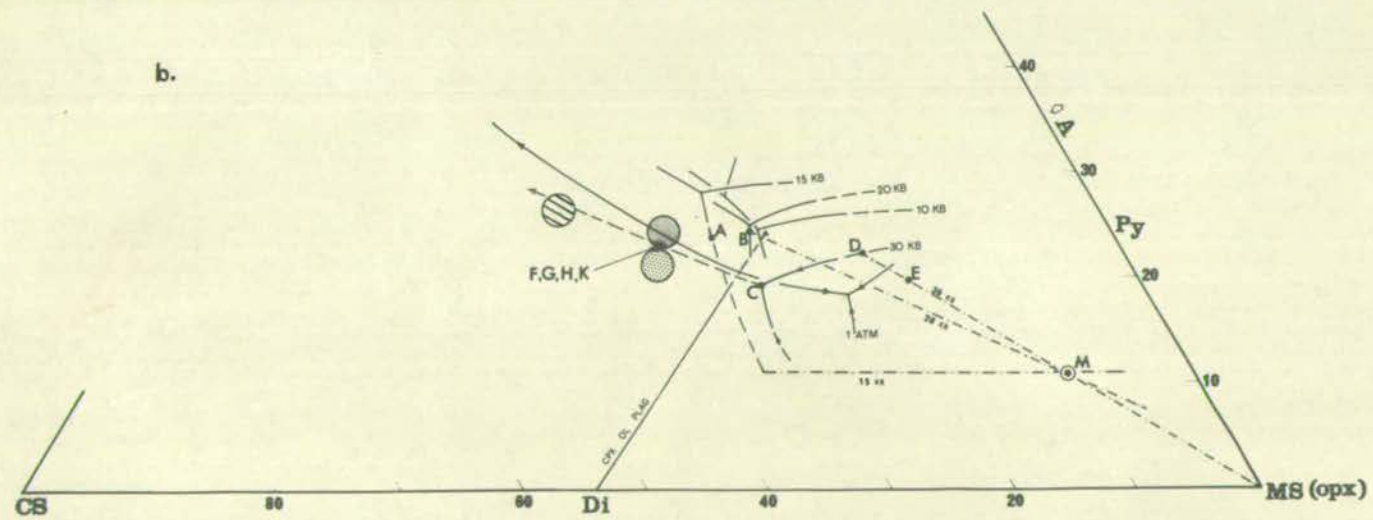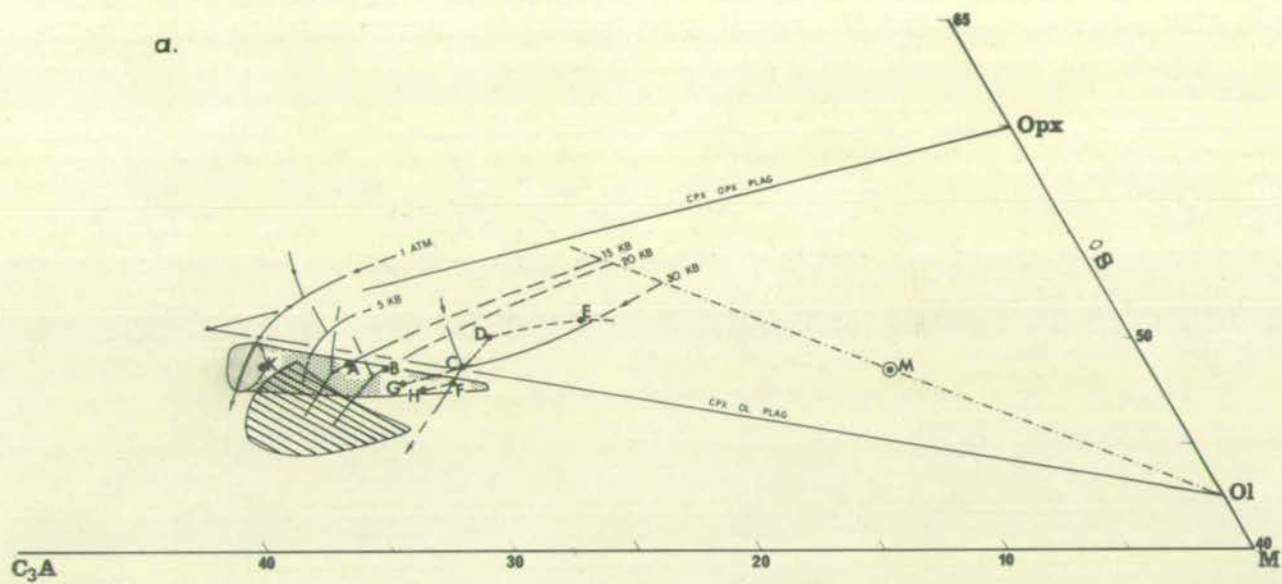
fractionation.   For example, if partial melting were advanced
to the stage where liquids A or B were formed at 15 or 20 kb
respectively (Fig. 33), these liquids could only yield the Kartala
lavas by rapid eruption to pressures close to one atmosphere, where
subsequent gabbro fractionation along the olivine + diopside +
plagioclase + liquid cotectic could yield the appropriate compositions.
However, it has been shown that plagioclase phenocrysts are very
rare in the Kartala lavas, and the trace element and rare-earth
data (Eu in particular) do not suggest that any substantial plagio-
clase fractionation has occurred during their development.

An alternative possibility is that partial melting occurred
at higher pressures, say 30 kb, during which increasingly advanced
partial melting should result in the loss of clinopyroxene (Fig.
33b) followed by the loss of garnet (Fig. 33a).   Because of this
early loss of clinopyroxene, the path of further melting along
C-D-E (Fig. 33b) will not be on the boundary of the diopside primary
phase volume, and therefore cannot be accurately projected in
Fig. 33a.   However, this path is schematically shown as the line
C-D-E in Fig. 33a, and the point E is arbitrarily taken as represen-
tative of a magma produced by advanced partial melting (involving
loss of both clinopyroxene and garnet) at 30 kb.   If this magma were
permitted to fractionate at any pressures above 25 kb, it would
follow a path such as E-D-C-F, fractionating harzburgite from E to
D, garnet harzburgite from D to C, and garnet wehrlite (olivine
eclogite) from C to F.

If olivine undergoes reaction in the equilibrium olivine +

clinopyroxene + garnet + liquid, as suggested by O'Hara and Yoder (1967, p. 106) and O'Hara (1968, pp. 75-76), the residual liquid would follow some path such as C-G or F-H across the garnet + clino-pyroxene + liquid surface (Fig. 33a), i.e. undergo eclogite fraction-ation instead of garnet wehrlite fractionation. Like the path C-D-E, however, the position of the residual liquids resulting from eclogite fractionation is not accurately known, and even if it were, it could not be adequately projected from olivine (Fig. 33b), a phase not involved in the equilibrium. Nevertheless, it is almost certain that either eclogite or garnet wehrlite fractionation at about 30 kb will increase the nepheline-normative character of the liquid, regardless of the exact position of C-G or F-H.

Considering now the effects of polybaric fractionation, as might occur during ascent of these magmas, a variety of fractionation paths are possible. For example, if the rate of ascent were just such that the residual liquid remained on the clinopyroxene + olivine + aluminous phase + liquid cotectic (Fig. 33), there could be a sequence of cumulates consisting of garnet wehrlite or eclogite, followed at lower pressures by spinel lherzolite or spinel wehrlite (or both in sequence), followed at still lower pressures by gabbro. (In this respect, it should be noted that eclogite fractionation need not be isobaric, but merely occurring at pressures above about 25 kb.) Such liquids, however, would not have satisfactory Al/Ca ratios without the gabbro fractionation, a process dismissed above, and such a sequence of events is not considered likely in the case of Kartala lavas.

Alternatively, if the magma was brought rapidly to shallower depths so that it was not capable of maintaining equilibrium with so many solid phases, it would fractionate correspondingly fewer of them, if any. Examples of such extremely rapid ascent with little or no fractionation have been postulated by Clarke (1970) for basalts in the Baffin Bay area, and by Jamieson (1966, 1969) for the Nuanetsi basalts of Rhodesia. With regard to the Kartala lavas, it can be seen from Fig. 33b that they have compositions which lie on the cotectics at atmospheric pressure, at 30 kb, possibly at higher pressures where the positions of phase boundaries are unknown, but not at any intermediate pressures. In this respect they are explicable in terms of fairly rapid ascent from 100 km or more so that they pre-cipitate only olivine or olivine + clinopyroxene (wehrlite), resulting in liquids such as $\underline{K}$ on the low-pressure cotectic (Fig. 33), equivalent in composition to No. 142 (Table 16). Collection of this magma in shallow magma chambers, as proposed in Section 6.2, would permit the precipitation of olivine and augite, producing the range of cumulus-enriched and aphyric lavas presently observed.

There is no difficulty, therefore, in explaining the major element chemistry of Kartala lavas by processes involving anhydrous crystal-liquid equilibria, and it remains to be shown whether the minor and trace element chemistry can be similarly accounted for. It has been proposed by Gast (1968) and O'Hara (1968) that wide ranges in the relative and absolute concentrations of incompatible elements in the liquid phase can be produced by slight variation in the degree of partial melting, especially in the earliest stages of

melting.   Further changes in absolute concentrations can be produced by variable amounts of crystal fractionation.   With such flexibility, one need only assume the appropriate combination of partial melting and crystal fractionation to suit the observed data, and objective evaluations become difficult.

With reference to the enrichment factors shown in Table 18, the following are possible combinations of melting and fractionation, assuming that the liquid $\underline{E}$ (Fig. 33) has similar enrichment factors to No. 18 (Table 18), since it plots in a similar position in Fig. 33. The average enrichment factor of 18 in such a liquid could be produced by, say, 10% partial melting and 50% fractionation of eclogite or wehrlite; or by 5% partial melting and no fractionation; or by 20% partial melting and 75% fractionation.   Subsequent fractionation of 50% olivine $\pm$ augite during ascent would result in the average enrichment factor of 48 found in No. 142 (Table 18).   (See Section 7.3. for the method of calculating these proportions.)

Although any exact estimates of the relative importance of fractional crystallization or partial melting would be impossible, even if high pressure partition coefficients were known exactly (cf. Schilling and Winchester, 1967; Gast, 1968) there is clearly no difficulty in producing the Kartala enrichment factors by these processes.

7.5. ORIGIN OF THE LA GRILLE LAVAS

7.5.1. Introduction

The close proximity of Kartala and La Grille volcanoes, and the overlap of La Grille lava compositions with those of Kartala,

require consideration of the possibility that both groups of lavas have a common origin. Furthermore, the significance of ultramafic inclusions in the La Grille lavas, but not those of Kartala, requires some consideration.

In spite of the overlap in chemistry of the lavas of the two volcanoes, it is useful to emphasize the differences between them. The La Grille lavas are not only more basic in average bulk composition, but the aphyric La Grille lavas are more basic than any from Kartala. This may mean that the La Grille lavas represent a greater degree of melting of peridotitic material in the source region, or that they have undergone less fractionation of ferromagnesian minerals during ascent, or some combination of both. If primarily due to the smaller degree of fractionation, then a faster rate of ascent is implied. Faster ascent of the La Grille lavas is also consistent with the elutriation of the large high density peridotite inclusions which they contain (see Section 3.3.3.) If, as suggested by the vesicle volumes (Fig. 10) and water contents (Fig. 13), there was no significant difference in volatile content of either group of lavas, the gentler slopes of La Grille may also be taken to reflect lower viscosity resulting from higher temperatures, and therefore faster ascent, than the lavas of Kartala.

7.5.2. Generation of La Grille lavas

The La Grille lavas are shown schematically in the C.M.A.S. projections in Fig. 33 following the same procedure to remove distortion from the olivine projection (Fig. 33b) as described for Kartala. Fig. 33 shows that the La Grille major element chemistry

can be derived from the same primary magma as that of the Kartala

lavas by greater fractionation of eclogite or garnet wehrlite

(olivine eclogite) at 30 kb.   Furthermore, eruption at different

stages of this high-pressure fractionation would account for the

overlap of La Grille and Kartala lava chemistry, specimens such as

No. 57 (see Section 5.7.2.) having undergone similar degrees of high-

pressure fractionation to Kartala lavas.   Such a process is con-

sistent with the higher average incompatible element enrichment

factors for the La Grille lavas (Table 18).   The average of 40 for

the most basic La Grille lavas (No. 54, Table 18) compared to 18 for

the most basic Kartala lava (No. 18, Table 18) is equivalent to

correspondingly greater high-pressure fractionation, depending upon

the degree of partial melting.   For example, with 20% partial

melting, 75% crystal fractionation would produce the Kartala enrich-

ment factors, and 87% fractionation would produce the La Grille

enrichment factors. (see Section 7.3. for method of calculation.)

Although this hypothesis is attractive in its simplicity, the

degree of high-pressure fractionation required by the incompatible

element enrichment factors seems excessively large.   It also does

not explain why the two types of lava are erupted from separate

centres 35 km apart.   Thus, it is necessary to subject this hypo-

thesis to a more rigorous test.

As discussed in Section 5.4.1., it is essential to the concept

of incompatible elements that they be excluded from any precipitating

phases, and thus all be passively concentrated in the liquid in equal

proportions, with a resulting linear relation between any two such

elements.   Therefore, if the concentrations of incompatible elements

in La Grille and Kartala lavas differ because of eclogite or wehrlite fractionation, there must be a linear relation between any two of them.

Because Ba has enrichment factors close to the average for each group (Table 18), and because of its importance in discriminating between them (Appendix D), it is used as an index of incompatibility in Fig. 34, in which various trace and minor elements are plotted against it. The same features are seen by plotting, for example, K_2O against each of these elements. This diagram shows that all elements regarded as incompatible in the Kartala lavas have more or less linear distributions (see Appendix D for correlation coefficients), in accordance with the petrogenetic scheme outlined in Section 7.4.2. Although roughly linear distributions are also apparent for the La Grille lavas, they tend to be more scattered than those of Kartala, as also reflected in the lower correlation coefficients (Appendix D). The most important feature of Fig. 34, however, is the offset of the fields for each volcano, showing that the two magma groups cannot be simply related by the high pressure fractionation of any minerals towards which these elements were behaving in an ideally incompatible manner. Neither does the scatter of points within the La Grille fields appear to be explicable in terms of the fractionation of such phases. It seems necessary, therefore, to investigate processes of deriving the La Grille lavas independently from those of Kartala, as one would have expected from their geographical separation.

It has been shown by Gast (1968) that a range of enrichment factors is possible for Ba, Sr, Rb, and K during the initial stages of

Fig. 34.

Concentration of some minor and trace elements
vs. Ba in Kartala and La Grille lavas.

    ○   = Kartala

    ●   = La Grille
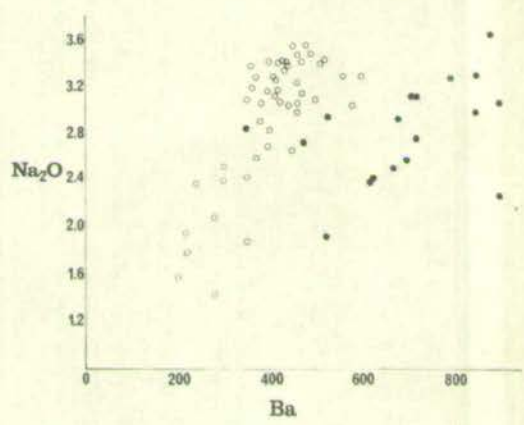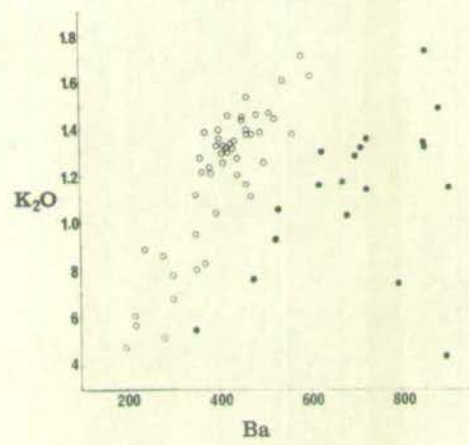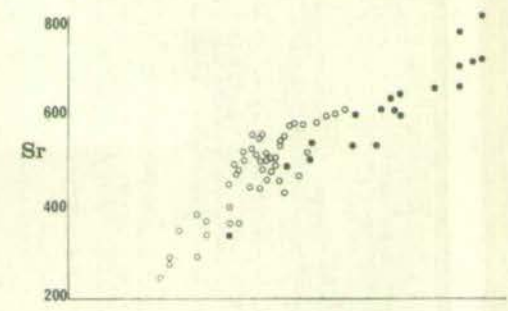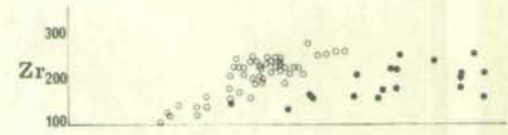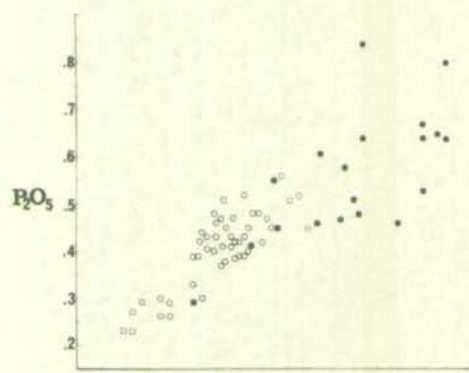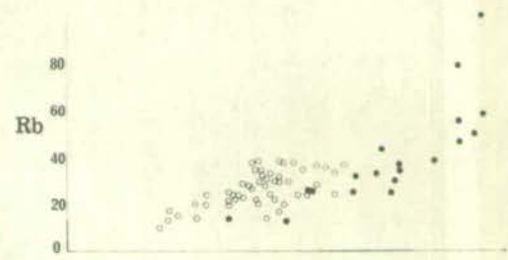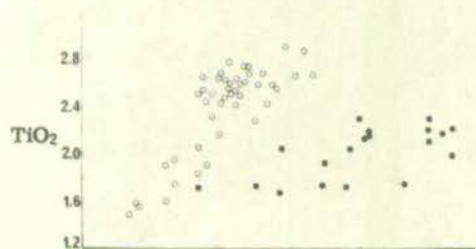
partial melting, i.e. before they are completely concentrated in the melt. With up to 10% partial melting, these enrichment factors are independently variable to a much greater degree than they are with more advanced melting and resulting greater dilution. Thus, with such low degrees of partial melting, no definite relation between any two incompatible elements can be predicted. Consequently, the La Grille lavas could have obtained their imprint of incompatible elements during the initial stages of partial melting (less than 10%), resulting in the apparently random scatter observed in diagrams such as Fig. 34.

Other processes involving fractionation or partial melting of hydrous phases such as phlogopite or amphibole have also been considered. These have been rejected, however, because the available trace element concentrations in such phases are not suitable, as outlined in detail by Gast (1968) and Wood (1968) (see Section 1.2.3.). Although there is no experimental data available regarding the effects of volatiles on trace elements, the available data for major elements (e.g. Morey and Hesselgesser, 1951; Luth and Tuttle, 1968), especially the SiO_2 - rich nature of vapours in equilibrium with silicates and silicate melts, suggest that volatiles were not important in the generation of these lavas. The hypotheses involving wall-rock reaction (Green and Ringwood, 1967; Kushiro, 1968; Harris, 1957) are regarded as even more untestable than volatile transport, and cannot be dismissed or accepted on completely objective grounds. However, the inferred faster rate of ascent of the La Grille lavas suggests that they would have lower enrichment factors than those of Kartala if wall-rock reaction during ascent had been the dominant

process dictating their final trace element contents.

7.6. PETROGENETIC SUMMARY

In the light of the above analysis of the chemistry and petrography of the Kartala and La Grille lavas, and accepting the phase diagrams constructed by O'Hara (1968), the following sequence of events, outlined in Fig. 35, seem to be reasonable explanations of their petrogenesis.

7.6.1. Kartala lavas

1. Partial melting of upper mantle of approximate composition M, at pressures of 25 kb or more, to form liquids represented by composition E, i.e. with more than 10% partial melting.

2. Removal of liquid from equilibrium with mantle material, e.g. by coalescence into large pockets or gradual ascent.

3. Cooling of these liquids at pressures above 25 kb so that they might fractionate any or all of the following: harzburgite along E-D, garnet harzburgite along D-C, and either garnet wehrlite along C-F or eclogite along some path such as C-G-Y or F-H-Z.

4. Interruption of this essentially isobaric fractionation by rapid upward migration of magma, at such a rate as to prevent the precipitation of garnet or spinel, while olivine and possibly clinopyroxene do precipitate and sink, producing liquids of composition K.

5. Collection and cooling of K in shallow magma reservoirs to precipitate olivine and augite, resulting in the cumulus-enriched and complementary aphyric lavas that reach the surface.

7.6.2. La Grille lavas

1. Partial melting of upper mantle of approximate composition $\underline{M}$ at pressures of 25 kb or more, yielding liquids of composition $\underline{C}$, i.e. with less than 10% partial melting.

2. Cooling of this liquid at similarly high pressures to fractionate the following: garnet harzburgite at $\underline{C}$, garnet wehrlite along $\underline{C-F-X}$ or eclogite along $\underline{C-G-Y}$ or $\underline{F-H-Z}$.

3. Interruption of this essentially isobaric fractionation at different stages by rapid upward migration of the liquids, during which olivine, clinopyroxene, orthopyroxene and spinel are precipitated in variable proportions, some being retained as the ultrabasic inclusions (wehrlites, lherzolites, and dunites) that are found in the La Grille lavas.

Fig. 35.

Schematic representation in the C.M.A.S. system of
the postulated sequence of processes involved in the
development of Kartala and La Grille lavas.

Thin solid arrows represent compositional changes
in the magmas resulting from polybaric fractionation
(see text for phases involved) during ascent.

Thin dashed arrows represent compositional changes
in the magmas caused by low pressure fractionation
and accumulation of olivine and augite during ascent.

Other lines and symbols as for Fig. 33.

BIBLIOGRAPHY

Abbott, M.J., 1969. Petrology of the Nandewar volcano, N.S.W., Australia. Contr. Mineral. and Petrol. 20, 115-134.

Bailey, D.K., 1964. Crustal warping - a possible tectonic control of alkaline magmatism. J. geophys. Res. 69, 1103-1111.

Baker, I., 1969. Petrology of the volcanic rocks of Saint Helena Island, South Atlantic. Bull. geol. Soc. Am. 80, 1283-1310.

Baker, P.E., Gass, I.G., Harris, P.G. and LeMaitre, R.W., 1964. The volcanological report of the Royal Society expedition to Tristan da Cunha, 1962. Phil. Trans. R. Soc., A 256, 439-578.

Birch, F., 1960. The velocity of compressional waves in rocks to 10 Kilobars. J. geophys. Res. 65, 1083-1102.

Bowen, N.L. and Schairer, J.F., 1935. The system $MgO-FeO-SiO_2$. Am. J. Sci. 229, 151-217.

Boyd, F.R., England, J.L. and Davis, B.T.C., 1964. Effects of pressure on the melting and polymorphism of enstatite, $MgSiO_3$. J. geophys. Res. 69, 2101-2109.

Brown, G.M., 1967. Mineralogy of basaltic rocks, pp. 103-162, in Basalts: the Poldervaart Treatise on rocks of basaltic composition, eds. Hess, H.H., and Poldervaart, A., N.Y.: Interscience.

Bryan, W.B., 1967. Geology and petrology of Clarion Island, Mexico. Bull. geol. Soc. Am. 78, 1461-1476.

Carswell, D.A. and Dawson, J.B., 1970. Garnet peridotite xenoliths in South African kimberlite pipes and their petrogenesis. Contr. Mineral. and Petrol. 25, 163-184.

Chayes, F., 1964. Variance-covariance relations in some published Harker diagrams of volcanic suites. J. Petrology 5, 219-237.

Clark, S.P. and Ringwood, A.E., 1964. Density distribution and constitution of the mantle. Rev. Geophys. 2, 35-88.

Clarke, D.B., 1970. Tertiary basalts of Baffin Bay: possible primary magma from the mantle. Contr. Mineral. and Petrol. 25, 203-224.

Coombs, D.S., 1963. Trends and affinities of basaltic magmas and pyroxenes as illustrated on the diopside-olivine-silica diagram. Spec. Pap. miner. Soc. Am. 1, 227-250.

Coombs, D.S. and Wilkinson, J.F.G. 1969. Lineages and fractionation trends in undersaturated volcanic rocks from the East Otago Volcanic Province (New Zealand) and related rocks. J. Petrology 10, 440-501.

Davidson, C.F., 1967. The so-called "cognate xenoliths" of kimberlite, pp. 342-346 in Ultramafic and Related Rocks, ed. Wyllie, P.J., N.Y.: John Wiley and Sons, Inc.

Davis, B.T.C. and Schairer, J.F., 1965. Melting relations in the join diopside-fosterite-pyrope at 40 Kilobars and at one atmosphere. Yb. Carnegie Instn Wash. 64, 123-126.

De Saint Ours, J., 1960. Etudes Geologiques dans L'extreme Nord de Madagascar et L'Archipel des Comores. Republique Malagache, Ministere de L'Economie Nationale, Service Geologique, Tananarive.

Dixey, F., 1956. The East African Rift System. Col. Geol. Min. Resources Supp. Ser. 1.

Esson, J., Flower, M.F.J., Strong, D.F., Upton, B.G.J. and Wadsworth, W.J., Geology of the Comores Archipelago. Geol. Mag. in press.

Fisher, R.L., Johnson, G.L. and Heezen, B.C., 1967. Mascarene Plateau, Western Indian Ocean. Bull. geol. Soc. Am. 78, 1247-1266.

Fisher, R.L., Engel, C.G. and Hilde, T.W.C., 1968. Basalts dredged from the Amirante Ridge, Western Indian Ocean. Deep Sea Res. 15, 521-534.

Fiske, R.S. and Kinoshita, W.T., 1969. Inflation of Kilauea Volcano prior to its 1967-1968 eruption. Science, N.Y. 165, 341-349.

Flower, M.F.J. and Strong, D.F., 1969. The significance of sandstone inclusions in lavas of the Comores Archipelago. Earth planet. Sci. Lett. 7, 47-50.

Francis, T.J.G., Davies, D. and Hill, M.N., 1966. Crustal structure between Kenya and the Seychelles. Phil. Trans. R. Soc., A 259, 240-261.

Gardiner, J.S., 1936. The reefs of the western Indian Ocean. I. Chagos Archipelago, II. The Mascarene region. Linn. Soc. Lond. Trans. (Zoology) 19, 393-436.

Gast, P.W., 1965. Terrestrial ratio of potassium to rubidium and the composition of the earth's mantle. Science, N.Y. 147, 858-860.

Gast, P.W., 1968. Trace element fractionation and the origin of tholeiitic and alkaline magma types. Geochim. cosmochim. Acta 32, 1057-1086.

Goulden, C.H., 1952. Methods of Statistical Analysis. N.Y., Lond.: John Wiley and Sons, Inc.

Green, D.H., 1969. The origin of basaltic and nephelenitic magmas in the earth's mantle. Tectonophys. 7, 409-422.

Green, D.H. and Ringwood, A.E., 1967. The genesis of basaltic magmas. Contr. Mineral. and Petrol. 15, 103-190.

Griffen, W.L. and Murthy, V.R., 1969. Distribution of K, Rb, Sr and Ba in some minerals relevant to basalt genesis. Geochim. cosmochim. Acta 33, 1389-1414.

Guilcher, A., 1965. Coral reefs and lagoons of Mayotte Island, Comoro Archipelago, Indian Ocean, and of New Caledonia, Pacific Ocean, pp. 21-45 in Submarine Geology and Geophysics. eds. Whittard, W.F. and Bradshaw, R. Lond.: Butterworths.

Harris, P.G., 1957. Zone-refining and the origin of potassic basalts. Geochim. cosmochim. Acta 12, 195-208.

Harris, P.G., 1967. Segregation processes in the upper mantle, pp. 305-317 in Mantles of the Earth and Terrestrial Planets, ed. Runcorn, S.K., New York: Interscience.

Harris, P.G. and Middlemost, E.A.K., 1970. The evolution of kimberlites. Lithos 3, 77-88.

Harris, P.G., Reay, A. and White, I.G., 1967. Chemical composition of the upper mantle. J. geophys. Res. 72, 6359-6369.

Haskin, L. and Gehl, M.A., 1962. The rare-earth distribution in sediments. J. geophys. Res. 67, 2537-2541.

Holmes, A., 1965. Principles of Physical Geology. London and Edinburgh: Thomas Nelson, Ltd.

Hope, K., 1968. Methods of Multivariate Analysis. Lond.: Univ. Lond. Press.

Hurley, P.M., 1957. Test on the possible chondritic composition of the earth's mantle and its abundance of uranium, thorium, and potassium. Bull. geol. Soc. Am. 68, 379-382.

Hurley, P.M., 1968a. Absolute abundance and distribution of Rb, K and Sr in the Earth. Geochim. cosmochim. Acta 32, 273-283.

Hurley, P.M., 1968b. Correction to: Absolute abundance and distribution of Rb, K and Sr in the Earth. Geochim. cosmochim. Acta 32, 1025-1030.

Ito, K. and Kennedy, G.C., 1967. Melting and phase relations in a natural peridotite to 40 kilobars. Am. J. Sci. 265, 519-538.

Jagger, T.A., 1947. Origin and Development of Craters. Geol. Soc. Am. Mem. 21.

Jamieson, B.G., 1966. Evolution of basalt magma at elevated pressures. Nature, Lond. 219, 1240-1241.

Jamieson, B.G., 1969. Natural rock projection into a pseudo-quaternary system, pp. 152-155 in Progress in Experimental Petrology, N.E.R.C. 1st Report, Manchester:Edinburgh.

Jamieson, B.G., 1970. Phase relations in some tholeiitic lavas illustrated by the system $R_2O_3-XO-YO-ZO_2$. Mineralog. Mag. in press.

Johannsen, A., 1938. A Descriptive Petrography of the Igneous Rocks, Vol. IV. Chicago: Univ. Chicago Press.

King, B.C. and Sutherland, D.L., 1960. Alkaline rocks of Eastern and Southern Africa. Sci. Prog. 48, pt. I, 298-321; pt. II, 504-523; pt. III, 709-720.

Krumbein, W.C. and Graybill, F.A., 1965. An Introduction to Statistical Models in Geology. N.Y.: McGraw-Hill.

Kushiro, I., 1968. Compositions of magmas formed by partial zone melting of the earth's upper mantle. J. geophys. Res. 73, 619-634.

Kushiro, I., Yashuhiko, S. and Akimoto, S., 1968. Melting of a peridotite nodule at high pressures and high water pressures. J. geophys. Res. 73, 6023-6029.

Kutolin, V.A., 1970. Ultrabasic nodules in basalts and the upper mantle composition. Earth planet. Sci. Lett. 7, 330-332.

Lacroix, A., 1922. La Constitution lithologique de l'Archipel des Comores. Proc. 23rd Internat. Geol. Congr., Brussels. 2, 947-979.

Lacroix, A., 1938. Le volcan actif de L'Ile de la Reunion et celui de La Grande Comore. Paris: Gauthier-Villars.

LeMaitre, R.W., 1962. Petrology of the volcanic rocks, Gough Island, South Atlantic. Bull. geol. Soc. Am. 73, 1309-1340.

Lovering, J.F., 1958. The nature of the Mohorovicic discontinuity. Trans. Am. geophys. Un. 39, 947-955.

Luth, W.C. and Tuttle, O.F., 1969. The hydrous vapour phase in equilibrium with granite and granite magmas, pp. 513-548 in Igneous and Metamorphic Geology, eds. Larsen, L., Manson,V. and Prinz, M. Geol. Soc. Am. Mem. 115.

Macdonald, G.A., 1949. Hawaiian petrographic province. Bull. geol. Soc. Am. 60, 1541-1595.

Macdonald, G.A., 1967. Forms and structures of extrusive basaltic rocks, pp. 1-61 in Basalts: the Poldervaart treatise on rocks of basaltic composition, eds. Hess, H.H. and Poldervaart, A., N.Y.: Interscience.

Macdonald, G.A., 1968a. Composition and origin of Hawaiian lavas, pp. 477-522 in Studies in Volcanology, eds. Coats, R.R., Hay, R.L. and Anderson, C.A. Geol. Soc. Am. Mem. 116.

Macdonald, G.A., 1968b. A contribution to the petrology of Tutuila, American Samoa. Geol. Rdsch. 57, 821-837.

Macdonald, G.A. and Katsura, T., 1964. Chemical composition of Hawaiian lavas. J. Petrology 5, 82-133.

Macdonald, G.J.F., 1959. Chondrites and the chemical composition of the Earth, pp. 476-494 in Researches in Geochemistry, ed. P.H. Abelson. N.Y.: John Wiley and Sons.

Macgregor, A.G., 1948. Problems of Carboniferous-Permian volcanicity in Scotland. Q. Jl. geol. Soc. Lond. 104, 133-153.

Manson, V., 1967. Geochemistry of basaltic rocks: major elements, pp. 215-269 in Basalts: the Poldervaart treatise on rocks of basaltic composition, eds. Hess, H.H. and Poldervaart, A., New York: Interscience.

Marshall, P., 1929. The volcanic rocks of the Cook Islands. 4th Pacific Sci. Congr., Proc. 2B. 901-903.

McBirney, A.R. and Aoki, K., 1968. Petrology of the Island of Tahiti, pp. 523-556 in Studies in Volcanology, eds. Coats, R.R., Hay, R.L. and Anderson, C.A. Geol. Soc. Am. Mem. 116.

Murata, K.J. and Richter, D.H., 1966a. The settling of olivine
        in Kilauean magma as shown by the lavas of the 1959
        eruption. Am. J. Sci. 264, 194-203.

Murata, K.J. and Richter, D.H., 1966b. Chemistry of the lavas
        of the 1959-60 eruption of Kilauea Volcano, Hawaii.
        Prof. Pap. U.S. geol. Surv. 537-A.

Murray, R.J., 1954. The clinopyroxenes of the Garbh Eilean sill,
        Shiant Isles. Geol. Mag. 91, 17-31.

Morey, G.W. and Hesselgesser, J.M., 1951. The solubility of some
        minerals in superheated steam at high pressure.
        Econ. Geol. 46, 821-835.

Nixon, P.H., Von Knorring, O. and Rooke, J.M., 1963. Kimberlites
        and associated inclusions of Basutoland: A mineralogical
        and geochemical study. Am. Miner. 48, 1090-1132.

O'Hara, M.J., 1965. Primary magmas and the origin of basalts.
        Scott. J. Geol. 1, 19-40.

O'Hara, M.J., 1967. Crystal-liquid equilibria and the origins of
        ultramafic nodules in basic igneous rocks, pp. 346-349
        in Ultramafic and Related Rocks, ed. Wyllie, P.J., N.Y.:
        John Wiley and Sons, Inc.

O'Hara, M.J., 1968. The bearing of phase equilibria studies in
        synthetic and natural systems on the origin and
        evolution of basic and ultrabasic rocks. Earth-Sci. Rev.
        4, 69-133.

O'Hara, M.J., 1970. Upper mantle composition inferred from
        laboratory experiments and observation of volcanic
        products. Phys. Earth Planet. Interiors 3, 236-245.

O'Hara, M.J. and Yoder, H.S., Jr., 1967. Formation and fractionation
        of basic magmas at high pressures. Scott. J. Geol.
        3, 67-117.

Pepper, J.F. and Everhart, G.M., 1963. The Indian Ocean, the
        geology of its bordering lands and the configuration
        of its floor. U.S. geol. Surv. Miscellaneous Geologic
        Investigations, Map 1-380 and accompanying text.

Presnall, D.C., 1969. The geometrical analysis of partial fusion.
        Am. J. Sci. 267, 1178-1194.

Press, F., 1969. The Suboceanic Mantle. Science, N.Y. 165, 174-176.

Prinz, M., 1967. Geochemistry of basaltic rocks: trace elements, pp. 271-323 in <u>Basalts: the Poldervaart treatise on rocks of basaltic composition</u>, eds. Hess, H.H. and Poldervaart, A., New York: Interscience.

Prosperi, F., 1957. <u>Vanished Continent: An Italian Expedition to the Comores Islands</u>. trans. by D. Moore. Lond.: Hutchinsons.

Reay, A. and Harris, P.G., 1964. The partial fusion of peridotite. <u>Bull. Volc.</u> 27, 115-127.

Robson, G.R. and Barr, K.G., 1964. The effect of stress on faulting and minor intrusions in the vicinity of a magma body. <u>Bull. volc.</u> 27, 315-330.

Saggerson, E.P. and Williams, L.A.J., 1964. Ngurumanite from southern Kenya and its bearing on the origin of rocks in the northern Tanganyika alkaline district. <u>J. Petrology</u> 5, 40-81.

Schilling, J.G. and Winchester, J.W., 1967. Rare-earth fractionation and magmatic processes, pp. 267-283 in <u>Mantles of the Earth and Terrestrial Planets</u>, ed. Runcorn, S.K., New York: Interscience.

Schilling, J.G. and Winchester, J.W., 1969. Rare-earth contribution to the origin of Hawaiian Lavas. <u>Contr. Mineral. and Petrol.</u> 23, 27-37.

Schmitt, R.A., Smith, R.H. and Olehy, D.A., 1964. Rare-earth, yttrium and scandium meteoritic and terrestrial matter - II. <u>Geochim. cosmochim. Acta</u> 28, 67-86.

Shaw, D.M., 1968. A review of K/Rb fractionation trends by covariance analysis. <u>Geochim. cosmochim. Acta</u> 32, 573-602.

Simmons, G., 1964. Velocity of shear waves in rocks to 10 kilobars. <u>J. geophys. Res.</u> 69, 1123-1130.

Smith, R.E., 1967. Segregation vesicles in basaltic lava. <u>Am. J. Sci.</u> 265, 696-713.

Spencer, A.B., 1969. Alkalic igneous rocks of the Balcones Province, Texas. <u>J. Petrology</u> 10, 272-306.

Stark, J.T. and Hay, R.L., 1963. Geology and petrography of volcanic rocks of the Truk Islands, East Caroline Islands. <u>Prof. Pap. U.S. geol. Surv.</u> 409.

Stearns, H.T. and Vaksvik, K.N., 1935. Geology and ground-water resources of the island of Oahu, Hawaii. U.S. geol. Surv. Bull. 1.

Stice, G.D., 1968. Petrography of the Manu'a Island, Samoa. Contr. Mineral. and Petrol. 19, 343-357.

Strong, D.F. and Jacquot, C., 1969. The Kartala caldera, Grande Comore, p. 109 in Symposium on Volcanoes and their Roots, vol. of abstr., Oxford, Sept. 1969. Int. Ass. Volc. Chem. Earth's Interior. (submitted to Bull. volc.)

Talwani, Manik., 1962. Gravity measurements in the Indian Ocean. Bull. geol. Soc. Am. 73, 1171-1182.

Thornton & Tuttle — see refs. for Appendix A .

Turekian, K.K. and Clark, S.P.Jr., 1969. Inhomogeneous accumulation of the earth from the primitive solar nebula. Earth planet. Sci. Lett. 6, 346-348.

Turner, F.J. and Verhoogen, J., 1960. Igneous and metamorphic petrology. New York: McGraw-Hill.

Upton,B.G.J. (ed.), 1969. Carboniferous volcanic rocks of the Midland Valley of Scotland, field excursion guide. Symposium on Volcanoes and their Roots, Int. Ass. Volc. Chem. Earth's Interior.

Upton, B.G.J. and Wadsworth, W.J. 1966. The basalts of Reunion Island, Indian Ocean. Bull. Volc. 29, 7-24.

Upton, B.G.J., Wadsworth, W.J. and Newman, T.C., 1967. The petrology of Rodriguez Island, Indian Ocean. Bull. geol. Soc. Am. 78, 1495-1506.

Urey, H.C., 1952. The Planets, their Origin and Development. Yale Univ. Press.

Van Padang, M. Neumann, ed., 1963. The volcanoes of the western part of the Indian Ocean, pp. 32-39 in Catalogue of the Active Volcanoes of the World, Including Solfatara fields, part XVI, Arabia and the Indian Ocean.

Varne, R., 1962. The petrology of Moroto Mountain, Eastern Uganda, and the origin of nephelinites. J. Petrology 9, 169-190.

Veeh, H.H., 1966. Ages of Pleistocene high sea level stand. J. geophys. Res. 71, 3379-3386.

Vienne, E., 1900. Colonies et Pays de Protectorates Mayotte et Comores. Paris: Exposition Universelle de 1900.

Vinogradov, A.P., 1962. Average contents of chemical elements in the principal types of igneous rocks of the Earth's crust. Geochemistry (trans. of Geokhimiya) 1962, 641-664.

Voeltzkow, A., 1906. Die Comoren, pp. 606-630 in Zeits. der Ges. für Erdkunde zu Berlin.

Walker, F. and Nicolaysen, L.O., 1953. The petrology of Mauritius. Col. Geol. Miner. Res. 4, 3-43.

Wilkinson, J.F.G., 1956. Clinopyroxenes of alkali olivine-basalt magma. Am. Miner. 41, 724-743.

Williams, H., 1933. Geology of Tahiti, Moorea, and Maio. B.P. Bishop Mus. Bull. 105.

Williams, L.A.J., 1969. Volcanic associations in the Gregory Rift Valley, East Africa. Nature, Lond. 224, 61-64.

Wood, C.P., 1968. A geochemical study of East African alkaline lavas and its relevance to the petrogenesis of nephelinites. Univ. Leeds Ph.D. thesis (unpubl.).

Wood, C.P., 1969. Geochemistry of volcanic rocks of the Cook Islands, pp. 38-39 in U.K. Information Sheet on the Upper Mantle, 4.

Yagi, K., 1960. Petrochemistry of the alkalic rocks of Ponape Island, western Pacific Ocean. Rep. 21st Internat. geol. Congr. (Norden) pt. 13, 108-122.

Yoder, H.S.,Jr. and Tilley, C.E., 1962. The origin of basalt magmas: an experimental study of natural and synthetic systems. J. Petrology 3, 342-532.

APPENDIX A

Analytical and Determinative Methods

A.1.   Preparation of rock powders

A.2.   X-ray fluorescence analysis

A.3.   Wet chemical methods

A.4.   Electron microprobe analysis

A.5.   Optical determinations

A.6.   Modal analysis

A.7.   Olivine X-ray diffraction method.

A. ANALYTICAL AND DETERMINATIVE METHODS

A.1. Preparation of rock powders

Rock powders were prepared using the methods currently
in use at the Grant Institute of Geology, and these methods are
summarized as a flow chart in Figure A-1.   For most hand specimens
three hundred to a thousand grams of one-quarter inch chips were
prepared, depending upon the grain size and percentage of phenocrysts
in the rock, as outlined by Wager and Brown (1960, Table 1, p. 6).
For some glassy or very fine-grained aphyric rocks less than one
hundred grams were prepared, since differences within the hand
specimen would be insignificant relative to those within the whole
flow.

Qualitative tests showed that the "Columboy" Tema disk mill
produces unacceptable $\underline{Ni}$ and $\underline{Cr}$ contamination (Table A-1), so
specimens analysed for these elements were ground in the agate or
tungsten carbide ball mills.   All powders from the ball mills were
sieved through 100 mesh B.S. nylon screen, and the few grains of
material commonly present after sieving were ground with an agate
mortar and pestle.   Initial checks showed that the Tema disk mill
produced -100 mesh powders (grinding time dependent upon the amount
of sample present), and sieving of these powders was therefore dis-
continued.   No equipment contamination was found for other elements
determined in this study (Table A-1).

HAND SPECIMEN

WASH UNDER HOT TAPWATER AND SCOUR WITH BRISTLE BRUSH

RINSE WITH DEIONIZED WATER

DRY OVERNIGHT AT ROOM TEMPERATURE

REDUCE TO 1 TO 2 INCH CHIPS WITH HYDRAULIC SPLITTER

DISCARD WEATHERED CHIPS

300-600 g REPRESENTATIVE SAMPLE

REDUCE TO $\frac{1}{4}$ INCH CHIPS WITH TUNGSTEN CARBIDE MORTAR AND PESTLE

100 g REPRESENTATIVE SAMPLE

Ni or Cr ANALYSIS ?   SEE TABLE B-I

YES → REDUCE TO -15 MESH ON THE MANCHESTER ROLLERS

NO → REDUCE TO -100 MESH IN "COLUMBOY" TEMA DISK MILL FOR 30-90 SEC.

REDUCE TO -100 MESH IN AGATE BALL MILL

SEPARATE PHENOCRYSTS

GROUNDMASS

PHENOCRYST ASSEMBLAGE

SIEVE IN 100 MESH SCREEN

REDUCE TO -100 MESH IN TUNGSTEN CARBIDE BALL MILL

SEPARATE INDIVIDUAL MINERALS

STORE IN TIGHTLY STOPPERED GLASS BOTTLES

DRY AT 110°C FOR 24 HOURS BEFORE ANALYSIS

Table A-1

Qualitative tests for contamination from grinding equipment

ppm		Ba	Zr	Sr	Rb	Zn	Cu	Ni	Cr
1	A	390	218	475	20	96	105	180	260
	T	450	205	500	26	106	89	1760	298
4	A	520	270	510	24	100	90	170	100
	T	485	238	524	32	116	85	1460	277
6	A	470	188	425	20	107	101	100	40
	T	470	159	444	25	114	94	1690	271
23	A	500	219	460	24	112	101	178	200
	T	390	207	480	26	112	95	1960	620
26	A	440	230	473	24	88	83	200	130
	T	400	222	492	26	104	99	1660	420
31	A	218	125	289	13	100	103	480	775
	T	250	127	305	13	93	90	770	800

Wt.%		SiO_2	TiO_2	Al_2O_3	Fe_2O_3	FeO	MnO	MgO	CaO	Na_2O	K_2O	P_2O_5
31	A	46·65	1·58	9·70	2·53	8·86	·19	15·60	11·95	1·98	·61	·22
	T	46·76	1·58	9·76	2·46	8·87	·19	15·98	11·00	1·93	·61	·25

A: "CUT ROCK"   Jaw-splitter ⟶ Manchester rollers ⟶ agate ball mill.

T: "   "   ⟶ Tema disk mill.

For the separation of phenocrysts, rocks were crushed to the phenocryst size (generally between 48 and 15 mesh), and run through a magnetic separator at very low current strength. This permits clean separation of the phenocrysts and groundmass, as all magnetite is concentrated in the groundmass and renders it highly magnetic. After separation, the phenocrysts were ground to -100 mesh in a tungsten carbide ball mill, and individual minerals were then separated on the magnetic separator. However, because of overlap in magnetic properties of olivine and some clinopyroxene fractions, clean olivine could not be obtained by this method. These clinopyroxene + olivine fractions were thus discarded and the olivine phenocrysts were hand-picked from the bulk powders. Because of this it must be noted that the clinopyroxene analyses do not represent the complete phenocrysts, but only the least magnetic part, about 90% of the total.

A.2. X-ray fluorescence analysis

The analyses for all trace elements and all major elements except FeO, Na_2O and H_2O were carried out by X-ray fluorescence spectroscopy, using Phillips PW 1212 twenty-four channel automatic or PW 1540 single channel spectrometers with standard instrument settings (e.g. see Norrish and Hutton, 1968). Trace elements were determined directly on the rock powders by calculating the ratios of peak to background and reading concentrations off linear calibration curves. The calibration curves were visually estimated as the best fit straight line through points obtained by plotting concentrations against ratios of peak to background for at least ten international standard rocks powders. The ratios of peak to background were calculated from counts corrected for instrument drift by means of a short computer program modified by the writer from a similar program written by D.H. Doff. The precision of this method has been determined on a single rock powder of the basalt No.1 (Table C-1) and th results are shown in Table A-2.

Major elements were determined on disks of fused rock powders prepared as shown in Figure A-2, after the method of Rose, et al. (1963). This method of preparation removes matrix effects so as to produce linear calibration curves, and renders unnecessary any mathematical corrections for matrix or mass absorption effects (cf. Holland, 1966, or Norrish and Hutton, 1969). The chemical results were calculated by means of a computer program (modified by J.D. Appelton after D.H. Doff) which corrects for instrument drift,

Table A-2

Precision of X-ray Fluorescence Analyses

p.p.m.	$\bar{x}$	R	s	c	n
Rb	29	18	6	20%	6
Cu	102	26	8	8%	6
Sr	512	22	8	2%	6
Ba	381	65	23	6%	6
Zn	93	15	5	5%	6
Zr	201	28	9	5%	6
Cr	337	40	37	11%	3
Ni	212	27	14	7%	4
wt. %					
SiO_2	47·05	0·33	0·13	0·27%	7
Al_2O_3	13·23	0·25	0·08	0·60%	7
Fe_2O_3	12·70	0·46	0·15	1·18%	7
MgO	9·21	0·21	0·10	1·09%	7
CaO	11·36	0·20	0·06	0·53%	7
K_2O	1·25	0·01	0·01	0·76%	7
P_2O_5	0·43	0·05	0·02	4·65%	7
TiO_2	2·38	0·09	0·03	1·14%	7

$\bar{x}$ Mean concentration

R   Range = maximum-minimum concentration obtained

s   standard deviation from the mean

c   coefficient of variation

n   number of determinations

Fe_2O_3 = total iron as Fe_2O_3

```
┌──────────┐      ┌──────────┐      ┌────────────────────┐      ┌──────────────┐
│  DRIED   │─────▶│   FOR    │─────▶│ WEIGH OUT          │─────▶│ CAREFULLY    │
│  POWDER  │      │  MAJOR   │      │ ·7500 g powder     │      │ MIX AND      │
│          │      │ ELEMENTS │      │ ·7500 g La₂O₃      │      │ TRANSFER     │
└────┬─────┘      └──────────┘      │ 6·00 g Li₂B₄O₇     │      │ TO GRAPHITE  │
     │                              └────────────────────┘      │ CRUCIBLE     │
     │                                                          └──────┬───────┘
     ▼
┌──────────┐
│   FOR    │
│  TRACE   │
│ ELEMENTS │
└────┬─────┘
```

- **DRIED POWDER** (circle) → **FOR MAJOR ELEMENTS** → **WEIGH OUT** ·7500 g powder, ·7500 g La_2O_3, 6·00 g $Li_2B_4O_7$ → **CAREFULLY MIX AND TRANSFER TO GRAPHITE CRUCIBLE**

- DRIED POWDER also → **FOR TRACE ELEMENTS**

- CAREFULLY MIX AND TRANSFER TO GRAPHITE CRUCIBLE → **PUT IN MUFFLE FURNACE PREHEATED TO 750°C. RAISE TEMP. TO 1050°C AND HOLD FOR 20 MIN.**

- → **REMOVE BEAD AFTER PARTLY COOLED AND PLACE IN DESSICATOR FOR COMPLETE COOLING**

- → **READJUST WEIGHT TO EXACTLY 7·5000 g WITH DRIED $Li_2B_4O_7$**

- → **PLACE BEAD IN W.C. VIAL, CRACK WITH STEEL CYLINDER, BALL MILL TO -100 MESH**

- → **PUT POWDER IN GLASS VIAL**

- → **DRY POWDER AT 110°C OVERNIGHT**

- → **PRESS POWDER INTO DISKS**

- → **STORE DISKS IN LOW HUMIDITY DRYING CABINET**

- STORE DISKS IN LOW HUMIDITY DRYING CABINET → **ANALYSE**

- FOR TRACE ELEMENTS → **ANALYSE**

calculates a regression line, and calculates the data from this regression. Along with the data the programme also prints out correlation coefficients for the regression line of each element, and reclaculates the concentration of each element in the standards used. This permits a rapid evaluation of the quality of each set of determinations, and the data for one such set of determinations are reproduced in Table A-3. The precision for each element has been determined on No.1, as shown in Table A-2. These data were obtained for separate fusion powders, and thus incorporate precision of the preparation technique as well as instrument precision. The accuracy of the method was determined from the three international rock standards DTS-1 (dunite), NBS-91 (silica brick), and BCR-1 (basalt), and the results are presented in Table A-4.

KEY TO TABLE BELOW:
M   COEFFICIENT OF REGRESSION   Y = M*X + C   (Y=CONC OF ELEMENT AND X=INTENSITY VALUE)
C   POINT OF INTERSECTION OF REGRESSION LINE ON Y AXIS
R   COEFFICIENT OF CORRELATION
D   COEFFICIENT OF DETERMINATION
SEE   STANDARD ERROR OF ESTIMATE
REE   RELATIVE ERROR OF ESTIMATE
N   NUMBER OF STANDARDS USED IN REGRESSION

M	0.01151	0.01922	0.10088	0.00816	0.23852	0.38782	1.29818	0.35674
C	-0.61912	-0.05806	-0.29009	-0.14986	4.49669	-0.21668	-0.19164	0.02545
R	0.999	1.000	0.998	1.000	1.000	1.000	1.000	0.991
N	9	8	12	11	10	10	10	9

STANDARDS   INTENSITIES , COMPUTED VALUES , AND DATA.

	CA	K	FE	TI	SI	AL	MG	P
PCC-1	95589	3758	88754	19842	157645	2563	33731	89
	0.481	0.000	6.663	0.012	42.146	0.777	43.597	0.001
	0.420	0.010	6.160	0.010	41.900	0.760	43.320	0.010
DX-24	916495	5667	114956	127567	173560	29098	12799	236
	9.930	0.029	11.310	0.891	45.894	11.378	16.424	0.110
	10.200	-1.000	11.790	0.900	45.980	11.450	16.810	-1.000
GSP-1	221489	362653	46703	100376	260989	39962	1066	639
	1.930	5.462	4.421	0.669	66.748	19.242	1.192	0.253
	2.060	5.500	4.240	0.660	67.260	19.300	0.950	0.280
M G	99771	254176	19166	32860	319718	26991	289	90
	0.529	3.811	1.643	0.118	80.756	10.096	0.184	0.008
	0.560	-1.000	1.690	0.110	80.570	10.020	0.120	0.010
NBS-76	27573	103561	23170	290551	203977	101116	580	35
	0.000	1.518	2.047	2.221	53.149	38.996	0.561	0.038
	-1.000	1.540	2.390	2.210	-1.000	-1.000	-1.000	0.070
NBS-77	27556	138140	11649	381959	115475	159164	515	1053
	0.000	2.046	0.887	2.966	32.040	61.910	0.477	0.401
	-1.000	2.110	0.900	-1.000	32.380	-1.000	0.500	-1.000
BCR-1	677906	118526	135369	292275	211560	35390	2851	978
	7.184	1.746	13.366	2.235	54.958	13.508	3.510	0.374
	6.920	1.690	13.280	2.250	54.120	13.660	3.480	0.350
AGV-1	469024	195464	68362	147442	227990	44461	1278	1273
	5.010	2.917	6.606	1.053	58.877	17.026	1.468	0.479
	4.900	2.860	6.650	1.050	59.000	17.140	1.500	0.490
NBS-91	969759	220514	5530	19851	262026	16015	162	115
	10.543	3.298	0.268	0.012	66.995	5.994	0.019	0.066
	10.480	-1.000	0.080	0.020	67.530	6.010	0.000	0.020
G-2	214501	298423	29498	80106	272436	41148	673	310
	1.850	4.484	2.686	0.504	69.478	19.741	0.682	0.136
	1.960	4.460	2.640	0.480	69.220	19.420	0.750	0.130
DTS-1	59135	3701	88752	19565	151657	1306	38431	60
	0.002	0.000	6.663	0.010	40.670	0.290	49.698	0.004
	0.020	0.000	6.640	0.010	40.600	0.280	49.820	0.000
NBS-1a	3455135	56265	18172	35013	55263	11252	1286	816
	39.152	0.829	1.539	0.136	17.678	4.147	1.478	0.317
	-1.000	-1.000	1.670	0.160	-1.000	4.160	-1.000	-1.000

Table A-4

Accuracy of X-ray Fluorescence Analyses

wt. %	NBS-91		DTS-1		BCR-1	
	A	B	A	B	A	B
SiO_2	67·59	67·53	40·66	40·45	55·20	54·48
TiO_2	·04	·02	·03	·02	2·20	2·23
Al_2O_3	6·37	6·01	·47	·55	13·80	13·65
$Fe_2O_3(T)$	·32	·08	8·89	8·85	13·31	13·50
MgO	·28	-	50·71	49·80	3·43	3·28
CaO	10·63	10·48	·06	·15	7·24	6·95
P_2O_5	·06	·02	·01	·01	0·38	0·36
K_2O	3·32	3·25	·00	·02	1·76	1·68

A: Data obtained during present study

B: Data given by Flanagan (1969).

$Fe_2O_3(T)$ = total iron as Fe_2O_3.

A.3. Wet chemical methods

P_2O_5 was determined on twelve specimens using the colorimetric method of Baadsgaard and Sandell (1954). However, because of the acceptable precision and accuracy of the X-ray fluorescence method (Tables A-3 and A-4), all further P_2O_5 analyses were made by this shorter method.

Ferrous iron was determined by the method of Wilson (1955), viz. cold HF attack of the rock powder in the presence of excess ammonium vanadate in plastic crucibles for about five days, and titration of the excess vanadate with ferrous ammonium sulfate in the presence of boric acid and sulphuric acid, using sodium diphenyl-amine sulphonate as indicator. The accuracy of this method was tested on the USGS standard basalt BCR-1, and the results are presented in Table A-5, column a. Precision of the method was determined from six duplicate analyses of No. 1 over a period of two months, during which time all other FeO analyses were made (Table A-5, column b). The precision was also calculated from the differences between duplicates on many different samples, as outlined by Gould (1966, p. 49), viz. if

X_1, X_2 = two determinations on a single sample,

$\overline{x}$ = mean of a number of determinations, n, and

s = standard deviation from the mean, then

$$s^2 = \frac{\Sigma(x - \overline{x})^2}{n - 1} = \frac{(x_1 - x_2)^2}{2} \quad \text{and} \quad s = \frac{x_1 - x_2}{\sqrt{2}}$$

The precision can thus be estimated by averaging $(x_1 - x_2)/\sqrt{2}$ for all the pairs of duplicate analyses. The results of this method

Table A-5

Precision and accuracy of ferrous iron analyses

	a	b	c
FeO obtained	8·90		
FeO accepted	8·91		
$\bar{x}$		9·16	9·00
R		·48	·34
s		·084	·067
c		·92%	·74%
n		12	72

a. Comparison of FeO content obtained for BCR-1 with that accepted by Flanagan (1969).

b. Precision of method calculated from repeat analyses of No.1

c. Precision of method calculated from differences between duplicate analyses of different rocks.

$\bar{x}$ = mean FeO concentration

R = range = maximum-minimum FeO concentration

s = standard deviation from the mean

c = coefficient of variation (relative deviation = $100\ s/\bar{x}$)

n = number of duplicate determinations

of calculation are given in Table A-5, column c, and it can be
seen that both methods of calculation yield similar results.

All Na_2O and twelve K_2O determinations were carried out
on an Evans Electroselenium Ltd. Model A flame photometer. The
K_2O results determined by X-ray fluorescence were found to be
satisfactory, however, so the faster X-ray method was used for
all subsequent determinations of K_2O. Two methods were used to
prepare sample solutions for flame photometry, as outlined in
Figure A-3. Method A, introduced by E.L.P. Mercy, was that
commonly used in the Grant Institute, and was used by the writer
for the first twelve samples, producing the precision shown in
Table A-6, column a. However, M.J. Saunders suggested that Ca
interference would be removed by allowing solid $CaSO_4$ to settle to
the bottom of the flask, and using a double Na filter on the photo-
meter. This cuts out the tedious steps 3 and 5, ignition and
filtration, and therefore two possible sources of error. Comparison
of columns a and b, Table A-6, shows that both methods have
comparable precision. Precision of method B was also calculated
from duplicates, column c, as outlined for FeO precision, and from
six analyses of BCR-1, column d. The accuracy of the method may
be seen from the analyses of BCR-1, column d, to be within the
limits of precision.
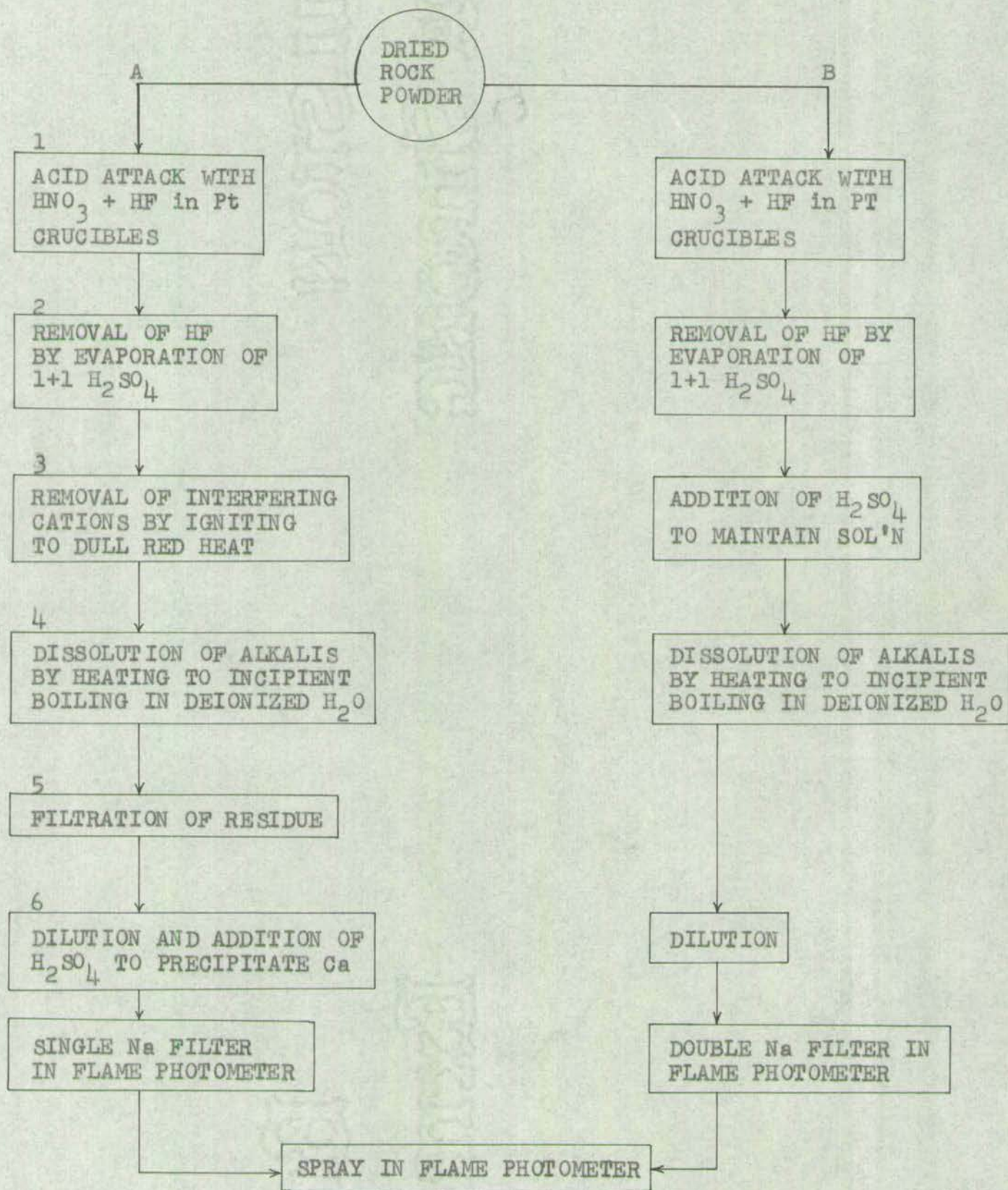
Table A-6

Precision and accuracy of Na$_2$O analyses

	a	b	c	d
ACCEPTED				3·30
$\bar{x}$	2·85	2·90	3·00	3·29
R	·23	·24	·10	·12
s	·069	·078	·043	·042
c	2·4%	2·7%	1·4%	1·3%
n	6	12	17	6

a. Precision of method A calculated from repeat analyses of No.1.

b. Precision of method B calculated from repeat analyses of No.1.

c. Precision of method B calculated from differences between
    duplicate analyses of different samples.

d. Comparison of Na$_2$O content obtained for BCR-1 with that
    accepted by Flanagan (1969), and precision of method B
    calculated from this data.

$\bar{x}$ = Mean Na$_2$O concentration

R = Range = maximum-minimum concentration

s = standard deviation from the mean

c = coefficient of variation

n = number of determinations

$\underline{H}_2\underline{O}$ was determined by a modified version of the method described by Shapiro and Brannock (1962). It consists of fusing one gram of the rock powder with three grams of lead oxide-lead chromate flux, collecting the evolved water on pre-dried, pre-weighed filter paper, and weighing the filter paper plus condensed water. The precision of this method is shown in Table A-7.

Table A-7

Precision of H$_2$O Analyses

	a	b
$\overline{x}$	·43	·40
R	·09	·17
s	·08	·04
c	20%	10%
n	6	99

a. Precision of method calculated from repeat analyses of No. 1

b. Precision of method calculated from differences between duplicate analyses of other rocks.

$\overline{x}$ = mean concentration

R = range = maximum-minimum concentration

s = standard deviation from the mean

c = coefficient of variation

n = number of duplicate determinations

A.4. Electron microprobe analysis

The microprobe analyses (Appendix E) were carried out at Durham University under the direction of Dr. C.H. Emeleus. The standards used were minerals close to the unknowns in composition, and after correction for instrument drift, linear calibrations were assumed. The error in this method is thought to be $\pm$ 2% of the values obtained for CaO, MgO, and FeO(total), $\pm$ 5% of TiO_2 values, and $\pm$ 10% of the Na_2O and K_2O values. (Dr. Emeleus, pers. comm.).

A.5. Optical determinations

Estimates of An contents of plagioclases were made according to the Michel Levy method on both the universal stage and flat stage, and some were also determined using the high temperature 2V curves of Smith (1958).

Refractive indices of olivines were measured on crushed grains in sodium light.

A.6. Modal analysis

Modal analyses were carried out using the "Shadowmaster" light table, on which an image of the thin section is projected onto an 18" glass plate. Points were counted by means of a 1 cm. grid, using at least 400 points for each rock. The reliability of this method was checked against the standard techniques using the mechanical stage and counting from 2000 to 5000 points. The results, shown diagrammatically in Fig. A-4, indicate that the only significant discrepancy arises from clinopyroxene counts.

Fig. A-4.

Comparison of modal data obtained using the
shadowmaster with that obtained using the
mechanical stage.   Numbers indicate volume
percent of different phases.

    •   = olivine phenocrysts

    Δ   = clinopyoxene phenocrysts

    O   = plagioclase phenocrysts

    ■   = groundmass.

SHADOWMASTER

100   80   60   40   20   0

0

20

MECHANICAL   STAGE

40

60

80

100

Ideal
Correspondence
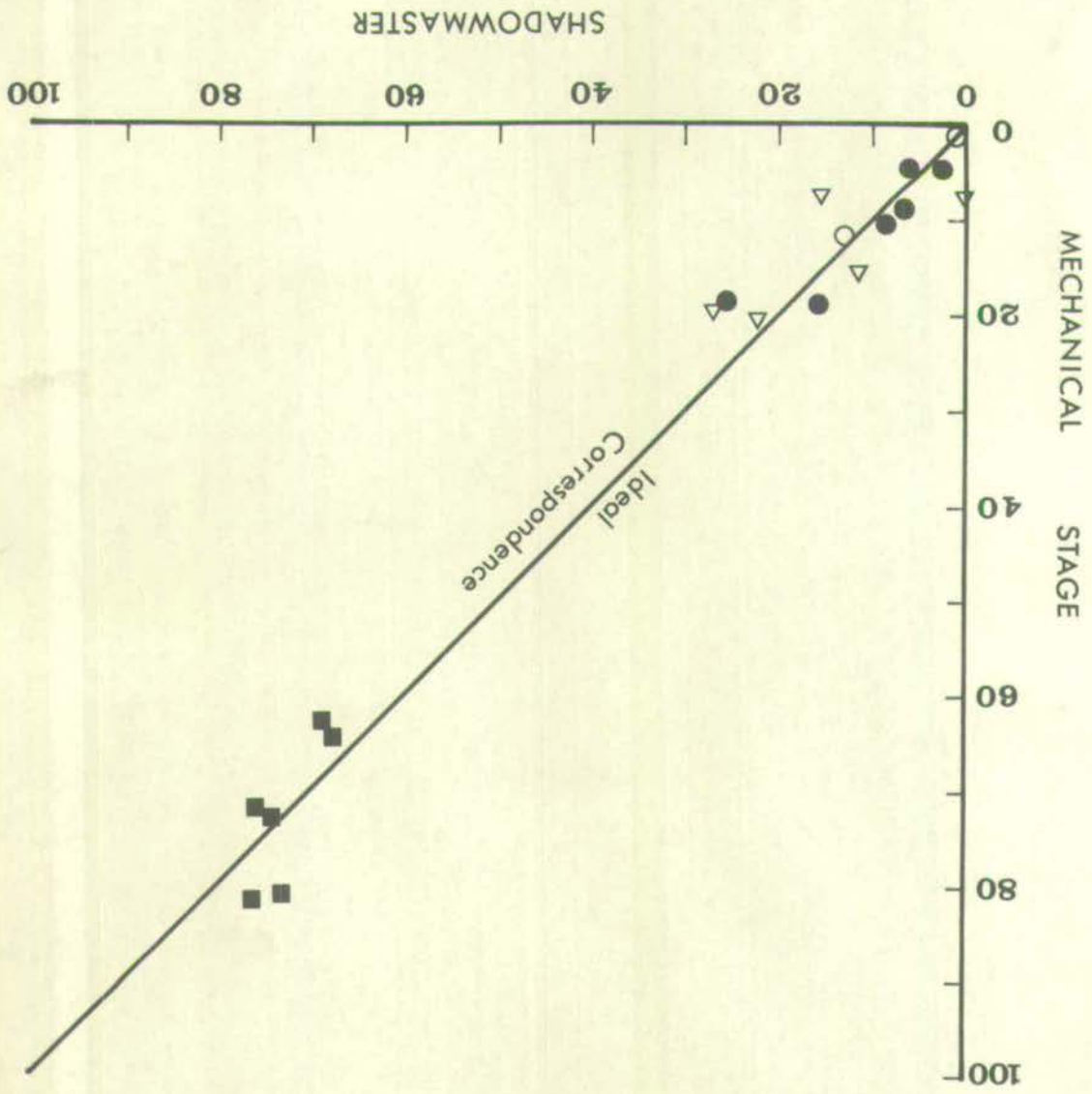
This is most likely a result of augite being mistaken for olivine during point counting on the mechanical stage, as this is unlikely to happen with the shadow master.   This writer feels that results obtained from the shadowmaster are in fact more reliable than those obtained from the mechanical stage.   The method was particularly well-suited to the present study because of the large size of phenocrysts in some thin sections, and the full view of thin sections that is projected permits rapid distinction between phenocryst and groundmass minerals and between different types of phenocrysts (e.g. xenocrysts, skeletal crystals, and euhedral crystals). Furthermore, it has the great advantage of being about five times more rapid than the mechanical stage.

A.7.   Olivine X-ray diffraction method

Olivines were determined according to the method of Yoder and Sahama (1957), which they estimate as accurate to $\pm$ 4%.

References cited

BAADSGAARD, H. and SANDELL, E.B. 1954. Photometric determination of phosphorus in silicate rocks. Analytica chim. Acta, 11, 183-187.

FLANAGAN, F.J. 1969. U.S. Geological Survey Standards - II. First compilation of data for the new U.S.G.S. rocks. Geochim. cosmochim. Acta, 33, 81-120.

GOULD, D. 1966. Geochemical and mineralogical studies of the granitic gneiss and associated rocks of Western Ardgour, Argyll. Univ. Edinburgh Ph.D. Thesis (unpubl.).

HOLLAND, J.G. 1966. A self-consistent mass absorption correction for silicate analysis by X-ray fluorescence. Spectrochimica Acta, 22, 2083-2093.

NORRISH, K. and HUTTON, J.T. 1969. An accurate X-ray spectrographic method for the analysis of a wide range of geological samples. Geochim. cosmochim. Acta, 33, 431-454.

ROSE, H.J., ADLER, I. and FLANAGAN, F.J. 1963. X-ray fluorescence analysis of the light elements in rocks and minerals. Appl. Spectrosc., 17, 81-85.

SHAPIRO, L. and BRANNOCK, W.W. 1962. Rapid analysis of silicate, carbonate and phosphate rocks. U.S. Geol. Surv. Bull. 1144-A.

SMITH, J.V. 1958. Effect of temperature, structural state and composition of the albite, pericline and acline-A twins of plagioclase feldspars. Am. Miner. 43, 546-551.

THORNTON, C.P. and TUTTLE, O.F. 1960. Chemistry of igneous rocks I: Differentiation Index. Am. J. Sci. 258, 664-684.

WAGER, L.R. and BROWN, G.M. 1960. Collection and preparation of material for analyses, in Methods in geochemistry, eds. Smales, A.A. and Wager, L.R. Interscience, New York and London; 4-32.

WILSON, A.D. 1955. A new method for the determination of ferrous iron in rocks and minerals. Bull. geol. Surv. Gt. Br., 9, 56-58.

YODER, H.S.jnr. and SAHAMA, T.G. 1957. Olivine X-ray determinative curve. Am. Miner., 42, 475-491.

APPENDIX B

Tables of Petrographic Data

B.1.   Kartala lavas

B.2.   La Grille lavas

B.3.   Badjini lavas

B.4.   Kartala intrusive rocks

B.5.   Miscellaneous rocks

Table B-1

Petrography of analysed lava flows from Kartala

Rock No.	Rock Type	Volume % Phenocrysts			Volume % Vesicles	Groundmass mineralogy				Comments
		Olivine	Augite	Plagio-clase		Olivine	Augite	Plagio-clase	Ore	
1	Ankaramite	7·6	8·9	-	0	X	X	An-48	X	
4	Alkali basalt	2·0	-	-	5·8	X	X	X	X	microphenocrysts 4·3% ol., 19·6% cpx, 11·6% plag of An-60. glassy groundmass; from 1872 flow.
6	Alkali basalt glassy chill	-	-	-	~50%	X	X	X	-	R.I. of glass = 1·610; from 1872 flow.
8	Alkali olivine basalt	7·0	-	-	22·6	-	X	X	X	from 1859 flow
13	Ankaramite	16·5	20·0	-	-	-	X	An-55	X	Block in N'Gouni tuff cone. Minor resorption of both olivine and augite.
17	Oceanite	14·5	4·8	-	-	X	X	An-48	X	Coarse doleritic groundmass. Ores elongate (= ilmanite?)
18	Oceanite	36·9	3·6	-	-	-	X	X	X	as above
19	Oceanite	22·0	14·3	-	-	-	X	X	X	as above
20	Alkali basalt	1·5	0·3	-	0	X	X	X	X	strong fluidal texture; coarse groundmass
21	Oceanite	21·0	11·7	-	-	X	X	X	X	Coarse dolerite groundmass. Elongate ore microphenocrysts. olivine phenocrysts resorbed. Augites zoned. gabbroic inclusion
22	Alkali basalt	2·0	2·5	-	-	X	X	An-58	X	1857 flow
23	Alkali olivine basalt scoria	7·8	5·9	-	21·8	X	X	X	-	R.I. of glass = 1·606
24	Alkali basalt	-	4·3	-	23·9	X	X	X	X	1859 flow
25	Alkali basalt	-	-	1·5	0	-	X	X	X	Microphenocryst of olivine, augite, plag.(=An-60) 1858 flow, upper end.
26	Alkali basalt	2·6	1·9	-	2·3	-	X	An-55	X	1858 flow, lower end
27(2)	Alkali basalt	-	-	-	23·7	X	X	X	X	
28	Alkali basalt	-	-	-	-	X	X	An-55	X	plagioclase microphenocrysts = An-68.
29	Alkali basalt	-	-	-	-	X	X	X	X	
31	Ankaramite	12·8	27·6	-	8·9	-	X	X	X	
32	Alkali basalt	2·6	1·9	-	2·5	-	X	An-55	X	Olivines skeletal in g'mass; some phenocrysts show resorption. Fluidal texture; 1904 flow.
39	Alkali basalt	1·4	-	-	13·3	X	X	X	X	Groundmass rich in plag.; few plag. and augite microphenocrysts.
40	Alkali basalt	-	2·1	3·6	2·8	-	X	An-57	X	Plag. and augite phenocrysts form glomeritic aggregates. dunitic inclusion.
41	Ankaramite	9·6	12·0	-	16·6	X	X	X	X	Olivine phenocrysts mostly euhedral, some resorbed. augite strongly zoned; 1860 flow.

Table B-1 (Contd.)

Rock No.	Rock Type	Volume % Phenocrysts			Volume % Vesicles	Groundmass mineralogy				Comments
		Olivine	Augite	Plagioclase		Olivine	Augite	Plagioclase	Ore	
45	Alkali basalt	1·0	-	-	0	X	X	X	X	Coarse doleritic groundmass with plag. interstitial. groundmass apatite.
46	Alkali basalt scoria				40·0	X	X	X	-	R.I. of glass = 1·610. 2% oxidized gabbroic inclusions.
47	Alkali basalt	-	-	-	6·0	X	X	X	X	Coarse doleritic groundmass, similar to 45. groundmass apatite.
48	Alkali basalt	-	1·4	1·4	29·3	X	X	X	X	as above
101	Alkali basalt	-	-	-	24·0	X	X	X	X	as above
102	Alkali basalt	-	-	-	0	X	X	X	X	as above
103	Alkali basalt scoria	3·9	-	-	28·8	X	X	X	-	Augite and plag. microphenocrysts clustered into rosettes. glassy groundmass.
112	Alkali basalt	-	-	-	24·2	X	X	X	X	
113	Alkali basalt	-	-	-	45·8	X	X	X	X	1860 flow
119	Alkali basalt scoria	tr	-	-	40·2	X	X	X	-	Olivines skeletal, much brown glass.
122	Alkali basalt scoria	-	-	-	45·7	X	X	X	-	as above
123	Alkali basalt scoria	-	-	-	50·0	X	X	X	-	as above ; 1965 flow
134	Alkali olivine basalt	2·0	6·0	-	35·3	X	X	X	X	1862 flow
139	Alkali basalt	0·4	1·8	-	35·5	X	X	X	X	1857 flow
142	Alkali basalt glass	-	-	-	>50%	X	X	-	-	very glassy (>95%), cellular structure, crystals of olivine and augite.
151	Oceanite	17·7	8·6	-	4·9	X	X	X	X	Slight resorption of larger phenocrysts; 1880 flow
154	Alkali basalt	1·6	-	-	12·0	X	X	X	X	
160	Alkali basalt	1·4	-	-	5·3	X	X	X	X	1857 flow
186	Ankaramite	5·4	17·3	-	35·6	X	X	X	X	glassy groundmass; 1860 flow
188	Feldspar-phyric basalt	2·1	4·2	12·8	16·0	X	X	X	X	
190	Alkali olivine basalt	3·4	3·4	-	4·5	X	X	X	X	
194	Ankaramite	8·2	24·6	-	0	X	X	X	X	doleritic g'mass
1כ5	Oceanite	16·6	16·3	-	-	X	X	X	X	

Table B-2

Petrography of analysed lava flows from La Grille

Rock No.	Rock Type	Volume % Phenocrysts Olivine	Augite	Volume % Vesicles	Olivine	Augite	Plag.	Ores	Neph.	Glass	Ultra-mafic inclusions	Comments
9	basanite	15·0	tr	8·0	X	X	X	X	X	X	-	small red spinel octahedra common. some elongate ore microphenocrysts. some skeletal olivine
10	basanite	10·6	-	15·6	X	X	X	X	X	X	-	as above.
36	nepheline basalt	8·8	-	4·5	X	X	-	X	X	X	X	Some olivines deformed and resorbed, some are large skeletal crystals. Ore microphenocrysts much glass. minor apatite.
37(2)	nepheline basalt	6·7	6·3	0	X	X	-	X	-	X	X	Groundmass much finer than above. Augite strongly zoned and polysynthetically twinned
37(3)	nepheline basalt	11·9	-	4·0	X	X	-	X	-	X	X	Small red spinel octahedra. Some olivines deformed and resorbed, some euhedral.
52	basanite	1·4	1·4	31·3	X	X	X	X	-	X	-	Olivine mostly euhedral, some resorbed. some augites have diopside cores.
53	basanite	6·1	1·3	-	X	X	X	X	X	-	X	Olivine mostly euhedral but some excellent skeletal crystals.
54	nepheline basalt	14·8	-	18·0	X	X	-	X	X	-	X	Much xenocrystal olivine; some spinel; incipient weathering near vesicles and cracks
55	basanite	10·9	-	13·3	X	X	X	X	X	-	X	Augites show complex intergrowths; some olivines resorbed but generally euhedral; plag. microphenocrysts.
56	nepheline basalt	13·6	-	7·4	X	X	-	X	-	X	X	The complex exsolution phenomena of the olivines indicate that this rock has undergone severe high temp. oxidation.
57	basanite	10·4	-	30·7	X	X	X	X	X	-	-	Slight resorption of olivine
58	basanite	4·0	-	0	X	X	X	X	X	-	X	Abundant ilmenite(?)microphenocrysts. some red spinel octahedra.
59	basanite	7·5	4·6	17·7	X	X	X	X	X	X	-	Coarse groundmass very rich in plag. olivine sometimes rimmed with augite residual liquid on vesicle

(Contd.)

Table B-2 (Contd.)

Rock No.	Rock Type	Volume % Phenocrysts Olivine	Augite	Volume % Vesicles	Groundmass mineralogy Olivine	Augite	Plag.	Ores	Neph.	Glass	Ultra-mafic inclusions	Comments
165	basanite	9·4	1·9	13·0	X	X	X	X	-	-	X	Some olivine and augite re-sorbed; sandstone inclusions present
171	nepheline basalt	13·5	-	4·8	X	X	-	X	-	-	X	
172	basanite	10·2	1·5	26·9	X	X	X	X	X	X	-	Small fine grained olivine glomerocrysts; olivines re-sorbed, have rare spinel inclusions
173	basanite	11·0	-	12·1	X	X	X	X	-	X	X	Abundant red spinel octahedra
178	nepheline basalt	< 1%	< 1%	24·1	X	X	-	X	-	X	-	Very glassy (= limburgite). Some olivine resorbed, but mostly skeletal. Augite in rosettes.
192	nepheline basalt	10·8	-	21·8	X	X	-	X	-	X	-	Olivines mostly large skeletal crystals, elongated, giving striking fluidal texture.

Petrography of analysed rocks, other than lava flows, from Grande Comore.

Table B-3. Badjini lavas

Rock No.	Rock Type	Volume % Phenocrysts				Volume % Vesicles	Groundmass mineralogy					Comments
		Olivine	Augite	Plagio-clase	Ores		Olivine	Augite	Plag.	Ore	Neph.	
132	Alkali Basalt	-	tr	tr		0	-	X	X	X		Microphenocrysts of augite and plagio-clase. fluidal texture.
146	Alkali basalt	-	-	-		26·0	X	X	X	X	X	Dendritic skeletal ore in glass. intersertal texture.
147	Feldspar-phyric basalt	-	1·0	7·5		11·7	X	X	X	X	X	Plagioclase microphenocrysts partly re-sorbed. strongly zoned. intersertal texture.
156	basanite	7·3	1·3	-		17·6	X	X	X	X	X	Olivines slightly iddingsitized. Striking microporphyritic texture. intersertal texture.
158	basanite	7·0	-	-		23·2	X	X	X	X	X	As above. Groundmass coarser

Table B-4. Intrusive rocks from the Kartala caldera

Rock No.	Rock Type	Olivine	Augite	Plagio-clase	Ores	Vesicles	Olivine	Augite	Plag.	Ore	Neph.	Comments
42	Alkali gabbro	2·5	30·6	53·2	13·7	0	X	X	X	X		Ores very skeletal; pyroxene zoned from purple titanaugite to pale green aegerine-augite rims; accessory biotite near ore minerals; apatite abundant.
44	Alkali dolerite	6·0	11·9	63·7	18·4	0	X	X	X	X		Layering results from different grain size; cpx less zoned than above; varioles filled by yellowish fibrous zeolites.
105	Alkali basalt	-	-	-	0	-	X	X	X	X		Some microphenocrysts of plag. and cpx. minor glass.
107	Alkali basalt	-	tr	-	0	14·5	X	X	X	X		Has inclusions of doleritic country rock (removed before analysis) Plag. strongly zoned.
110	Alkali basalt	-	-	-	0	30·0	X	X	X	X		

Table B-5. Miscellaneous analysed rocks

Rock No.	Rock Type	Olivine	Augite	Plagio-clase	Ores	Vesicles	Olivine	Augite	Plag.	Ore	Neph.	Comments
16a	Vitric crystal tuff	10·8	10·9	-		0	-	-	-		X	(R.I. of glass = 1·554, but varies with oxidation. Minerals fragmented. Pyroxene is distinctly green diopside.
b	"	20·4	11·1	-		0	-	-	-		X	(
30	Feldspar-phyric basalt	9·1	15·6	11·9		2·3	-	X	An-35	X		Plagioclase, phenocrysts strained, but un-zoned, = An-60. Groundmass extremely fine-grained. Augite, strongly zoned. Olivines iddingsitized, some in cores, some rims.
35	Spinel lherzolite											The particular nodule analysed has ~90% olivine, ~5% chrome diopside, ~5% enstatite, and < 1% red spinel. The enstatite is oxidized, and partially remelted, leaving a granular mosaic of olivine and diopside. Coarser diopside appears interstitial to olivine, i.e. formed later than it.
38A	altered basanite											
130	Feldspar-phyric basalt	11·6	-	19·0		7·2	X	X	X	X		Feldspar is An-66. N.B. This is the only rock on Grande Comore with the ol+plag. phenocryst assemblage, and also the only one with hy in the norm.

APPENDIX C

Tables of chemical data

C.1.   Kartala lavas

C.2.   La Grille lavas

C.3.   Badjini lavas

C.4.   Kartala intrusive rocks

C.5.   Miscellaneous rocks

* indicates that Fe_2O_3 has been reduced to
2.00 wt.% before calculation of the norm.

D.I. = differentiation index (Thornton and Tuttle, 1960).

Table C-1

Chemical Analysis of Lavas from Kartala

	1	4	6	8	13	17	18	19	20
SiO_2	47·12	47·30	47·45	47·99	45·40	46·05	44·91	45·85	46·60
TiO_2	2·32	2·56	2·29	2·55	1·60	1·94	1·49	1·56	2·67
Al_2O_3	13·20	14·68	14·19	14·32	8·46	10·02	7·78	8·14	14·40
Fe_2O_3	2·53	2·31	1·69	3·07	3·29	1·75	2·02	2·19	4·78
FeO	9·16	9·29	10·22	8·21	8·42	9·80	9·76	9·73	7·89
MnO	·19	·20	·19	·20	·20	·19	·20	·19	·30
MgO	9·38	6·66	6·69	6·65	17·43	15·60	21·07	19·66	5·92
CaO	11·48	11·71	12·82	11·50	11·79	10·85	9·07	9·58	11·28
Na_2O	2·89	3·41	3·12	3·40	1·42	2·34	1·56	1·76	3·39
K_2O	1·24	1·44	1·12	1·32	·52	·89	·48	·57	1·28
P_2O_5	·41	·45	·40	·47	·26	·29	·23	·27	·39
H_2O	·42	·25	·14	·38	·86	·71	·49	·31	·80
Total	100·34	100·26	100·32	100·06	99·65	100·43	99·06	99·81	99·70
Or	7·32	8·51	6·60	7·82	3·11	5·27	2·88	3·38	7·65
Ab	15·86	16·48	14·93	21·38	11·58	10·94	12·50	13·74	21·39
An	18·65	20·52	21·35	19·97	15·36	14·25	12·99	12·69	20·52
Ne	5·37	6·70	6·18	4·05	·31	4·83	·48	·67	4·12
Di	28·78	28·29	32·48	27·71	33·53	30·35	24·83	26·59	27·04
Ol	15·05	10·24	10·72	8·63	27·58	27·43	39·92	36·12	6·22
Mt	3·59	3·35	2·44	4·46	4·83	2·54	2·97	3·19	7·01
Ilm	4·40	4·86	4·34	4·86	3·08	3·69	2·87	2·98	5·13
Ap	·97	1·07	·94	1·12	·62	·69	·55	·64	·93
Rest	·42	·25	·14	·38	·86	·71	·49	·31	·80
Rb	29	24	20	28	14	15	10	17	24
Cu	102	90	101	80	93	85	73	73	76
Sr	512	510	425	510	288	345	245	275	485
Ba	381	520	470	430	280	240	200	220	360
Zn	93	100	107	92	85	95	104	95	103
Zr	201	270	188	228	121	138	110	120	220
Cr	337	125	70						112
Ni	212	55	77						90
DI	28·56	31·68	27·71	33·25	15·01	21·04	15·86	17·79	33·16

Table C-1 (Contd.)

	21	22	23	24	25	26	27	28
SiO_2	47·20	47·63	47·13	47·25	48·32	47·60	46·73	46·90
TiO_2	1·95	2·65	2·43	2·55	2·45	2·50	2·51	2·76
Al_2O_3	12·86	14·22	13·61	14·11	14·83	14·26	13·89	15·10
Fe_2O_3	1·84	1·34	2·83	2·09	2·97	3·12	3·37	3·50
FeO	9·83	9·86	9·11	9·47	9·24	8·27	8·30	8·75
MnO	·19	·19	·20	·26	·19	·19	·18	·22
MgO	10·92	6·65	8·43	6·60	5·50	6·66	6·86	5·44
CaO	11·24	11·51	11·72	12·02	11·42	12·20	12·65	11·18
Na_2O	2·37	3·40	3·07	3·17	3·26	3·37	3·04	3·54
K_2O	·68	1·35	1·26	1·22	1·39	1·28	1·22	1·45
P_2O_5	·26	·43	·42	·42	·44	·42	·43	·42
H_2O	·13	·32	·22	·32	·24	·10	·72	·15
Total	99·47	99·55	100·43	99·48	100·26	99·97	99·90	99·41
Or	4·04	8·04	7·43	7·27	8·21	7·57	7·27	8·63
Ab	19·36	18·16	16·45	17·90	22·55	18·08	16·35	19·83
An	22·59	19·70	19·59	20·84	21·72	20·01	20·82	21·18
Ne	·45	5·87	5·13	4·96	2·72	5·66	5·19	5·60
Di	25·77	28·73	28·91	29·90	26·31	30·67	32·09	26·07
Ol	20·75	11·45	12·80	10·20	8·50	7·75	7·53	7·29
Mt	2·69	1·96	4·09	3·06	4·30	4·53	4·93	5·11
Ilm	3·73	5·07	4·60	4·88	4·65	4·75	4·81	5·28
Ap	·62	1·03	·99	1·00	1·04	1·00	1·03	1·00
Rest	·13	·32	·22	·32	·24	·10	·72	·15
Rb	24	31	24	23	24	24	23	30
Cu	108	115	101	123	65	83	146	77
Sr	364	495	460	465	475	473	497	500
Ba	300	432	500	365	370	440	382	450
Zn	98	118	112	110	110	88	96	105
Zr	160	240	219	235	240	230	222	240
Cr		130	253	175	35	145	124	60
Ni		118	190	103	55	94	104	48
D.I.	23·85	32·06	29·01	30·12	33·48	31·31	28·81	34·06

Table C-1 (Contd)

	29	31	32	*39	*40	41	45
SiO_2	46·50	46·76	47·70	46·10	47·77	47·37	46·25
TiO_2	2·62	1·58	2·42	2·64	2·76	1·91	2·78
Al_2O_3	14·21	9·76	14·71	14·80	14·99	11·75	14·90
Fe_2O_3	3·11	2·46	2·33	4·45	4·36	1·88	3·25
FeO	9·00	8·87	9·53	8·07	8·15	9·19	8·89
MnO	·48	·19	·20	·26	·24	·18	·23
MgO	6·02	15·98	6·12	5·52	5·94	11·22	5·23
CaO	11·80	11·00	11·32	11·30	10·57	12·92	11·33
Na_2O	2·64	1·93	3·32	3·10	3·04	2·58	3·46
K_2O	1·42	·61	1·34	1·33	1·17	·83	1·54
P_2O_5	·39	·23	·41	·37	·39	·30	·43
H_2O	·55	·25	·25	·77	·76	·13	·52
Total	98·74	99·62	99·55	98·71	100·14	100·26	98·81
Or	8·54	3·63	7·96	8·06	6·97	4·90	9·26
Ab	18·81	15·60	20·25	18·17	24·79	12·86	17·91
An	23·14	16·27	21·40	23·12	24·01	18·00	20·93
Ne	2·13	·45	4·34	4·73	·63	4·84	6·43
Di	27·70	29·69	26·59	26·34	21·59	35·55	27·34
Ol	9·07	27·21	10·46	10·57	12·77	16·79	6·94
Mt	4·59	3·59	3·40	2·97	2·92	2·72	4·79
Ilm	5·07	3·02	4·62	5·14	5·29	3·62	5·37
Ap	·94	·55	·98	·90	·93	·71	1·04
Rest	·55	·25	·25	·77	·76	·13	·52
Rb	22	13	14	22	17	24	32
Cu	90	103	83	101	43	116	90
Sr	485	289	451	504	450	360	535
Ba	450	218	432	410	460	370	460
Zn	112	100	127	125	101	85	100
Zr	220	125	228	230	224	168	240
Cr	92	740	70	65	60	450	37
Ni	91	444	76	81	53	176	53
D.I.	29·49	19·68	32·55	32·14	32·83	22·60	33·60

Table C-1 (Contd.)

	46	47	48	*101	*102	103	112
SiO_2	46·40	47·25	47·50	47·18	47·46	47·76	47·15
TiO_2	2·57	2·70	2·52	2·44	2·60	2·79	2·48
Al_2O_3	14·20	15·34	14·98	13·90	14·45	14·80	15·06
Fe_2O_3	2·32	3·02	2·88	7·52	3·25	2·13	2·16
FeO	10·04	9·59	9·06	4·51	9·53	10·28	10·11
MnO	·21	·23	·21	·18	·19	·19	·19
MgO	6·19	5·63	5·85	6·50	5·78	5·23	5·84
CaO	12·08	10·97	11·45	12·06	11·49	10·83	11·75
Na_2O	3·24	3·40	3·07	2·81	3·54	3·39	3·27
K_2O	1·32	1·40	1·12	1·36	1·46	1·46	1·30
P_2O_5	·41	·46	·33	·43	·48	·51	·47
H_2O	·24	·63	·30	1·19	·32	·35	·29
Total	99·22	100·62	99·27	100·07	100·55	99·72	99·97
Or	7·88	8·27	6·69	8·18	8·60	8·68	7·70
Ab	15·05	20·71	22·57	18·17	17·66	22·37	17·89
An	20·51	22·46	24·03	21·67	19·16	20·98	22·62
Ne	6·85	4·36	1·99	3·26	6·60	3·51	5·33
Di	30·68	23·77	25·52	29·77	28·35	24·58	26·97
Ol	9·73	9·83	9·36	10·26	10·25	10·21	10·52
Mt	3·40	4·38	4·22	2·95	2·89	3·11	3·14
Ilm	4·93	5·13	4·83	4·71	5·28	5·33	4·72
Ap	·98	1·09	·79	1·04	1·20	1·22	1·12
Rest	·24	·63	·30	1·19	·35	·35	·29
Rb	20	27	21	38	30	35	35
Cu	99	98	68	80	79	53	57
Sr	437	517	443	550	568	540	515
Ba	415	400	350	400	480	418	408
Zn	109	120	114	104	81	113	102
Zr	200	242	202	195	207	222	187
Cr	83	49	83	60	45		
Ni	80	62	88	75	50		
D.I.	29·78	33·35	31·25	32·16	33·47	34·57	30·92

Table C-1 (Contd.)

	113	119	122	123	134	139	142
SiO_2	47·72	47·71	48·11	47·96	47·59	48·08	46·48
TiO_2	2·70	2·60	2·61	2·52	2·17	2·69	2·61
Al_2O_3	14·99	14·83	14·54	14·37	13·27	14·15	14·18
Fe_2O_3	2·59	2·73	·85	2·22	3·00	3·77	1·49
FeO	9·64	9·79	10·69	9·66	8·26	8·04	10·63
MnO	·18	·19	·18	·18	·19	·18	·20
MgO	5·49	5·75	6·16	6·33	7·83	6·47	6·95
CaO	11·20	11·11	11·60	12·00	13·38	11·55	11·04
Na_2O	3·47	3·38	3·15	3·05	2·68	3·22	2·96
K_2O	1·39	1·47	1·26	1·30	1·04	1·40	1·38
P_2O_5	·48	·47	·38	·45	·40	·52	·52
H_2O	·39	·47	·27	·25	·47	·31	·34
Total	100·24	100·50	99·79	100·70	100·28	100·38	98·78
Or	8·22	8·68	7·48	7·68	6·16	8·27	8·28
Ab	21·19	20·58	19·70	19·45	16·36	22·48	17·87
An	21·25	20·94	21·91	21·66	21·14	20·00	21·66
Ne	4·45	4·34	3·83	3·43	3·44	2·57	4·10
Di	25·70	25·55	27·62	28·62	34·57	27·36	25·09
Ol	9·16	9·91	12·34	10·09	8·89	7·53	14·52
Mt	3·76	3·96	1·34	3·22	4·36	5·46	2·19
Ilm	5·13	4·94	4·98	4·78	4·13	5·10	5·03
Ap	1·14	1·11	·90	1·06	·95	1·23	1·25
Rest	·39	·47	·27	·25	·47	·31	·34
Rb	38	35	30	33	28	38	30
Cu	81	57	73	82	140	85	68
Sr	573	570	496	475	440	528	530
Ba	490	510	418	422	395	460	460
Zn	113	113	108	106	93	97	107
Zr	223	208	221	198	160	229	213
Cr							
Ni							
D.I.	33·86	33·60	31·01	30·56	25·96	33·31	30·25

Table C-1 (Contd.)

	151	154	160	186	188	190	194	195
SiO_2	46·40	47·70	47·48	48·25	48·76	47·64	46·30	46·55
TiO_2	1·75	2·60	2·68	2·06	2·68	2·66	1·84	1·90
Al_2O_3	10·04	14·26	14·22	12·50	15·70	13·61	10·18	10·08
Fe_2O_3	1·91	3·22	3·06	2·83	2·63	2·31	2·76	3·41
FeO	9·63	9·02	8·80	7·95	8·36	9·31	8·63	8·32
MnO	·19	·19	·18	·17	·18	·18	·19	·19
MgO	14·82	6·87	6·49	9·16	5·21	6·75	13·87	14·02
CaO	11·17	11·78	11·47	13·40	10·29	11·36	12·12	12·18
Na_2O	2·50	3·03	3·40	2·40	3·28	3·14	1·86	2·06
K_2O	·78	1·21	1·38	·95	1·63	1·33	·80	·86
P_2O_5	·29	·39	·45	·39	·45	·48	·39	·30
H_2O	·25	·26	·24	·32	·73	·41	·66	·44
Total	99·73	100·46	99·85	100·38	99·86	99·18	99·60	100·31
Or	4·63	7·13	8·19	5·61	9·71	7·96	4·78	5·09
Ab	12·27	20·34	19·73	17·69	26·63	21·18	13·93	13·05
An	13·94	21·67	19·54	20·51	23·49	19·35	17·25	15·74
Ne	4·87	2·83	4·95	1·41	·73	3·10	1·07	2·38
Di	32·01	27·70	28·17	34·91	20·46	28·19	32·77	34·16
Ol	25·46	9·83	8·79	10·93	8·93	10·58	21·70	20·31
Mt	2·78	4·66	4·45	4·10	3·84	3·39	4·04	4·95
Ilm	3·34	4·92	5·11	3·91	5·13	5·11	3·53	3·61
Ap	·69	·92	1·07	·92	1·07	1·15	·93	·71
Rest	·25	·26	·24	·32	·73	·41	·66	·44
Rb	20	33	38	25	37	28	20	20
Cu	108	128	88	91	60	87	88	91
Sr	335	498	545	398	600	520	360	382
Ba	300	440	470	350	600	395	350	278
Zn	98	103	90	86	93	88	83	90
Zr	137	210	221	152	252	233	148	136
Cr		110	150	575	75			
Ni		98	98	170	50			
D.I.	21·78	30·30	32·87	24·71	37·07	32·23	19·78	20·52

Table C-2

Chemical Analyses of Lavas from La Grille

	9	10	36	37(2)	37(3)	52	53
SiO_2	43·49	43·61	42·70	43·16	43·33	43·50	44·92
TiO_2	2·13	2·04	1·92	1·72	1·74	2·20	1·75
Al_2O_3	12·66	12·64	9·95	10·36	10·44	12·09	12·98
Fe_2O_3	2·06	·55	2·86	2·99	3·23	3·41	3·43
FeO	9·45	10·86	8·67	8·16	8·26	7·80	8·56
MnO	·23	·20	·28	·19	·20	·20	·21
MgO	12·68	12·24	16·70	17·36	17·19	12·26	12·25
CaO	12·44	12·03	11·79	11·31	11·57	12·22	11·17
Na_2O	3·08	2·91	2·37	2·47	2·35	3·26	3·24
K_2O	1·32	1·05	1·30	1·18	1·16	1·34	·74
P_2O_5	·48	·45	·61	·47	·46	·64	·46
H_2O	·30	·48	1·08	·41	·41	1·13	·51
Total	100·32	99·08	100·23	99·78	100·34	100·05	100·22
Or	4·84	6·29	3·88	6·88	6·86	8·00	4·38
Ab	-	1·57	-	-	·12	2·63	11·62
An	16·81	18·59	12·78	13·78	14·52	14·55	18·74
Ne	14·11	12·68	10·95	11·39	10·71	13·67	8·59
Lc	2·32	-	3·03	·10	-	-	-
Di	33·59	31·62	33·63	31·49	31·74	33·90	27·11
Ol	20·16	23·44	26·41	27·59	26·96	16·49	20·14
Mt	2·99	·81	4·18	4·36	4·69	5·00	4·99
Ilm	4·04	3·93	3·68	3·29	3·31	4·22	3·33
Ap	1·14	1·08	1·46	1·12	1·09	1·53	1·09
Rest	·30	·48	1·08	·41	·41	1·13	·51
Rb	30	26	32	33	25	55	39
Cu	75	83	89	81	81	80	83
Sr	600	530	590	525	526	690	645
Ba	710	530	625	670	620	850	794
Zn	80	89	105	85	71	87	85
Zr	217	155	202	152	158	197	234
Cr			650	910	820	590	
Ni			540	2430	525	310	
D.I.	21·27	20·54	17·86	18·38	17·69	24·31	24·60

Table C-2 (Contd.)

	54	55	56	57	58	59
SiO_2	42·04	44·91	41·41	46·59	42·73	43·26
TiO_2	1·67	1·73	2·18	1·72	2·17	2·30
Al_2O_3	9·06	12·75	11·87	14·00	12·81	13·56
Fe_2O_3	3·46	1·81	3·79	2·33	3·93	2·34
FeO	7·58	10·47	8·42	10·01	8·17	9·14
MnO	·20	·21	·20	·21	·23	·20
MgO	20·01	12·00	12·81	9·48	10·96	9·74
CaO	10·85	11·14	13·06	11·08	12·01	12·76
Na_2O	1·88	2·68	2·73	2·81	3·62	2·54
K_2O	·93	·76	1·36	·55	1·49	1·29
P_2O_5	·55	·41	·84	·29	·65	·51
H_2O	·60	·52	1·11	·68	·35	1·37
Total	98·83	99·39	99·78	99·75	99·18	99·01
Or	5·59	4·54	·34	3·28	8·91	7·81
Ab	·47	11·33	-	19·82	1·03	3·92
An	13·78	20·75	16·33	24·18	14·47	22·31
Ne	8·52	6·29	12·60	2·26	16·22	9·80
Lc	-	-	6·12	-	-	-
Di	29·57	25·28	34·94	23·91	33·22	31·60
Ol	32·41	23·86	17·82	19·15	14·66	15·38
Mt	5·11	2·65	5·57	3·41	5·76	3·47
Ilm	3·23	3·32	4·19	3·30	4·17	4·47
Ap	1·33	·98	2·02	·69	1·56	1·24
Rest	·60	·52	1·11	·68	·35	1·37
Rb	26	13	37	14	50	25
Cu	80	78	69	60	70	77
Sr	495	480	590	331	700	625
Ba	525	475	720	350	880	700
Zn	90	100	100	105	87	85
Zr	157	130	242	145	245	216
D.I.	14·58	22·15	19·13	25·36	26·17	21·52

Table C-2 (Contd.)

	165	171	172	173	178	192
SiO_2	42·03	41·97	42·80	42·82	41·72	43·14
TiO_2	1·98	2·16	2·11	2·04	2·22	2·30
Al_2O_3	11·76	10·88	12·10	11·47	12·69	13·35
Fe_2O_3	4·53	3·25	3·57	2·62	3·40	3·92
FeO	7·28	8·76	8·07	8·82	9·07	8·20
MnO	·20	·21	·20	·21	·21	·22
MgO	14·42	14·22	12·44	14·21	10·92	10·36
CaO	12·24	12·45	12·67	12·23	13·53	11·11
Na_2O	2·23	3·08	2·95	2·89	3·03	4·27
K_2O	·44	1·14	1·44	1·03	1·15	1·74
P_2O_5	·64	·64	·53	·58	·80	·67
H_2O	2·30	·53	·64	·34	1·31	·51
Total	100·05	99·29	99·51	99·26	100·01	99·79
Or	2·66	·74	5·72	6·15	1·91	10·35
Ab	7·10	-	-	·19	-	1·78
An	21·25	12·65	15·69	15·45	17·85	12·21
Ne	6·61	14·29	13·67	13·28	14·06	18·74
Lc	-	4·77	2·26	-	3·90	-
Di	28·99	36·46	35·42	33·65	36·05	31·15
Ol	21·28	20·64	16·68	22·14	15·06	14·05
Mt	6·72	4·77	5·23	3·84	4·99	5·72
Ilm	3·85	4·15	4·05	3·92	4·27	4·40
Ap	1·55	1·53	1·27	1·39	1·92	1·60
Rest	2·30	·53	·64	·34	1·31	·51
Rb	101	35	47	44	58	79
Cu	72	71	80	80	79	77
Sr	655	635	645	600	792	762
Ba	900	720	850	680	900	850
Zn	80	88	84	92	92	112
Zr	152	174	176	173	207	200
Cr			600			
Ni			290			
D.I.	16·37	19·80	21·65	19·63	19·87	30·88

Table C-3

Analyses of rocks other than lava flows from Kartala and La Grille

	Badjini lavas				
	132	146	147	156*	158*
SiO_2	48·61	47·10	46·80	45·86	46·58
TiO_2	2·78	2·56	2·48	2·60	2·51
Al_2O_3	15·32	14·05	14·12	12·81	14·02
Fe_2O_3	5·03	3·38	1·76	5·57	5·77
FeO	7·29	9·04	9·78	6·91	7·19
MnO	·19	·19	·48	·17	·19
MgO	5·09	6·60	5·64	9·95	8·02
CaO	10·42	12·58	11·20	11·47	10·86
Na_2O	3·41	2·66	4·36	2·26	2·52
K_2O	1·55	1·12	·85	1·14	1·17
P_2O_5	·54	·42	·38	·46	·40
H_2O	·51	·70	·66	1·13	1·07
Total	100·74	100·40	98·51	100·33	100·30
Or	9·14	6·64	5·13	6·85	7·00
Ab	28·65	18·93	19·81	15·91	19·70
An	21·86	23·15	16·80	21·79	23·76
Ne	·07	1·97	9·69	1·91	1·02
Di	21·07	29·86	30·92	26·69	22·98
Ol	5·40	8·66	9·31	17·77	16·83
Mt	7·27	4·91	2·61	2·95	2·93
Ilm	5·27	4·88	4·81	5·02	4·82
Ap	1·28	1·00	·92	1·11	·96
Rest	·51	·70	·66	1·13	1·07
Rb	38	25	16	24	17
Cu	54	93	92	82	68
Sr	600	545	435	497	540
Ba	490	420	350	625	590
Zn	103	82	107	82	95
Zr	230	187	175	173	214
Cr				480	
Ni				210	
D.I.	37·86	27·54	34·63	26·06	28·45

Table C-4

Analyses of rocks other than lava flows from Kartala and La Grille

	Kartala Intrusive Rocks				
	42	44	105	107	110
SiO_2	47·37	45·60	47·55	47·57	47·06
TiO_2	3·77	3·53	2·68	2·88	2·91
Al_2O_3	13·09	13·70	14·85	15·71	15·74
Fe_2O_3	2·23	3·29	2·68	1·31	1·98
FeO	12·12	10·87	9·44	10·75	10·11
MnO	·35	·23	·19	·20	·20
MgO	4·38	5·23	5·79	4·96	5·08
CaO	10·00	10·92	11·43	10·39	10·48
Na_2O	3·53	3·40	3·27	3·03	3·64
K_2O	1·74	1·49	1·38	1·72	1·61
P_2O_5	··53	·45	·51	·52	·56
H_2O	·34	·97	·52	·21	·55
Total	99·45	99·68	100·29	99·25	99·92
Or	10·37	8·92	8·17	10·26	9·57
Ab	23·50	18·12	20·67	21·92	20·17
An	14·86	17·95	21·81	24·41	21·99
Ne	3·59	5·97	3·82	2·14	5·86
Di	26·50	28·00	25·98	20·11	22·03
Ol	9·43	8·35	9·34	12·46	10·59
Mt	3·26	4·83	3·89	1·92	2·89
Ilm	7·22	6·79	5·10	5·52	5·56
Ap	1·27	1·08	1·21	1·24	1·33
Rest	·34	·97	·52	·21	·55
Rb	24	36	36	34	37
Cu	120	127	51	50	51
Sr	418	480	584	593	572
Ba	580	275	560	580	540
Zn	121	125	115	117	112
Zr	302	200	249	252	245
Cr	23	50			
Ni	18	55			
D.I.	37·47	33·01	32·66	34·33	35·60

Table C-5

Analyses of rocks other than lava flows from Kartala and La Grille

Miscellaneous Analysed Rocks

	16	30	35	38A	130	Mo-125
SiO_2	40·55	46·94	41·78	43·72	48·73	
TiO_2	1·71	2·60	·08	1·63	2·11	
Al_2O_3	8·57	14·40	·95	11·86	13·95	
Fe_2O_3	5·32	2·42	·05	3·80	2·93	
FeO	7·44	9·50	9·02	8·29	9·08	
MnO	·21	·21	·20	·20	·18	
MgO	19·22	7·23	44·70	12·64	8·61	
CaO	8·65	9·85	1·80	12·14	10·54	
Na_2O	·88	3·58	·20	1·72	2·90	
K_2O	·09	1·36	·01	·66	·68	
P_2O_5	·51	·69	·02	·43	·34	
H_2O	5·93	·69	·19	2·44	·27	
Total	99·08	99·47	99·00	99·53	100·32	

	16	30	35	38A	130	Mo-125
Or	·57	8·13	·06	4·02	4·02	
Ab	7·99	22·81	1·71	11·60	24·52	
An	20·57	19·44	1·68	23·37	23·02	
Ne	-	4·25	-	1·83	-	
Di	17·30	20·76	5·70	28·61	21·89	
Hy	15·95	-	1·47	-	5·83	
Ol	24·56	14·40	89·09	20·66	11·66	
Mt	8·28	3·55	·07	5·67	4·25	
Ilm	3·49	5·00	·15	3·19	4·00	
Ap	1·30	1·65	·05	1·05	·80	
Rest	5·93	·69	·19	2·44	·27	

	16	30	35	38A	130	Mo-125
Rb	<5	42	<5	17	11	33
Cu	80	57	30	98	82	7
Sr	84	846	20	1260	360	158
Ba	140	870	<5	475	255	610
Zn	85	125	97	91	93	24
Zr	127	347	20	162	152	242
Cr		123				
Ni		94				

	16	30	35	38A	130	Mo-125
D.I.	8·56	35·19	1·77	17·45	28·54	

APPENDIX D

Statistical analysis of chemical data

D.1. Discriminant function analysis

D.2. Correlation and variance

D. STATISTICAL ANALYSIS OF CHEMICAL DATA

D.1. Discriminant function analysis

The multivariate statistical technique of discriminant function analysis is ideally suited to the present problem of distinction between two groups of chemical variables. It is useful not only to determine the statistical significance of differences between two populations, but the discriminant function so calculated can be used to assign samples of unknown provenance to one population or another. Without reproducing the complex mathematics involved, the procedure may be paraphrased as follows:

Given: a) a normally distributed population, $\underline{U}$, with n_1 samples and
    k variables, and with $n_1 > k$; and

b) a normally distributed population $\underline{V}$, with n_2 samples and
    k variables, and with $n_2 > k$;

Calculate:

c) the discriminant functions

$$D = d_1 x_1 + d_2 x_2 + \cdots d_k x_k$$

for each analysis;

and   d) the mean discriminant functions D_u and D_v for each
    population $\underline{U}$ and $\underline{V}$;

and   d) the "deciding discriminant function" D_o.

Determine;

f) the confidence with which the two populations $\underline{U}$ and $\underline{V}$
    can be separated by carrying out an F-ratio test of the
    null hypothesis that $D_u = D_v$.

Calculate: g) for unassigned samples, the discriminant function,
D, by multiplication of each variable $x_1, x_2, \ldots x_k$
by the "characteristic numbers" $d_1, d_2, \ldots d_k 1$ and
adding these products. If $D > D_0$, then the sample
belongs in population $\underline{U}$; if $D < D_0$, then it belongs
in population $\underline{V}$.

Discriminant function analysis was employed in the present study
to determine a) the statistical significance of chemical differences
between Kartala and La Grille lavas, and b) whether the geomorpholo-
gical boundary between each volcano (see Chapter 2) accords with the
geochemical boundary, and c) test the petrographic affinity of the
Badjini lavas, and d) if any particular variable is suitable alone
for distinguishing between the two groups of lavas.

The characteristic numbers and deciding discriminant functions
for major elements and trace elements are given in Table D-1.

In order to apply the F-ratio test of significance it is
necessary that each population has a normal distribution. However,
it was shown that MgO in particular has a skewed distribution in
Kartala lavas. Rather than exclude this important variable or the
samples which cause the skew, or normalize them as logarithms, etc.,
the variables were separated into two groups consisting of the
twelve major elements and five trace elements. Cr and Ni were
not used because there was insufficient data for La Grille.
Separate discriminant functions were calculated for each group of var-
iables, but the F-ratio test was applied only to the trace elements.

Table D-1

Characteristic numbers and deciding discriminant functions

VARIABLE (x)	CHARACTERISTIC NUMBER (d)
wt.%	
SiO_2	4·1497
Al_2O_3	-4·3954
Fe_2O_3	0·4094
FeO	-0·6041
MgO	-2·3352
CaO	-2·6257
Na_2O	-9·0274
K_2O	5·2013
H_2O	-1·8756
TiO_2	5·1049
P_2O_5	-3·5413
MnO	-17·2550

Deciding discriminant function $D_o = 56·841$

ppm	
Rb	0·3992
Cu	-0·0304
Sr	-0·0292
Ba	-0·0765
Zn	-0·1124
Zr	0·1773

Deciding discriminant function $D_o = -23·0350$

In order to decide which variables are most effective in discriminating between Kartala and La Grille lavas, the correlation coefficients (r) between each variable and the discriminant function (D) have been calculated. These show (Table D-2) that SiO_2, Ba, and P_2O_5 are effective discriminators at the 99·9% level and Sr is suitable at the 99·0% level of significance. The sign of $\underline{r}$ indicates whether the variable makes a negative or positive contribution to the discriminant function. Thus, the opposing signs of $\underline{r}$ for P_2O_5 in Kartala and La Grille lavas will tend to cancel out its effectiveness as a discriminator.

D.2. Correlation and variance

The matrix of correlation coefficients has been calculated for each group of lavas according to the standard equation

$$r = \frac{n\sum xy - \sum x \sum y}{(n\sum x^2 - (\sum x)^2)(n\sum y^2 - (\sum y)^2)}$$

and these are presented in figures D-1 and D-2.

Some of these cannot be accepted as shown, however, because the variables are not independent, being restricted to the constant sum of 100%. As emphasized by Chayes (1960, 1962), the effect of the constant sum is to enhance any negative correlations between variables which make an important contribution to the variance. In order to determine the extent of this effect, the variance for

Table D-2

Importance of individual variables (x) in discriminating between Kartala and La Grille lavas, as indicated by their correlations (r) and the discriminant functions (D)

Variable (x)	(r) Kartala	(r) La Grille
SiO_2	$\cdot$49 **	$\cdot$73 **
TiO_2	$\cdot$33	$-\cdot$33
Al_2O_3	$\cdot$09	$-\cdot$15
Fe_2O_3	$\cdot$18	$-\cdot$45
FeO	$-\cdot$05	$\cdot$24
MnO	$\cdot$03	$-\cdot$24
MgO	$-\cdot$20	$\cdot$16
CaO	$-\cdot$14	$-\cdot$34
Na_2O	$-\cdot$06	$-\cdot$30
K_2O	$-\cdot$24	$-\cdot$36
P_2O_5	$\cdot$19	$-\cdot$74 **
H_2O	$-\cdot$06	$-\cdot$31
Rb	$-\cdot$05	$\cdot$28
Cu	$-\cdot$15	$\cdot$43
Sr	$\cdot$09	$\cdot$65 *
Ba	$\cdot$38 *	$\cdot$70 **
Zn	$-\cdot$05	$-\cdot$53
Zr	$-\cdot$07	$\cdot$28

* Significant at the 99·0% level of confidence.

** Significant at 99·9% level of confidence.

CORRELATION MATRIX FOR DATA MATRIX KARTALA   1

	SI / NA / ZN	TI / K / ZR	AL / P / DI	FE_2O_3 / H_2O	FED / RB	MN / CU	MG / SR	CA / BA
SI	1.000000	0.547437	0.670224	-0.031285	-0.042229	-0.135941	-0.667680	0.293390
	0.614187	0.559183	0.575560	-0.293689	0.580803	-0.145770	0.597154	0.606112
	0.058924	0.557553	0.659789					
TI	0.547437	1.000000	0.940875	0.212180	-0.017814	0.070039	-0.943101	0.075070
	0.920177	0.946328	0.834938	0.012584	0.654413	-0.211503	0.917710	0.814778
	0.401315	0.926030	0.959941					
AL	0.670224	0.940875	1.000000	0.168814	-0.008620	0.037626	-0.986502	0.196629
	0.928643	0.911057	0.784902	-0.090352	0.629392	-0.166998	0.887554	0.829783
	0.435240	0.898269	0.957214					
FE_2O_3	-0.031285	0.212180	0.168814	1.000000	-0.898783	0.044680	-0.213066	0.100223
	0.085439	0.203834	0.123201	0.647224	0.176763	-0.081504	0.253604	0.108331
	-0.039827	0.143095	0.235135					
FEO	-0.042229	-0.017814	-0.008620	-0.898783	1.000000	-0.013283	0.063606	-0.251518
	0.082886	-0.039439	0.006749	-0.604819	-0.117896	-0.080608	-0.103739	-0.016015
	0.251821	-0.017641	-0.065337					
MN	-0.135941	0.070039	0.037626	0.044680	-0.013283	1.000000	-0.063895	0.038054
	-0.099451	0.096219	-0.049181	0.084749	-0.103963	0.017627	0.015566	0.062157
	0.144243	0.052027	-0.005557					
MG	-0.667680	-0.943101	-0.986502	-0.213066	0.063606	-0.063895	1.000000	-0.302110
	-0.916905	-0.915236	-0.810346	0.063175	-0.641433	0.119660	-0.893730	-0.823280
	-0.384835	-0.883477	-0.945102					
CA	0.293390	0.075070	0.196629	0.100223	-0.251518	0.038054	-0.302110	1.000000
	0.110757	0.082815	0.170945	-0.128759	0.134967	0.536902	0.108324	0.177195
	-0.236525	0.041673	0.024895					
NA	0.614187	0.920177	0.928643	0.085439	0.082886	-0.099451	-0.916905	0.110757
	1.000000	0.915270	0.801988	-0.200115	0.625337	-0.151771	0.871937	0.794419
	0.381281	0.899371	0.951109					
K	0.559183	0.946328	0.911057	0.203834	-0.039439	0.096219	-0.915236	0.082815
	0.915270	1.000000	0.881078	0.012603	0.693388	-0.236940	0.952671	0.861253
	0.366501	0.912777	0.955817					
P	0.575560	0.834938	0.784902	0.123201	0.006749	-0.049181	-0.810346	0.170946
	0.801988	0.881078	1.000000	-0.035000	0.741771	-0.225370	0.889768	0.707508
	0.183980	0.776306	0.831075					
H_2O	-0.293689	0.012584	-0.090352	0.647224	-0.604819	0.084749	0.063175	-0.128759
	-0.200115	0.012603	-0.035000	1.000000	-0.024378	-0.102364	0.080717	-0.077259
	-0.024965	-0.054756	-0.025951					
RB	0.580803	0.654413	0.629392	0.176763	-0.117896	-0.103963	-0.641433	0.134967
	0.625337	0.693388	0.741771	-0.024378	1.000000	-0.144693	0.818777	0.658041
	0.023193	0.535614	0.682862					
CU	-0.145770	-0.211503	-0.166998	-0.081504	-0.080608	0.017627	0.119660	0.536902
	-0.151771	-0.236940	-0.225370	-0.102364	-0.144693	1.000000	-0.202479	-0.177086
	-0.102929	-0.130918	-0.277786					
SR	0.597154	0.917710	0.887554	0.253604	-0.103739	0.015566	-0.893730	0.108324
	0.871937	0.952671	0.889768	0.080717	0.818777	-0.202479	1.000000	0.851857
	0.250431	0.852063	0.931408					
BA	0.606112	0.814778	0.829783	0.108331	-0.016015	0.062157	-0.823280	0.177195
	0.794419	0.861253	0.797508	-0.077259	0.658041	-0.177086	0.851857	1.000000
	0.207674	0.811135	0.823150					
ZN	0.058924	0.401315	0.435240	-0.039827	0.251821	0.144243	-0.384835	-0.236525
	0.381281	0.366501	0.183980	-0.024965	0.023193	-0.102929	0.250431	0.207674
	1.000000	0.403265	0.400929					
ZR	0.557553	0.926030	0.898269	0.143095	-0.017641	0.052027	-0.883477	0.041673
	0.899371	0.912777	0.776306	-0.054756	0.535614	-0.130918	0.852063	0.811135
	0.403265	1.000000	0.924538					
DI	0.659789	0.959941	0.957214	0.235135	-0.065337	-0.005557	-0.945102	0.024895
	0.951109	0.955817	0.831075	-0.025951	0.632362	-0.277786	0.931408	0.823150
	0.400929	0.924538	1.000000					

CORRELATION MATRIX FOR DATA MATRIX GRILLE   1

	SI / NA / ZN	TI / K / ZR	AL / P / DI	FE2O3 / H2O	FEO / RB	MN / CU	MG / SR	CA / BA
SI	1.000000	-0.463781	0.511073	-0.477091	0.537710	-0.003374	-0.377168	-0.572806
	0.137063	-0.400891	-0.830455	-0.331523	-0.451508	-0.180619	-0.570869	-0.552916
	0.177657	-0.285219	0.481820					
TI	-0.463781	1.000000	0.399642	0.162151	-0.073652	0.086553	-0.552883	0.724609
	0.573605	0.646337	0.639290	0.248345	0.448350	-0.123302	0.739449	0.637262
	0.091767	0.579960	0.364023					
AL	0.511073	0.399642	1.000000	-0.211167	0.471834	-0.090645	-0.967749	0.164303
	0.606866	-0.003934	-0.152146	0.051717	0.087418	-0.437697	0.147136	0.112968
	0.229081	0.271071	0.755646					
FE2O3	-0.477091	0.162151	-0.211167	1.000000	-0.892156	-0.030432	0.152040	0.097993
	0.119692	0.146862	0.591854	0.381310	0.682818	-0.176364	0.511416	0.671785
	-0.063563	0.328054	0.020438					
FEO	0.537710	-0.073652	0.471834	-0.892156	1.000000	0.088339	-0.435994	-0.016891
	0.079931	-0.198572	-0.472349	-0.318927	-0.602681	-0.076072	-0.423897	-0.605171
	0.268230	-0.221321	0.185586					
MN	-0.003374	0.086553	-0.090645	-0.030432	0.088339	1.000000	0.021481	-0.054302
	0.144484	0.243319	0.108516	-0.057390	-0.033795	0.225500	0.128323	-0.006377
	0.403191	0.330822	0.116639					
MG	-0.377168	-0.552883	-0.967749	0.152040	-0.435994	0.021481	1.000000	-0.310904
	-0.660847	-0.123870	-0.013648	-0.093829	-0.118994	0.443101	-0.259575	-0.197276
	-0.297713	-0.349295	-0.761419					
CA	-0.572806	0.724609	0.164303	0.097993	-0.016891	-0.054302	-0.310904	1.000000
	0.060459	0.299176	0.615568	0.419275	0.246146	-0.083912	0.525491	0.519371
	-0.229949	0.436569	-0.180886					
NA	0.137063	0.573605	0.606866	0.119692	0.079931	0.144484	-0.660847	0.060459
	1.000000	0.524758	0.225455	-0.320115	0.329851	-0.162604	0.551772	0.452505
	0.319643	0.466068	0.893890					
K	-0.400891	0.646337	-0.003934	0.146862	-0.198572	0.243319	-0.123870	0.299176
	0.524758	1.000000	0.452987	-0.290659	0.099721	0.218618	0.535316	0.424294
	0.126367	0.541388	0.350188					
P	-0.830455	0.639290	-0.152146	0.591854	-0.472349	0.108516	-0.013648	0.615568
	0.225455	0.452987	1.000000	0.410092	0.580044	0.005485	0.740710	0.682747
	0.149588	0.544420	-0.078403					
H2O	-0.331523	0.248345	0.051717	0.381310	-0.318927	-0.057390	-0.093829	0.419275
	-0.320115	-0.290659	0.410092	1.000000	0.552916	-0.106446	0.274125	0.353524
	-0.035082	0.042672	-0.289536					
RB	-0.451508	0.448350	0.087418	0.682818	-0.602681	-0.033795	-0.118994	0.246146
	0.329851	0.099721	0.580044	0.552916	1.000000	-0.035204	0.713376	0.796501
	-0.029041	0.184884	0.149121					
CU	-0.180619	-0.123302	-0.437697	-0.176364	-0.076072	0.225500	0.443101	-0.083912
	-0.162604	0.218618	0.005485	-0.106446	-0.035204	1.000000	0.237864	0.114587
	-0.162838	-0.018373	-0.269038					
SR	-0.570869	0.739449	0.147136	0.511416	-0.423897	0.128323	-0.259575	0.525491
	0.551772	0.535316	0.740710	0.274125	0.713376	0.237864	1.000000	0.929051
	-0.077618	0.601366	0.269375					
BA	-0.552916	0.637262	0.112968	0.671785	-0.605171	-0.006377	-0.197276	0.519371
	0.452505	0.424294	0.682747	0.353524	0.796501	0.114587	0.929051	1.000000
	-0.263339	0.568944	0.199206					
ZN	0.177657	0.091767	0.229081	-0.063563	0.268230	0.403191	-0.297713	-0.229949
	0.319643	0.126367	0.149588	-0.035082	-0.029041	-0.162838	-0.077618	-0.263339
	1.000000	0.031023	0.420985					
ZR	-0.285219	0.579960	0.271071	0.328054	-0.221321	0.330822	-0.349295	0.436569
	0.466068	0.541388	0.544420	0.042672	0.184884	-0.018373	0.601366	0.568944
	0.031023	1.000000	0.338671					
DI	0.481820	0.364023	0.755646	0.020438	0.185586	0.116639	-0.761419	-0.180886
	0.893890	0.350188	-0.078403	-0.289536	0.149121	-0.269038	0.269375	0.199206
	0.420985	0.338671	1.000000					

the Kartala and La Grille lavas has been calculated (Tables D-3 and D-4, respectively). The six oxides SiO_2, Al_2O_3, Fe_2O_3, FeO, CaO, and MgO make up 97·9% and 92·7% of the total variance for Kartala and La Grille respectively, and MgO contributes more than all other variables together in each volcano.

Because of the large variance given by MgO, any correlations between MgO and the other five variables will have a strong negative component artificially imposed by the constant sum effect. This component can be calculated by the equation

$$E(r_{1j}) = \frac{\sigma_1}{\sigma_c(1 - M')}$$

where variable 1 is MgO and variables j are SiO_2, Al_2O_3, Fe_2O_3, FeO, and CaO, σ_c is the mean standard deviation of variables j, and M' is the reduced number of variables (i.e. six) (see Chayes, 1962, p. 442). This calculation indicates that the constant sum effect contributes -0·72 and -0·55 to the Kartala and La Grille correlation coefficients respectively. For those elements which make insignificant contributions to the total variance and are consequently free of constant sum effects, the correlation co-efficients can be accepted as given.

Table D-3

Variance of Kartala chemistry

Variable	Minimum	Mean	Maximum	Variance(σ^2)	% Variance
SiO_2	44·91	47·16	48·76	·63	2·48
TiO_2	1·49	2·38	2·79	·14	·55
Al_2O_3	7·78	13·41	15·70	4·29	16·88
Fe_2O_3	·85	2·80	7·52	1·14	4·48
FeO	4·51	9·06	10·69	1·02	4·01
MnO	·17	·19	·47	·006	*
MgO	5·21	8·38	21·07	17·15	67·47
CaO	9·07	11·53	13·40	·65	2·56
Na_2O	1·42	2·93	3·54	·31	1·22
K_2O	·48	1·19	1·63	·09	·35
P_2O_5	·23	·40	·52	·006	*
H_2O	·10	·41	1·19	·05	**
Rb	10	26	38	53	*
Cu	43	89	146	466	*
Sr	245	461	600	7359	*
Ba	200	399	600	7135	*
Zn	81	102	127	124	*
Zr	110	200	270	166	*

* Insignificant

** Omitted.

Table D-4

Variance of La Grille chemistry

Variable	Minimum	Mean	Maximum	Variance (σ^2)	Variance %
SiO_2	41·41	43·16	46·59	1·56	11·07
TiO_2	1·67	2·00	2·30	·05	·35
Al_2O_3	9·06	11·97	14·00	1·74	12·35
Fe_2O_3	0·55	3·03	4·53	·84	5·96
FeO	7·28	8·72	10·86	·89	6·32
MnO	·19	·21	·28	·004	*
MgO	9·48	13·28	20·01	8·03	56·99
CaO	10·85	11·98	13·53	·56	3·97
Na_2O	1·88	2·86	4·27	·29	2·06
K_2O	·44	1·13	1·74	·11	·78
P_2O_5	·29	·56	·84	·02	·14
H_2O	·30	·77	2·30	·25	**
Rb	13	40	101	469	*
Cu	60	77	89	42	*
Sr	331	601	792	11339	*
Ba	350	703	900	24193	*
Zn	71	90	112	102	*
Zr	130	186	245	1218	*

* Insignificant

** Omitted

References Cited

Chayes, F., 1960. On correlation between variables of constant sum. *J. geophys. Res.* 65, 4185-4193.

Chayes, F., 1962. Numerical correlation and petrographic variation. *J. Geol.* 70, 440-452.

APPENDIX E

Electron microprobe data

Table E.1. Augites

	CaO	MgO	FeO	TiO_2	Al_2O_3	Na_2O	Mol % Ca	Mol % Mg	Mol % Fe
GC-1									
Core	21·8	13·9	8·1	2·0	-	-	46·0	41·2	12·8
Rim	21·8	14·6	7·8	1·7	-	-	45·4	41·8	12·8
Core	22·7	17·6	4·4	0·6	-	-	44·4	48·9	6·7
Rim	22·0	15·0	7·8	2·6	-	-	44·9	42·7	12·4
G'mass	22·6	12·1	7·1	2·1	-	-	50·0	37·6	12·5
G'mass	20·3	14·4	8·2	2·1	-	-	46·1	41·4	12·5
GC-2									
Core	22·0	16·5	5·4	1·0	3·5	0·5	44·9	47·2	7·9
Rim	22·3	17·6	4·6	0·8	2·6	0·2	44·4	48·9	6·7
Core	22·2	15·2	5·4	1·2	3·9	1·5	46·5	44·2	9·3
Rim	21·6	15·5	6·6	2·5	7·1	0·5	44·8	44·8	10·4
Core	-	16·0	5·1	1·1	3·7	-	-	-	-
Rim	-	13·9	6·6	1·8	5·9	-	-	-	-
G'mass	21·2	7·5	11·1	2·0	6·0	1·3	52·8	26·4	20·6
G'mass	21·3	13·8	7·2	2·6	7·0	0·7	45·8	42·2	12·0
GC-26									
Core	21·1	15·2	5·6	1·5	-	-	45·2	45·2	9·6
Rim	21·7	14·7	5·4	1·5	-	-	46·5	44·1	9·5
Core	20·6	16·3	5·5	1·2	-	-	43·1	47·7	9·2
Rim	22·3	15·2	5·2	1·7	-	-	47·1	44·7	8·2
Core	19·9	15·8	5·5	2·4	-	-	43·4	47·0	9·6
Rim	22·5	16·5	5·4	1·2	-	-	45·0	46·1	8·9
G'mass	20·1	13·7	6·7	2·3	-	-	45·6	43·0	11·4
G'mass	21·0	15·1	7·2	1·1	-	-	44·2	44·2	13·5
GC-30									
Core	21·8	14·0	5·8	1·6	-	-	47·5	42·6	10·0
Rim	19·5	13·2	7·6	2·0	-	-	44·4	42·1	13·5
Dark	22·0	12·7	7·8	3·1	-	-	48·1	38·9	13·0
Light	21·7	13·8	7·5	2·4	-	-	46·4	41·2	12·4
Light Core	18·2	11·9	7·1	1·6	-	-	45·3	41·2	14·4
Dark	21·2	12·0	7·4	2·7	-	-	48·4	38·5	13·2
Light	21·5	13·8	7·4	1·8	-	-	46·3	41·4	12·4
G'mass	21·7	12·2	8·0	3·5	-	-	48·3	38·0	13·8

	CaO	MgO	FeO	TiO_2	Al_2O_3	Na_2O	Cr_2O_3	Mol % Ca	Mol % Mg	Mol % Fe
GC-31										
Brown Core	22·5	16·1	5·2	1·6	3·1	2·6		45·7	45·9	8·4
Light Core	22·5	16·7	4·9	0·8	3·4	0·9		45·4	46·9	7·7
Light Core	-	17·3	4·5	0·9	-	1·0		-	-	-
Dark Rim	-	15·9	6·2	1·6	-	2·0		-	-	-
Core	22·2	17·7	4·5	0·7	3·3	0·8		45·4	46·9	7·7
Rim	21·9	16·1	6·0	1·8	4·2	1·4		44·5	46·0	9·6
Core	-	-	-	1·6	-	2·1		-	-	-
Rim	-	-	-	1·1	-	0·2		-	-	-
G'mass	21·7	17·1	5·4	1·3	3·8	1·1		43·7	47·0	8·3
G'mass	-	13·5	5·4	1·0	-	0·1		-	-	-
GC-35										
Core	18·7	16·2	3·8	-	4·6	-	1·0	42·3	51·3	6·4
Rim	19·6	16·4	-	-	-	-	-	-	-	-
Core	20·2	16·2	-	-	5·3	-	1·2	-	-	-
Rim	21·5	16·3	-	-	5·5	-	1·1	-	-	-
G'mass	-	16·5	4·0	-	5·7	-	1·1	-	-	-
G'mass	-	16·3	3·9	-	6·4	-	1·0	-	-	-
G'mass	-	15·9	2·7	-	7·0	-	0·8	-	-	-
G'mass	21·0	16·8	-	-	4·5	-	1·0	-	-	-
G'mass	20·5	16·1	4·9	-	3·1	-	1·2	44·1	47·6	8·3
G'mass	-	-	3·9	-	1·7	-	1·2	-	-	-
GC-41										
Core	21·7	15·4	5·3	1·1	-	-		45·9	45·9	8·2
Rim	22·4	15·5	5·0	1·1	-	-		46·5	45·4	8·1
Core	22·9	15·4	4·0	0·8	-	-		47·7	45·4	6·9
Rim	22·7	15·4	4·0	0·5	-	-		48·3	45·4	5·9
Core	20·7	16·0	4·0	0·4	-	-		45·2	48·8	6·1
Rim	20·7	16·4	6·0	1·7	-	-	·	43·0	47·7	9·3
G'mass	21·9	16·7	7·8	1·8	-	-		42·4	45·8	11·8
G'mass	22·5	15·8	6·6	1·4	-	-		45·0	45·0	10·0

	CaO	MgO	FeO	TiO$_2$	Al$_2$O$_3$	Na$_2$O		Mol % Ca	Mol % Mg	Mol % Fe
GC-44										
Core	19·2	12·5	11·2	1·6	2·2	1·8		38·3	42·0	19·7
Rim	19·7	11·5	11·4	2·4	2·5	3·5		36·3	43·7	20·0
Core	-	12·5	10·7	1·4	-	2·0		-	-	-
Rim	-	11·1	10·8	2·1	-	2·9		-	-	-
Core	19·6	13·0	10·6	1·5	2·0	1·5		39·7	42·2	18·1
Rim	20·5	11·8	11·1	1·9	3·5	3·2		36·2	44·5	19·3
Core	21·7	12·5	5·3	1·5	5·4	0·6		40·3	50·7	9·0
Rim	-	-	-	-	-	-		-	-	-
Core	-	12·8	11·0	1·5	-	2·1		-	-	-
Rim	-	11·0	12·8	2·1	-	3·9		-	-	-
Core	21·3	21·3	7·4	1·4	3·6	1·6		44·2	44·2	11·6

Table E-2. Olivine Microprobe Analyses

	Total as FeO	MgO	Mol % Fo		Total as FeO	MgO	Mol % Fo
GC-1				**GC-30 (Contd.)**			
Core	14·2	44·6	84·8	Micro-Pheno.			
Core	14·9	43·8	83·9	Core	29·1	31·3	66·4
Rim	14·2	45·3	85·1	Rim	29·1	31·9	66·1
Core	13·2	45·6	86·4	Core	25·1	35·8	71·5
Rim	13·2	45·6	86·4				
Core	12·7	45·2	86·2	G'mass	28·2	33·1	67·9
Rim	13·2	44·5	86·0	G'mass	25·1	33·6	70·6
G'mass	20·5	37·5	77·0	**GC-31**			
G'mass	29·6	30·1	64·5	Core	18·2	41·9	80·9
G'mass	28·5	31·2	66·2	Rim	16·3	43·2	82·4
GC-2				Core	16·1	42·5	82·8
Core	13·7	46·0	86·0	Rim	15·7	42·6	82·8
Rim	15·0	43·7	83·7	Core	17·2	40·6	80·7
Core	14·7	43·7	83·7	Rim	17·1	40·7	80·7
Rim	14·7	44·2	84·6	G'mass	16·8	42·3	82·2
Core	18·8	40·3	79·6	G'mass	17·9	40·8	80·4
Rim	20·1	38·2	77·3	**GC-35**			
G'mass	25·9	33·6	70·0	Core	13·8	49·6	86·7
G'mass	25·8	34·5	70·5	Rim	14·0	46·0	86·0
GC-26				Small Grains			
Core	19·3	42·9	80·0	1	13·5	45·4	86·4
Rim	19·0	43·9	80·9	2	13·2	48·9	87·4
G'mass	20·6	40·4	77·7	3	13·6	45·8	85·8
GC-30				4	13·8	48·4	86·4
Pheno.				5	13·3	44·8	85·4
Core	26·4	34·2	69·8	6	13·5	43·7	85·3
Rim	28·7	32·4	67·0	**GC-41**			
Core	27·7	32·6	67·2	Core	15·0	45·0	84·5
Rim	29·2	32·4	66·2	Rim	16·7	43·0	81·5
Resorbed Xeno.				Core	15·6	43·7	83·3
Core	21·6	37·1	75·5	Rim	14·5	44·9	84·9
Rim	22·5	34·2	73·5	Core	14·7	44·4	84·7
				Rim	15·4	43·7	84·0

Table E-2 (Contd.)

	FeO	MgO	Mol % Fo
GC-44			
Core	36·0	25·2	55·6
Rim	48·7	16·1	37·0
Core	43·4	20·0	45·4
Rim	57·2	14·9	31·9
Core	34·8	25·8	57·5
Rim	27·8	19·3	55·2
Micro-pheno.	45·2	18·6	42·8
Micro-pheno.	37·7	23·3	52·7
G'mass	45·8	16·2	38·4

Plate 1.

Typical coastal exposure, southeast
Grande Comore.

Plate 2.

Columnar-jointed lavas exposed in walls of
Chagnoumeni pit crater. Note interfingering
and pinching out of upper flows.   The
central thick flow is about 10 metres thick.

1

2
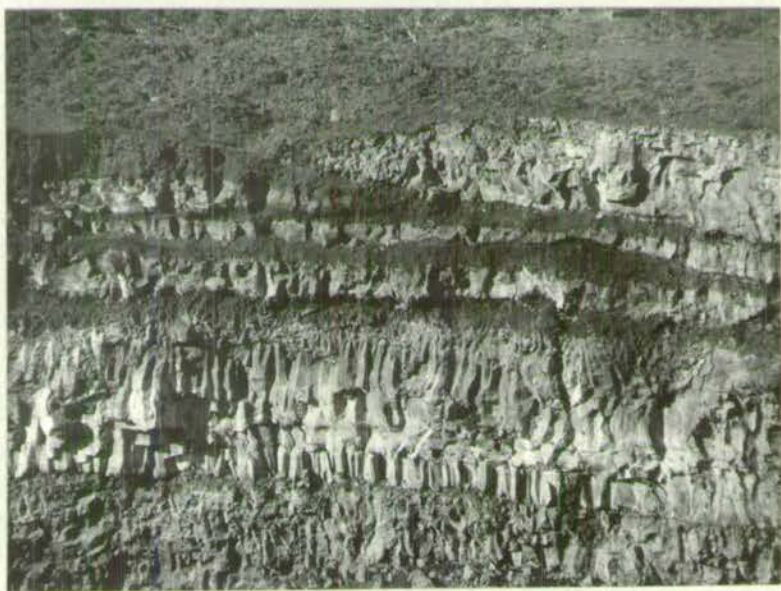
Plate 3.

Plagioclase-phyric flow, Foumboudzivouni.
Note baked contacts and flow alignment of
plagioclase phenocyrsts in upper flow, and
rosette-like clusters in lower ones.

<u>Plate 5.</u>

Haboho cinder cone, northwest rift zone of
Kartala (see Fig. 5). Note soil layers about
50 cm. from top on right side.

<u>Plate 6.</u>

Sima cinder cone, showing characteristic colours
caused by weathering, western Kartala (see Fig. 5).
Note curved sub-horizontal dyke truncating bedding.

5

6

a.

b.

Plate 10.

Panoramic view of the Kartala caldera from its eastern side.
The area of overlap of the upper and lower photos can be
positioned from the 1965 flow.
Compare with Fig. 7a.

W   NNW

1965   FLOW   PORTE D'ITSANDRA

S   SSW

CHAHALE

Plate 11.

Vertical basaltic dyke in wall of Chagnoumeni pit
crater. Note characteristic zoning, with vesicular
centre, massive outer parts, and glassy margins.
Dyke is about 25 cm. thick.

Plate 12.

Alkali basalt (No.32)

Plate 13.

Alkali olivine basalt (No.2)

Plate 14.

Oceanite (No.18)

Plate 15.

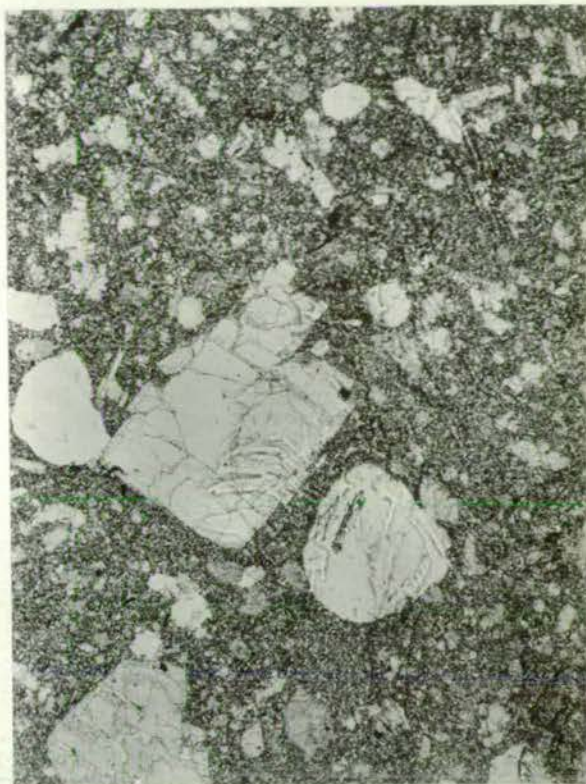Ankaramite (No. 31)

12.   1 cm.
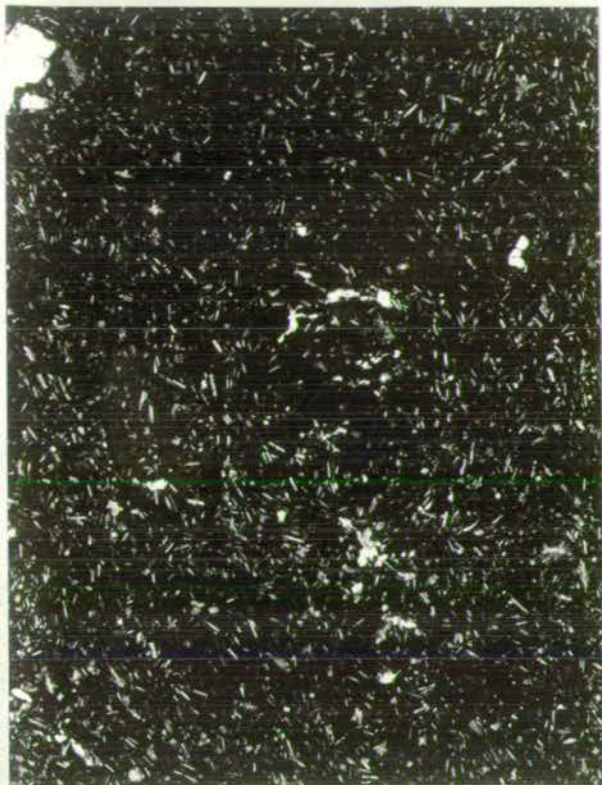
13.   5 mm.
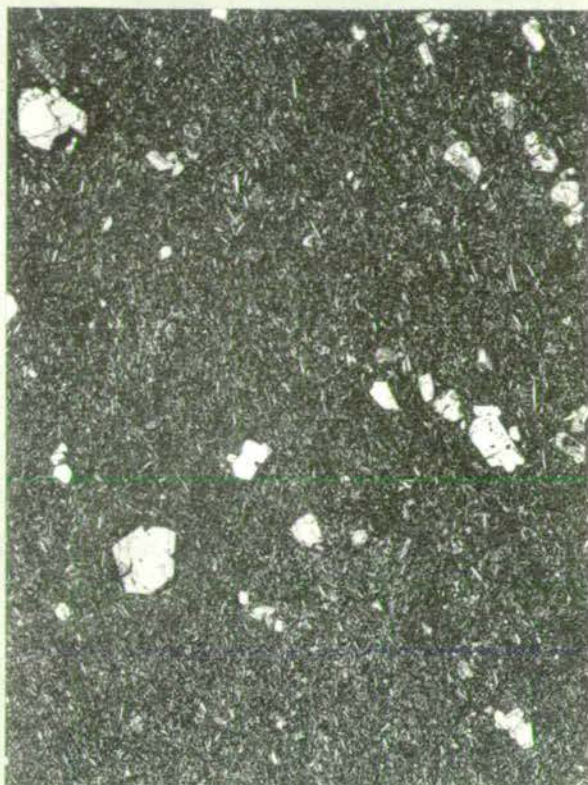
14.   5 mm.
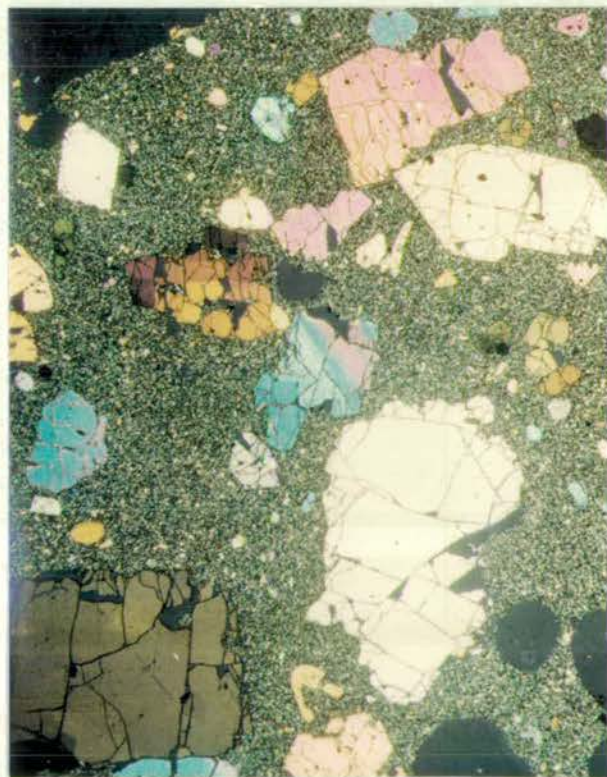
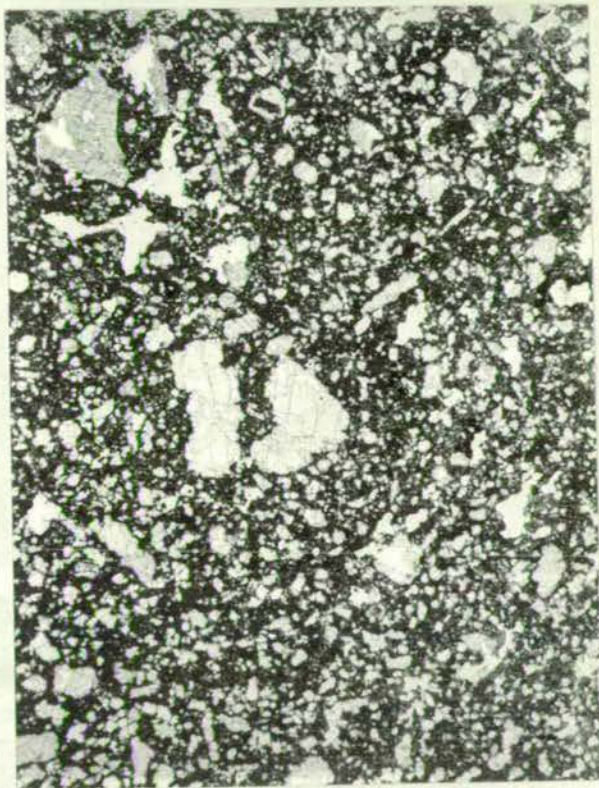15.   5 mm.
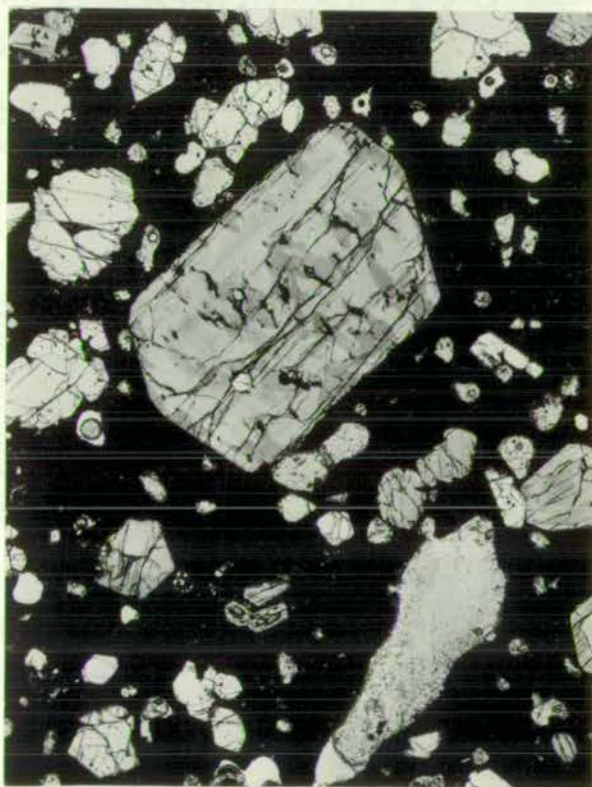
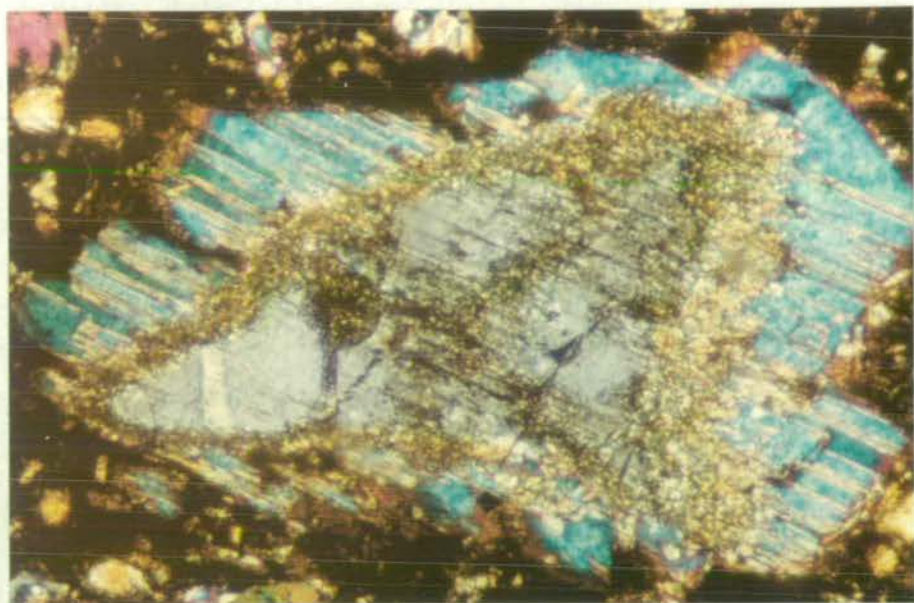16.   5 mm.

17.   5 mm.

18.   5 mm.

Plate 19.

Orthopyroxene xenocryst in La Grille lava,
surrounded by polysynthetically twinned
clinopyroxene. (~1 mm. dia.)

Plate 20.

Quartz xenocryst in La Grille lava,
surrounded by clinopyroxene. (~1 mm. dia.)

19.

20.